Vestibular Processing and its Cortical Signature in Humans

THÈSE N^{O} 6469 (2015)

PRÉSENTÉE LE 19 FÉVRIER 2015

À LA FACULTÉ DES SCIENCES DE LA VIE

CHAIRE FONDATION BERTARELLI DE NEUROPROSTHÉTIQUE COGNITIVE

PROGRAMME DOCTORAL EN NEUROSCIENCES

ÉCOLE POLYTECHNIQUE FÉDÉRALE DE LAUSANNE

POUR L'OBTENTION DU GRADE DE DOCTEUR ÈS SCIENCES

PAR

Steven GALE

acceptée sur proposition du jury:

Prof. C. Petersen, président du jury
Prof. O. Blanke, directeur de thèse
Prof. B. Day, rapporteur
Prof. C. Michel, rapporteur
Prof. J. D. R. Millán Ruiz, rapporteur

ÉCOLE POLYTECHNIQUE
FÉDÉRALE DE LAUSANNE

Suisse
2015

Abstract

The vestibular system encodes rotations and translations of the head in space. While much is known about cortical processing of the classical Aristotelian sensory modalities, such as vision and touch, knowledge of how vestibular stimulation is encoded in the human brain is lacking, probably due to the inherent technical difficulties of recording human brain function while providing natural vestibular stimulation. Here, I used electroencephalography (EEG), psychophysics, and a custom-built rotating chair to elucidate how natural vestibular stimulation is encoded and processed in the brain, and identified novel markers of vestibular processing in the brain in the frequency domain. Specifically, in one set of experiments the spectral response to rotations were analyzed during constant velocity stimulation and short, transient stimulations in healthy subjects and bilateral vestibular-loss patients (BVPs). In another set of experiments the time course of spectral modulations was compared to that of the vestibulo-ocular response (VOR), which decays exponentially during constant velocity rotational stimulation with a time constant of 10-30s. Throughout all EEG experiments, spectral power in the alpha (8-13 Hz) band was found to consistently encode vestibular stimulation. Furthermore, the multisensory nature of the vestibular system was studied statistically by using a Bayes-optimal integration model to better understand how visual and vestibular information are combined in the brain to form a percept. Results across these experiments indicate that visual and vestibular information are not just integrated optimally, but also “fused” at the perceptual level.

Keywords: vestibular system; electroencephalography; multisensory integration; Bayesian inference; psychophysics; brain-machine interface

Résumé

Le système vestibulaire encode les rotations et translations de la tête dans l’espace. Chez l’humain, bien que le traitement cortical des modalités sensorielles aristotéliciennes classiques, telles que la vision et le toucher, soit plutôt bien caractérisé, la représentation de l’activation du système vestibulaire au niveau cérébral est encore mal connue. Ceci est probablement dû aux difficultés inhérentes à la stimulation du système vestibulaire humain de façon naturelle tout en enregistrant simultanément l’activité cérébrale. Ici, j’ai utilisé l’électroencéphalographie (EEG) et la psychophysique en combinaison avec l’emploi d’une chaise rotative construite sur mesure afin d’élucider comment une stimulation naturelle du système vestibulaire est encodée et traitée au niveau du cerveau, en particulier au niveau des composantes fréquentielles de l’activité cérébrale. Plus spécifiquement, j’ai tout d’abord analysé la réponse spectrale enregistrée lors de mouvements de rotation à vitesse constante ou lors de courtes rotations transitoires, et ceci chez des sujets sains, mais aussi chez des sujets atteints de perte bilatérale de la fonction vestibulaire. Ensuite, j’ai comparé l’évolution temporelle des modulations spectrales avec celles générées lors d’une réponse vestibulo-oculaire, qui décroit exponentiellement lors de stimulations rotationnelles à vitesse constante avec une constante de temps de 10 – 30 s. Dans tous les enregistrements EEG obtenus, j’ai observé que la puissance spectrale dans la bande alpha (8-13 Hz) encodait de manière consistante l’activation vestibulaire. Finalement, j’ai étudié statistiquement la nature multisensorielle du système vestibulaire, en appliquant un modèle d’intégration optimal de Bayes pour mieux comprendre comment les informations visuelles et vestibulaires sont combinées au niveau du cerveau afin de constituer une perception. En conclusion, les résultats de ces différentes expériences semblent indiquer que l’information visuelle et l’information vestibulaire ne sont pas simplement intégrées de manière optimale, mais qu’elles sont « fusionnées » au niveau perceptuel.

Mots-clés: Système vestibulaire; électroencéphalographie; intégration multisensorielle; inférence bayésienne; psychophysique; interface cerveau-machine.

Table of Contents

1. INTRODUCTION

The vestibular system, which at its periphery in the inner ear is composed of an elegant structure of linear (two otolith organs: utricle and saccule) and rotational (three semicircular canals: horizontal, posterior, and anterior) sensors, encodes movements and orientations of the head in space, and contributes to a wide array of functions that allow us to process physical motion. It plays a central role in our everyday lives: from reflexes that stabilize our gaze during movement to high-level perception of self-motion, and yet its multimodal and distributed nature does not give rise to a distinct sensation (Angelaki and Cullen, 2008). Although considered our "sixth sense", research and knowledge of how vestibular stimuli are processed in the human cortex lags behind that of the other senses, such as vision and touch. For example, electroencephalography (EEG) has been used extensively for almost 100 years to study the human visual system (Berger, 1929; Niedermeyer, 2005), while EEG studies of the human vestibular system have been limited both in scope and number, failing to converge on an EEG correlate of natural vestibular stimulation (Hood and Kayan, 1985; Durrant and Furman, 1988; Probst et al., 1995).

One explanation for the dearth of cortical vestibular research in humans is technical. Visual stimuli for studies of the visual system are easily compatible with EEG and neuroimaging (fMRI, PET) techniques, ranging from simply opening and closing the eyes to visual stimuli delivered via a computer screen while subjects remain stationary (Niedermeyer, 2005). However, delivering a precise natural vestibular stimulation (VS) requires complex motion platforms while subjects are physically displaced, making neuroimaging studies impossible and EEG difficult. For this reason most studies of cortical vestibular function in humans used artificial VS techniques (i.e. caloric VS, galvanic VS), which have coarsely mapped some vestibular regions of cortex. However, these techniques co-excite other sensory modalities (Lopez et al., 2012) and thus cannot selectively stimulate structures in the peripheral vestibular apparatus.

Further complicating the issue, vestibular processing is complex and multimodal, even at the subcortical level; visual, motor, and proprioceptive information are integrated with signals from vestibular afferents at the level of the first synapse in the brainstem (Angelaki and Cullen, 2008). Additionally, the cortical vestibular system is distributed throughout the cortex, with no primary vestibular cortex, and is composed of bimodal neurons that respond to vestibular as well as visual, somatosensory, and

proprioceptive input (Brandt and Dieterich, 1999), a stark contrast to the localized and unimodal cortical areas that encode other senses.

The primary goal of the research described here was to overcome these challenges and discover how, and where, vestibular information is processed in the human brain, bringing it in line with knowledge of other sensory modalities such as vision and touch. Using a custom-built cockpit style centrifuge chair (the rotator) this thesis details investigations of the horizontal semicircular canals' contribution to the cortical and perceptual response to natural passive whole-body VS. In one set of experiments, I used EEG to determine if cortical oscillations responded to rotational VS in the same manner as for other senses (i.e. alpha band for vision, mu rhythm for touch; Niedermeyer, 2005). Building on this work, I asked if properties and temporal dynamics established in non-human primate recordings of sub-cortical vestibular neurons (Fernandez and Goldberg, 1971; Waespe and Henn, 1977), as well as human studies of the vestibulo-ocular reflex (VOR) and perception of rotation (Cohen et al., 1981; Okada et al., 1999; Bertolini et al., 2011), were also present at the cortical level in humans. In another series of experiments, I used statistical models and psychophysics to probe how visual and vestibular information are combined in the brain to form a percept of rotation. This technique facilitated an investigation into whether these two idiothetic cues were integrated in a Bayes-optimal manner, and whether the cues were "fused" at the perceptual level.

For the remainder of this introduction, some of the core concepts and background of the vestibular system will be presented.

1.1 Sub-Cortical Processing.

The peripheral vestibular system encodes linear accelerations and tilt (two otolith organs: utricle and saccule) and rotational accelerations (three orthogonal semicircular canals: horizontal, posterior, and anterior) of the head. Our rotation platform was oriented to stimulate only the horizontal semicircular canals, which will be described in further detail here (for a full description of the vestibular apparatus see Purves et al., 2007). Each ring-shaped canal is filled with fluid (endolymph), which relative to the canal itself, flows in the opposite direction of angular

accelerations of the head. At the base of each canal is a bulbous structure called the ampulla, in which mechano-gated hair cells housed in the cupula modulate an otherwise constant firing rate in cell bodies in the vestibular nerve when they are displaced by endolymph flow during movement (Fig. 1.1). The resting state firing rates of these neurons are high, allowing direction specific modulation of firing rates (i.e. firing rates for afferents from one canal increase for clockwise (CW) and decrease for counterclockwise (CCW) rotations. Note: left and right canals are complimentary; for CW rotations afferents from the right horizontal canal will increase their firing rate while decreasing for afferents in the left horizontal canal, and vice versa in response to CCW rotations).

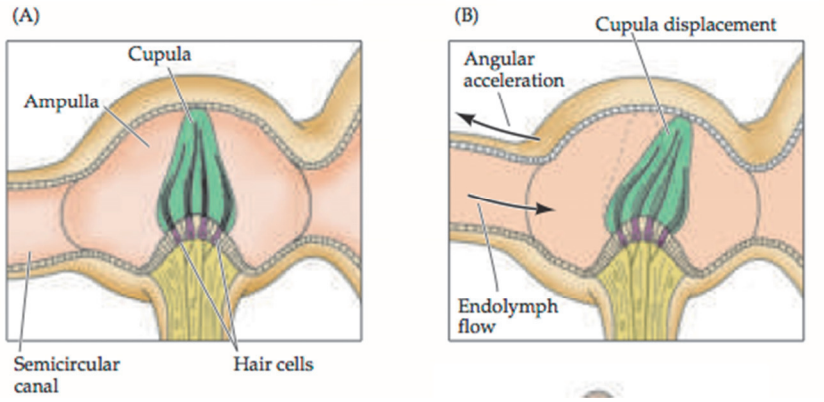

Figure 1.1: Physiology of the sensing structure of the semicircular canals at rest (LEFT) and with angular acceleration (RIGHT) as shown by the displacement of the cupula and hair cells (taken from: Purves et al., 2007).

Signals from the vestibular nerve, which faithfully encode hair cell displacement in both the semicircular canals and otolith organs, connect directly with a group of neurons in the brainstem called the vestibular nucleus. At this first synapse, signal integration and processing occurs between vestibular otolith and canal afferents, and with descending signals from the visual, motor, and proprioceptive systems (Purves et al., 2007; Angelaki and Cullen, 2008). It is important to note that although angular accelerations act on the canals, this signal is mathematically integrated due to the small diameter of the canals and the viscous properties of the endolymph, and therefore encodes the velocity of the VS (Purves et al., 2007; Cullen and Sadeghi, 2008).

1.2 The Vestibulo-Ocular Reflex (VOR)

Of the several reflexes driven by the vestibular system, the vestibulo-ocular reflex (VOR) is the most pertinent to the studies presented here. The VOR is a reflexive eye-movement that stabilizes our gaze while we move. Neurons in the vestibular nuclei connect directly with oculomotor neurons that terminate on the medial and lateral recti of the eyes, which mediate compensatory eye movements in the opposite direction to rotational or translational VS with a gain of roughly 1. The latency of this response is low, on the order of 5ms (Angelaki and Cullen, 2008), making it an accessible and precise marker of vestibular activity, as demonstrated by the correlation between VOR and firing rates of subcortical vestibular neurons in non-human primates (Büttner and Waespe, 1981). The yaw rotational VS induced a horizontal VOR in our experiments, and special consideration was taken to remove this signal from recorded EEG (for preprocessing details see methods section of paper 1).

1.3 Response to Constant Velocity VS and Velocity Storage

Most of what we know about vestibular processing has been learned from non-human primate studies reporting single unit activity in the vestibular nerve and vestibular nuclei in response to passive whole-body rotations. In their seminal study, Fernandez and Goldberg (1971) studied firing rates of vestibular afferents in the vestibular nerve during constant velocity rotational VS (Fernandez and Goldberg, 1971). During an acceleration pulse from rest, the head will begin to turn immediately, but the endolymph in the semicircular canals will lag the rotation (much like when turning a glass of water; the glass moves faster than the water at first) displacing the hair cells in the cupula and modulating vestibular afferent firing rates. Fernandez and Goldberg found maximal firing rates during the acceleration pulse, although due to the viscosity of the endolymph and small diameter of the canals, the acceleration stimulus was mathematically integrated by the canals and resulted in firing rates that encoded its velocity. During the constant velocity phase, firing rates returned to baseline levels following an exponential trajectory with a time constant of 7-10s (Fig. 1.2; Fernandez and Goldberg, 1971; Büttner and Waespe, 1981). The same modulation of firing rates occurred when the monkey was decelerated to rest from constant velocity (when you stop turning the glass of water, the water will

continue turning at first even though the glass is at rest). This property was exploited for the EEG experiments presented in this thesis in order to circumvent confounds related to somatosensory cues and other movement related artefacts in the recordings. Analyzing the post-rotation period allowed recording of periods when vestibular cortical areas were active but the subject was immobile.

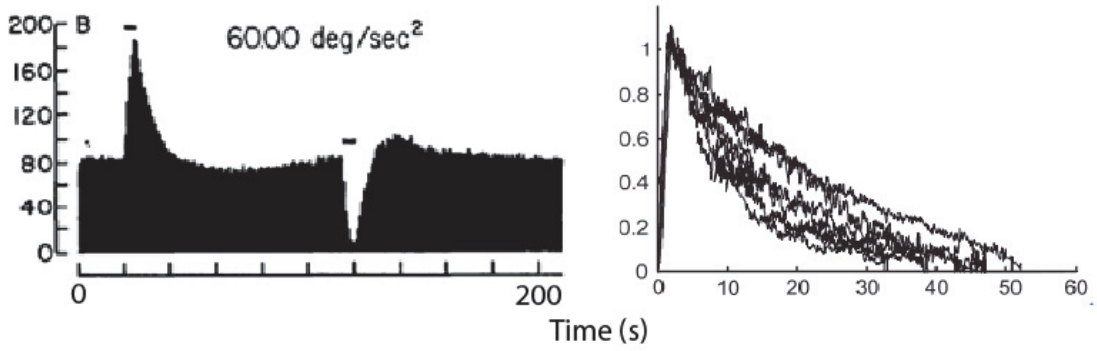

Figure 1.2: Firing rate of a single neuron in the vestibular nerve of a squirrel monkey during constant velocity VS (LEFT; taken from Fernandez and Goldberg, 1971). Note the exponential trajectory in response after acceleration and deceleration pulses (horizontal bars). RIGHT: single trials of the VOR response in humans during the period immediately following constant velocity VS (taken from Bertolini et al., 2011).

Interestingly, when vestibular nuclei neurons in the brainstem were recorded during the same constant velocity VS, the firing rates decayed with a longer time constant, in the range of 15-20s (Waespe and Henn, 1977). This increase in time constant is referred to as “velocity storage”, the mechanism and function of which is not well understood (Raphan et al., 1979; Bertolini et al., 2011). In humans, studies of the VOR and perception of rotation during constant velocity VS (Fig. 1.2; Cohen et al., 1981; Okada et al., 1999; Bertolini et al., 2011) yielded the same exponential decay during the constant velocity phase with time constants similar to those in the vestibular nuclei, confirming the velocity storage effect is propagated to oculomotor and perceptual functions humans, and therefore would presumably be present in the human cortex.

1.4 The Vestibular Cortex

To date no primary vestibular cortex, that is a cortical area whose neurons respond solely to VS, has been found in either humans or non-human primates (Angelaki and Cullen, 2008). In non-human primates, a network of distributed and multimodal areas in somatosensory, temporal, frontal, and parieto-insular cortices respond to

VS, with the parieto-insular vestibular cortex (PIVC) presumed to be the core due to its high percentage of vestibular responsive neurons (~50%) and strong interconnectivity with other vestibular cortical areas (Fig. 1.3; see reviews by Guldin and Grüsser, 1998; Lopez and Blanke, 2011).

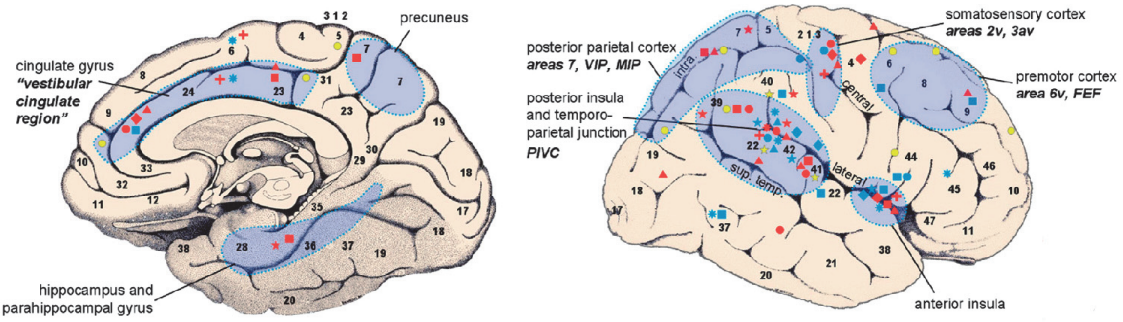

Figure 1.3: Human cortical areas activated by caloric VS (red), galvanic VS (blue), or auditory clicks (yellow). Corresponding vestibular areas in monkeys are written in bold (taken from Lopez and Blanke, 2011).

Neuroimaging studies in humans have identified a similar cortical representation of VS (Fig. 1.3; Brandt and Dieterich, 1999; Lopez and Blanke, 2011; Lopez et al., 2012). As found in monkeys, neurons in frontal, parietal, and temporal regions of the human cortex also responded to VS. These regions largely overlapped with those identified in studies of non-human primates. However it should be noted when comparing results across species that non-human primate studies were performed using natural VS on motion platforms, which allowed for a specific stimulation of individual canal and otolith organs. In contrast, human studies were performed using artificial VS techniques (i.e. galvanic and caloric VS), which provided a less precise VS and simultaneously excited multiple semicircular canals and otolith organs, as well as co-exciting other sensory modalities (e.g. somatosensory response to warm/cold water caloric VS).

The distributed and multimodal vestibular cortical network identified further complicates localizing cortical vestibular processing in humans, but makes it clear that new approaches are necessary to broaden the understanding of how VS is represented by the brain. Ideally, methods that allow the recording of neural signals during natural vestibular VS would facilitate a more direct comparison to recordings of non-human primates. As EEG records cortical activity at the network level with millisecond temporal resolution while allowing physical motion, it has the potential to

identify important new aspects of vestibular function (and dysfunction) during natural VS in the human cortex.

1.5 Vestibular EEG

To our knowledge, all prior electrophysiological investigations of the human vestibular system in response to natural VS (Hood and Kayan, 1985; Durrant and Furman, 1988; Probst et al. 1995) looked at evoked potentials. Interestingly, all of these studies demonstrated a similar long latency vestibular evoked potential (LLVEP), a consistent dome-shaped negativity that matched the rotation profile and persisted for the duration of the stimulus. Hood and Kayan (1985) first used the raised-cosine rotational stimuli and measured full-scalp EEG (10-20 montage referenced to the tip of the nose) in cohorts of healthy subjects and BVPs (Fig. 1.4), resulting in a negativity that was maximal at Cz and peaked halfway through the rotation profile for both groups. No statistical differences between the groups were reported. Probst et al. (1995) used similar experimental procedures to Hood and Kayan and found a similar LLVEP in healthy subjects by recording from a single vertex electrode referenced to the nasion (Fig. 1.4). Again, a long latency negativity that followed the angular velocity profile of the VS was recorded. Note that only one electrode was used in these recordings so this effect could not be localized. Furthermore, patients with vestibular deficiencies were not recorded from to confirm the negativity was vestibular in origin. Durrant and Furman (1988) gave short constant velocity pulses to healthy subjects and BVPs and found nearly identical LLVEP in both healthy subjects and BVPs. Again, recordings were made with only one vertex electrode referenced to the mastoid. The protocol was repeated with both cohorts but with the eyes closed, and no discernable differences were found from eyes-opened recordings. Again, healthy subjects and BVPs had nearly identical responses.

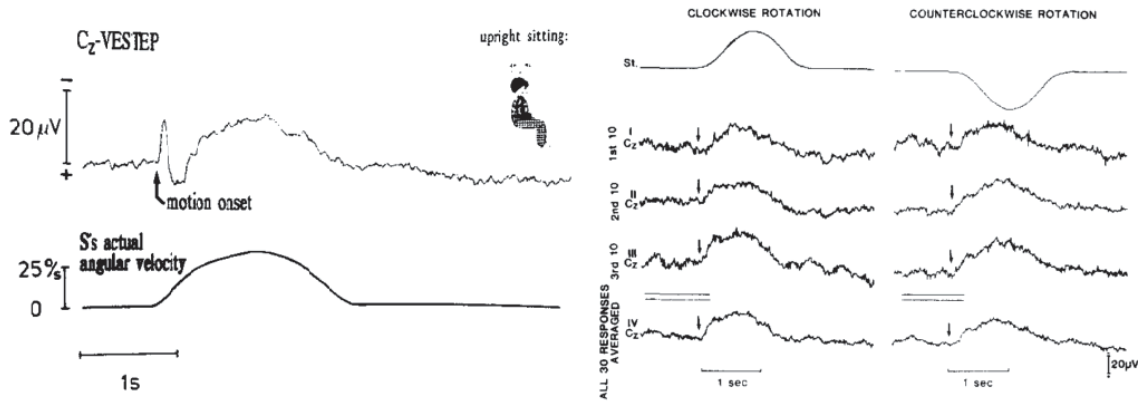

Figure 1.4: Vestibular evoked potential in response to natural vestibular stimulation with a "raised-cosine" velocity profile. LEFT: Grand average results from Probst et al. (1995). RIGHT: 10-trial average evoked potentials in response to the same "raised-cosine" VS in both clockwise and counterclockwise directions (Hood and Kayan, 1985).

The similarity of the evoked response between healthy subjects and BVPs makes it unlikely that this signal is vestibular in origin. I offer several explanations for why this type of paradigm/analysis is not suitable for capturing a cortical vestibular response. Although each of the aforementioned vestibular EEG studies made specific mention of the need to deal with the inevitable artefacts inherent to this type of stimulation, I argue that the countermeasures they employed were not sufficient to control for these artefacts. For example, sparse electrode montages do not allow for the use of an average reference to remove common-mode noise caused by rotation, such as movement of the electrodes relative to the head. A standard remote reference, such as the nose or forehead, used in previous studies would be susceptible to this type of artefact. Furthermore, dense scalp recordings including frontal electrodes, which can be used to detect and remove components related to VOR, were not utilized in these studies. Ocular nystagmus is a major source of artefacts in vestibular electrophysiology, and yet no methods apart from asking subjects to visually suppress the VOR and qualitatively monitoring of EOG traces have been employed in these previous studies.

Classical sensory-evoked potential studies (e.g. visual or somatosensory) are usually an average of hundreds of time series time-locked to short, discrete stimuli (Niedermeyer, 2005). Due to the long time constant of the peripheral vestibular system, and the artefacts/confounds present during most VS, evoked potentials are an insufficient analysis technique for decoding cortical vestibular processing. This claim is reinforced by the inconsistent results obtained in previous vestibular EEG

literature, and a central reason for hypothesizing that cortical oscillations in the alpha band, being multimodal and distributed in the cortex, might better reflect cortical processing of VS.

1.6 The Alpha Band

Alpha band (8-13Hz) oscillations have been linked to a wide array of sensorimotor and cognitive functions. Oscillations in the alpha band (referred to as mu rhythm over parietal and frontal areas) are generally suppressed or blocked during mental effort and/or cortical activation (Niedermeyer, 2005). In his landmark study, Berger showed spectral power in the alpha band power to be suppressed when the eyes were opened (and the visual system was engaged) and enhanced when the eyes were closed and no visual stimuli were processed (Berger, 1929). This effect has been shown to be dominant over visual cortex/occipital areas of the scalp (Niedermeyer, 2005). Gastaut expanded on these findings by demonstrating that oscillations in the alpha band were also modulated by the performance or observance of motor actions over sensorimotor areas of the scalp (Gastaut, 1952; Niedermeyer, 2005). Since then, alpha band oscillations have been shown to react to a dizzying array of sensorimotor, cognitive, and multisensory tasks over occipital, parietal, temporal, and frontal scalp regions (reviewed in: Hari and Salmelin, 1997; Klimesch, 1999; Niedermeyer, 2005; Pineda, 2005). Additionally, alpha band oscillations have been strongly linked to attentional processes; alpha band power decreases during visual (Sausang, et al., 2005; Romei et al., 2008) and somatosensory (Haegens et al., 2011, 2012) attention. Because alpha band power is generally suppressed when corresponding cortices are active (e.g. lower alpha band power over visual cortex with the eyes opened, lower alpha band power over somatosensory cortex during direct touch), it has been referred to as a resting or priming rhythm for cortical areas (Haegens et al., 2011; Niedermeyer, 2005). We would therefore expect vestibular cortical areas to react in a similar manner when activated to that of other senses (i.e. vision and touch) that also modulate alpha band oscillations.

When predicting the neural correlate of VS as measured by EEG, knowledge of subcortical (sections 1.1 to 1.3) and cortical (sections 1.4 to 1.5) vestibular processing provides strong guidance as to its representation in humans. Said

correlate should be responsive to sensory input, widely distributed over cortex, and multisensory. As outlined in this section, each of these criteria can also describe reactivity of alpha band oscillations in the human cortex. Finally, vestibular cortical areas overlap with many parieto-temporal areas shown to modulate alpha band oscillations. Furthermore, vestibular cortical neurons and alpha band oscillations are both responsive to visual, motor, and proprioceptive stimuli, strengthening the possible link between the two.

1.7 Bayesian Integration of Visual and Vestibular Cues

When perceiving the world, we regularly combine cues from different sensory modalities with redundant information. For example, a professor turning in their chair to address a frantic PhD student will combine vestibular (semicircular canals) and visual (optic flow during rotation) information to gauge the speed and amount of rotation. It has been shown that the variability of this final estimate at both the perceptual and neuronal levels is reduced when compared to the variability of its component cues in a statistically optimal manner (reviews: Knill and Pouget, 2004; Angelaki et al., 2009; cortical visual-vestibular integration: Gu et al., 2008; Fetsch et al., 2009; Butler et al., 2010). Maximum-likelihood estimation (MLE), a statistical model based on a Bayesian framework, quantifies this theory by equating a statistical perceptual estimate with the weighted sum of its component sensory cues in situations where the distribution of prior knowledge is flat. One such situation might be rotations over a small (5º) range (i.e. a person would not perform better at detecting rotations of 15º than 20º).

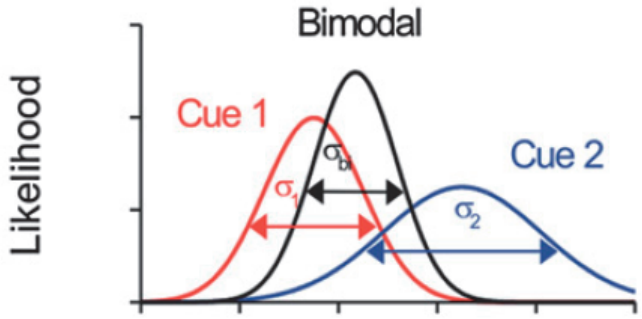

Figure 1.5: Schematic representation of MLE. The reliability of a bimodal cue (black) is increased (i.e. smaller variance) compared to its constituent cues (cue 1, red; cue 2, blue) (Taken from Angelaki et al., 2009).

Formally, according to the model a bimodal estimate combining two sensory cues will be more reliable (i.e. have a smaller variance) than each cue on their own if they are integrated (Fig. 1.5). In some cases, the two cues are “fused”, meaning that we no longer have access to the constituent cues, only the combined bimodal estimate (Hillis et al., 2004).

Here, we studied how visual and vestibular information were processed in humans at the perceptual level by having subjects judge the relative size of successive rotations when given visual (optic flow), vestibular (yaw rotation), and bimodal (visual and vestibular stimulation together) feedback. As visual and vestibular signals interact in vestibular nuclei neurons, the VOR, and in the cortex (Dieterich and Brandt, 2000), our goal was to better understand the perceptual interaction between the two sensory cues. Do visual and vestibular cues integrate following the MLE model at the level of human perception? Do we still have access to these individual cues or are they discarded and replaced by a fused cue? By answering these questions we can better understand how vestibular information is processed and combined in the human cortex.

2. PERSONAL CONTRIBUTIONS

2.1 Thesis Articles

1. Gale S, Prsa M, Schurger A, Gay A, Paillard A, Herbelin B, Guyot JP, Lopez C, Blanke O (submitted) Oscillatory neural responses evoked by natural vestibular stimui in humans.

Personal contribution: design, implementation, recording, analysis, writing.

2. Gale S, Schurger A, Blanke O (in prep) Temporal dynamics of cortical oscillations under natural vestibular stimulation.

Personal contribution: design, implementation, recording, analysis, writing.

3. Prsa M, **Gale S**, Blanke O (2012) Self-motion leads to mandatory cue fusion across sensory modalities. J Neurophysiol 108:2282-2291.

Personal contribution: design, implementation, recording, analysis (interpretation), writing (revisions).

2.2 Appendix Articles

4. Evans N, **Gale S**, Schurger A, Blanke O (submitted) Visuo-neural discrepancies modulate the sense of agency for brain-machine actions.

Personal contribution: design, implementation, recording, analysis, writing (revisions).

5. Kaliuzhna M, Prsa M, **Gale S**, Lee S, Blanke O (in press – Journal of Vision) Learning to integrate contradictory multisensory self-motion cue pairings.

Personal contribution: design, implementation, recording (pilot).

3. SCIENTIFIC ARTICLES

3.1

Paper I – Oscillatory neural responses evoked by natural vestibular stimuli in humans.

Oscillatory neural responses evoked by natural vestibular stimuli in humans.

Steven Gale[1,2], Mario Prsa[1,2], Aaron Schurger[1,2], Annietta Gay[3], Aurore Paillard[2], Bruno Herbelin[1,2], Jean-Philippe Guyot[3], Christophe Lopez[4], Olaf Blanke[1,2,5]

[1] Center for Neuroprosthetics, École Polytechnique Fédérale de Lausanne, Switzerland
[2] Laboratory of Cognitive Neuroscience, Brain-Mind Institute, École Polytechnique Fédérale de Lausanne, Switzerland
[3] Department of ORL, University Hospital Geneva, Switzerland
[4] Aix Marseille Université, CNRS, NIA UMR 7260, 13331, Marseille, France
[5] Department of Neurology, University Hospital Geneva, Switzerland

Corresponding Author:
Olaf Blanke
Center for Neuroprosthetics & Brain-Mind Institute
Bertarelli Foundation Chair in Cognitive Neuroprosthetics
School of Life Sciences
École Polytechnique Fédérale de Lausanne
Station 19
CH – 1015 Lausanne
Tel: +41 21 693 69 21
E-mail: olaf.blanke@epfl.ch

Abstract

While there have been numerous studies of the vestibular system in mammals, less is known about the brain mechanisms of vestibular processing in humans, probably due to the technical challenges of measuring brain activity during natural vestibular stimulation (VS) in cortical and subcortical structures. Although several electroencephalography (EEG) studies have been carried out in humans over the last 30 years the reported data are not conclusive, did not use modern electrode montages or EEG analyses, and did not investigate how VS relates to cortical oscillations. Here, we measured changes of cortical oscillations in response to transient (raised-cosine velocity profile) and constant velocity passive whole body yaw rotations using high-density 192-channel EEG in healthy subjects and a group of patients with bilateral vestibular loss (BVPs). The present approach overcame significant technical challenges associated with combining natural VS with human electrophysiology and reveals that transient and constant velocity VS is associated with a prominent suppression of alpha power (8-13Hz). Alpha band suppression was localized over bilateral parieto-temporal scalp regions and these alpha modulations were significantly smaller in BVPs. No other comparable modulation that was consistent across transient and constant velocity VS were observed in the other frequency bands. We propose that suppression of oscillations in the alpha band over parieto-temporal scalp regions reflects cortical vestibular processing, potentially comparable with alpha and mu oscillations in the visual and sensorimotor systems respectively, opening the door to the investigation of human cortical processing under various experimental conditions during natural VS.

Introduction

The vestibular system encodes three-dimensional displacements of the head and its position relative to gravity. Vestibular signals are used for oculomotor and postural control, but also underpin perceptual and cognitive functions, including visual perception according to internal models of gravity, spatial navigation, and bodily awareness (Brandt et al., 2005; Indovina et al., 2005; Lopez et al., 2010). In strong contrast with the growing number of functions shown to be under vestibular influence is the relative lack of data on the vestibular cortex in animals and humans (Brandt and Dieterich, 1999; Angelaki and Cullen, 2008; Lopez and Blanke, 2011).

Electrophysiological investigations in non-human primates have revealed vestibular responses in several areas of the cortex. These include the intraparietal sulcus, the somatosensory, temporal, frontal and parieto-insular cortices (Schwarz and Fredrickson, 1971; Grüsser et al., 1990a,b; Bremmer et al., 2002; Gu et al., 2008; Liu et al., 2011). These areas form a cortical network of which the core is presumed to be located in the 'parieto-insular vestibular cortex' (PIVC; Guldin and Grüsser, 1998). Recently, descriptions of vestibular neurons' spatiotemporal tuning in these cortical regions have been achieved during three-dimensional passive rotations/translations on motion platforms in non-human primates (e.g. Takahashi et al., 2007; Chen et al., 2011; Shinder and Newlands, 2014).

Investigations of the human vestibular cortex are challenging because neuroimaging techniques (fMRI, PET) do not allow head and body movements and thus the application of natural vestibular stimulation (VS). Consequently, human neuroimaging studies have used a variety of artificial VS devoid of physical head motion, such as cold and warm caloric VS, galvanic VS, auditory clicks or short tone bursts (Lopez et al., 2012). These studies revealed vestibular activations in the insular, temporo-parietal, somatosensory, cingulate and frontal cortices (e.g. Bottini et al., 1994; Lobel et al., 1998; Dieterich et al., 2003; Schlindwein et al., 2008). Yet these stimulation techniques activate otolithic and semicircular canal receptors to different degrees, rendering the comparisons between the obtained results difficult. Furthermore, since

artificial VS has no physiological equivalent, its use in humans precludes direct comparisons with data about the vestibular cortex in non-human primates collected during VS on motion platforms (e.g. Grüsser et al., 1990b; Liu et al., 2011; Chen et al., 2011).

While electroencephalography (EEG) has been used extensively to describe visual, somatosensory and auditory cortical responses (Niedermeyer, 2005), a detailed description of EEG responses to natural vestibular stimuli and their neural generators is still lacking. Building on prior studies that have attempted to measure vestibular evoked potentials (Hood and Kayan, 1985; Elidan et al., 1991; Probst et al., 1995; Todd et al., 2014 a,b,c), here we report data from a new research platform that allowed us to investigate human cortical processing of natural VS by recording high-density 192-channel EEG while participants underwent passive whole body yaw rotations. We performed two studies (total of four experiments) and analyzed event-related desynchronization of cortical oscillations and vestibular evoked potentials during transient and constant velocity rotations in healthy participants and a cohort of patients diagnosed with bilateral vestibular loss.

Materials and Methods

Participants.

A total of 22 healthy subjects participated in these experiments: ten healthy subjects (mean age 29.9 ± 3.6 years; 3 women) in study 1 and twelve healthy subjects (mean age 30.4 ± 4.3 years, 3 women) participated in study 2. All healthy subjects were right handed and had normal or corrected to normal vision. Nine patients (mean age 54.7 ± 20; 6 women) diagnosed with bilateral vestibular loss participated in studies 1 and 2. Patients had idiopathic (n=4), ototoxic (n=2), congenital (n=1), ischemic (n=1) or surgical (n=1) related vestibular loss. The protocol was approved by the ethics research committee at the University of Geneva, and the experiments were performed in accordance with the ethical standards as declared in the Declaration of Helsinki.

Experimental Setup.

Rotational stimuli around the yaw axis were delivered by a custom-built centrifuge chair centered on the axis of rotation (Fig. 1*A*), therefore providing angular stimulation to the vestibular organs. The chair was digitally servo-controlled (PCI-7352) with precise positioning (±0.1°). Actual displacement kinematics were externally recorded by a triaxial accelerometer (Summit Instruments, 34203A) attached to the chair and positioned directly behind the subjects' head. Rotation profiles were pre-programmed and specified the chair's instantaneous angular position at a rate of 100Hz. Constant velocity stimuli were specified manually.

Subjects were restrained in the chair via a 5-point racing harness, with face paddles pressing on the subjects' cheekbones in order to restrain head movements. Additionally, foot straps and cushioning were used to further reduce subject movement. The rotator was housed in a lightproof and soundproof Faraday cage. White noise was administered to mask auditory cues from the chair during rotation. The vestibulo-ocular reflex (VOR) was suppressed by having subjects fixate straight-ahead on a chair-fixed LED target. We eliminated airflow cues and any residual light reflections emanating from

the surroundings by physically enclosing the chair with a dark blanket. Subjects were also monitored throughout the experiment with an infrared camera positioned directly below the fixation target.

Experimental Procedures.

In study 1, we investigated neural responses to transient vestibular stimuli. High-density EEG (see below) was recorded while participants were given a total of 100 rotations with a duration of 1.3s in each direction following a "raised-cosine" velocity profile (Fig. 1*B*) (Hood and Kayan, 1985; Probst et al., 1995). The peak velocity of the rotation, which occurs at the midway point of the profile (i.e. 650ms) was 110°/s resulting in a total angular displacement of 72°. The angular velocity profile was therefore a single cycle of a 0.77Hz raised cosine function. The inter-stimulus interval separating two consecutive rotations was randomly drawn from a uniform distribution between 1.5s and 2.5s in order to avoid anticipatory signals. Clockwise (CW) and counterclockwise (CCW) rotations were presented in randomized order in 4 sessions (each lasting less than 3 minutes). The subjects were instructed to stay immobile during each 3-minute session, maintain visual fixation, and avoid blinking of the eyes during rotation intervals.

In study 2, the effects of a constant vestibular stimulus were investigated. We recorded high-density EEG while the participants were rotated at a constant angular velocity of 80°/s for a minimum of 105 seconds (Fig. 1*C*) in both the CW and CCW direction. Subjects were accelerated to and decelerated from constant velocity in 2s pulses at an average of 40°/s^2. A shorter post-rotation period, directly after rotation had stopped, was also recorded. No explicit cues were given to subjects about when rotation would start and end. We also recorded EEG for each participant during a static baseline control condition, without any rotation, for the same length of time. As in study 1, subjects were instructed to remain immobile, maintain fixation, and minimize blinking.

EEG Recordings.

EEG was recorded using a 192-channel pre-amplified scalp electrode system (BioSemi, Inc., Amsterdam, Netherlands) sampled at 2048 Hz and downsampled to 512Hz for analysis. An active reference electrode pair (CMS-DRL) was positioned at the apex of the skull, and offline analysis was performed with an average reference. Data were transferred for monitoring in real-time to a dedicated recording computer via optical link. Eye movements were recorded by an electro-oculogram (EOG) system composed of four electrodes, placed above and below the right eye and one near each of the left and right lateral canthi.

EEG Data Analysis.

Preprocessing. As a whole body rotation inevitably induces VOR, we ensured preprocessing steps were taken to remove the associated artefacts from the recorded EEG. Residual artefacts were removed from EEG recordings using the FASTER algorithm (Nolan and Whelan, 2010), a fully automated statistical thresholding approach to artefact removal in EEG signals. EOG signals were used by the algorithm to remove eye-movement components in the signal related to the VOR. Channels with artefacts were removed and linearly interpolated from neighboring electrodes for each recording (average of 15 ± 1 out of 192 channels rejected for each subject).

We examined EOG traces before and after artefact removal using FASTER to ensure that eye movements had been removed from our recordings before analysis. Examination of average horizontal and vertical EOG traces of healthy subjects from study 1 aligned with rotation onset before and after preprocessing confirmed that artefacts caused by the VOR not successfully suppressed by fixation were either removed or strongly attenuated by FASTER.

Study 1: Transient Vestibular Stimulation.

Power spectrum analysis. After preprocessing, we computed the power spectral density for each electrode from -0.5s to 2s relative to rotation onset for all trials using the multitaper method (Fieldtrip Matlab toolbox, Mathworks, Natick, Massachusetts, USA).

Spectral estimates were calculated for 33 logarithmically scaled frequencies from 1 to 100Hz (i.e. 5 frequencies per octave) and at a 32ms time step. For frequencies above 20Hz, we used a constant smoothing frequency window of 5Hz and a 500ms temporal window yielding 4 multitapers. For frequencies below 20Hz, we applied 2 multitapers using the same temporal window of 500ms and therefore a frequency window of 3Hz. Power was normalized for all frequency bins with respect to baseline power between -0.5s and -0.1s. The time-frequency method that we used allows for a better visualization of the different natural brain oscillation frequencies whose bandwidths typically follow a linear progression on a logarithmic scale. To remove signal components driven by events phase-locked to rotation onset, we subtracted the evoked potential (i.e. the EEG signal averaged across all trials) from each trial. The computed time-frequency values therefore correspond only to signals that are not stimulus-locked. All spectral powers are reported as the average over all 192 electrodes. To compare maximal spectral power during rotation, we averaged spectral power in the same temporal window of interest commencing 650ms after rotation onset (peak velocity) through the end of rotation (1300ms after rotation onset) for both groups (healthy subjects and BVPs). This window contained stimulus peaks in velocity and acceleration and accounted for any potential phase lag between VS and the evoked cortical response (Hood and Kayan, 1985; Probst et al., 1995; Grüsser et al., 1990a; Chen et al., 2011). In this manner we compared spectral power in each band, both within and between groups, using the same electrodes (average over all 192 electrodes) and epoch.

Vestibular-evoked potentials. We performed an evoked potential analysis on the same transient rotation data of study 1. Data were preprocessed in two ways: 1) with a standard vertex reference and no techniques to remove movement related artefacts (i.e. VOR, movement of EEG cap relative to the skull) and 2) using an average reference and the FASTER algorithm to remove artefacts from the signal. In this manner we were able to compare the results obtained using the same preprocessing as used in previous studies (first preprocessing method used here, as used by Hood and Kayan, 1985; Probst

et al., 1995) with the results obtained using the present methods (the second preprocessing method). All data were filtered using a zero-phase second-order Butterworth filter between 1 and 100 Hz, and a subsequent notch filter at 50 Hz was used to remove line noise. A grand average was then performed on the data.

Study 2: Constant Velocity Vestibular Stimulation.

Power spectrum analysis. The firing rates of vestibular afferents from the semicircular canals are proportional to angular velocity but respond to non-zero acceleration stimuli (Goldberg and Fernandez, 1971). During a constant velocity rotation, the afferents modulate their activity in response to the initial acceleration pulse as velocity increases from zero to a constant level, and then return to baseline firing rates with a time constant of 5-6s (Büttner and Waespe, 1981) despite an ongoing rotation. In the vestibular nuclei, during the first stage of neural processing of vestibular inputs, the time constant of the return to baseline of the stimulus-induced activity is increased (Waespe and Henn, 1977), also known as velocity storage. The slow phase of the VOR as well as the reported perception of rotation follow the same dynamics as the activity of vestibular nuclei neurons in response to the acceleration stimulus, both having typical time constants in the 10-30s range (Bertolini et al., 2011). It follows that if we select an "early" period corresponding to the first 5s of constant velocity rotation and a "late" 5s period beginning 100s later (which is between 3 and 10 times the velocity storage time constant), then we can compare the measured cortical oscillations between conditions with and without VS but identical in other aspects (i.e. extra-vestibular sensory cues). Furthermore, this modulation of vestibular activity is also present in the period directly after constant velocity rotation ends (post-rotation); vestibular afferents encode the deceleration from constant to zero velocity and this activity returns to baseline levels with the same time constant as after the initial rotation onset. We therefore selected the first 5s of rest after rotation offset as the "post-rotation" period, and compared this with average activity during the static condition. The duration of our recordings did not

allow for a comparison of early and late post-rotation periods, however note that late and static conditions are equivalent in terms of vestibular activity.

Spectral power was calculated for each electrode during each period (i.e. early, late, post-rotation, etc…) using a Fast Fourier Transform (Matlab, Mathworks, Natick, Massachusetts, USA). A 2s epoch was used for the transform, which was shifted by 1s increments to fill each period (0.5 Hz resolution). Epochs within a period were then averaged to give spectral power for that period. To minimize edge effects of the transform, a Hann window was applied and the linear trend was removed. Relative changes in spectral power (P) at frequency (f) for each electrode (n) were calculated for each subject (s) according to equation 1:

$$P_n(s,f) = 10log_{10}\frac{P_{n,test}(s,f)}{P_{n,base}(s,f)} \quad (1)$$

where $P_{n,test}(s,f)$ is either the first 5 seconds of rotation (early) or post-rotation (post-rotation), and $P_{n,base}(s,f)$ is either the late period or the average over the entire static condition.

We averaged the spectral power during the test period in the alpha (8-13Hz) band. We also examined spectral power in the beta (14-30Hz) and gamma (30-100Hz, excluding Fourier coefficients between 49-51Hz due to electrical noise) bands. The logarithm of this power change was calculated so that the data would be approximately normally distributed (Oberman et al., 2005). This process was also applied to the control condition (static baseline), using the first 5 seconds of the recording as the early period and another 5-second interval (100 seconds later), as the late period. As in study 1, spectral power was averaged across all 192 electrodes in order to avoid biases that can be introduced by post-hoc selection of clusters of electrodes.

Topographical analysis.

For descriptive purposes we localized the set of 10 electrodes with the largest magnitude change in each frequency band with respect to baseline for each direction. The sets for each direction were then combined. In this manner we detected whether or not spectral changes in a given band formed a coherent topography on the scalp

(clustered) or were sparsely distributed. For study 1, electrodes with the largest power suppression/enhancement were sorted by spectral band during the temporal window of interest. For study 2, electrodes were calculated in each spectral band and for each test versus baseline comparison.

EEG Statistical Analysis

Study 1: Transient Vestibular Stimulation. A bootstrap analysis was used on each electrode to delineate frequency and time bins with power estimates significantly different from their corresponding pre-rotation baseline. To this end, the power estimates for the average of all electrodes were computed 999 times on a different subset of trials by randomly taking for each subset N trials, with replacement, from the complete set of N trials pooled from all subjects. Bins with significant power changes were deemed to be those that had more than 95% of their bootstrapped estimates that were either greater or smaller than the corresponding pre-stimulus average power (for detailed description see: Prsa et al., 2012). Furthermore, statistical comparisons between band power within the temporal window of interest between groups used a bootstrap test that randomly selected M control subjects or L BVPs, with replacement, from the complete set of M control subjects or L BVPs and compared them as above. Finally, band power at every timepoint was compared between healthy subjects and BVPs by performing a running bootstrap to test for significance. We corrected for multiple comparisons with a cluster-based permutation test. The labels of healthy subjects and BVPs were randomly shuffled 999 times and the same running bootstrap test was performed on this shuffled data as above, and we recorded the number of consecutive significant timeframes for every permutation. Consecutive timeframes had to be larger than 95% of cluster sizes to be considered significant.

Study 2: Constant Velocity Vestibular Stimulation. We used a cluster-based permutation test (electrode-wise threshold of $p < 0.01$) to identify contiguous clusters of electrodes that were significantly different when comparing the log spectral power during the test

(either the early rotation or post-rotation) periods and baseline (either the late rotation or static baseline) periods, while controlling for multiple comparisons. More specifically, for each subject we applied a two-tailed t-test at each electrode to the difference in log spectral power between the test period (i.e. early rotation) and baseline epochs. As described in Lenggenhager et al. (2011), we randomly permuted the labels on half of our data for each comparison and then looked for the largest contiguous cluster of significant electrodes in this permuted dataset. This process was repeated for each way of choosing half of the participants within a group (i.e. healthy subjects and BVPs), resulting in a distribution of maximum cluster sizes. Only those clusters larger than 99% of permuted max cluster sizes passed our test (for a detailed description see: Lenggenhager et al., 2011).

EEG Source Localization.

The sLORETA software package (Pascual-Marqui, 2002) was used for estimating the cortical neural generators for spectral modulations in each band (alpha, beta, gamma) of the EEG scalp recordings (as in Lenggenhager et al., 2011; Evans and Blanke, 2012). Neural generators were computed from scalp potentials by using the pseudo-inverse of the electrical lead field, which was derived from a head model based on the MNI152 template (Fuchs et al., 2002). EEG recordings were preprocessed in the same manner as for scalp-level analysis, using the FASTER algorithm to remove artefacts. The subject-wise cross-spectra were first calculated at every electrode for each spectral band, and an inverse transformation matrix (signal to noise regularization of 1) was applied to each cross-spectra. Statistical comparisons within a spectral band and between conditions were carried out at the voxel level using an F-ratio of the log-transformed data (type I errors were corrected as per Nichols & Holmes, 2002). We set our F-ratio threshold for significant voxels to be 1.3 ($-1.3 \geq F \geq 1.3$).

Results

Study 1- Transient Vestibular Stimulation.

Analysis of EEG responses to transient VS in healthy subjects and BVPs focused on relative changes in spectral power during the rotation period as compared to the pre-rotation baseline. This analysis revealed prominent suppression in the alpha and beta bands and enhancement in gamma band.

Alpha Band. Alpha band power was significantly suppressed in healthy subjects: time-frequency bins in the alpha band were significantly suppressed compared to pre-rotation baseline for both CW and CCW displacements (bootstrap t-test, $p<0.05$; Fig. 2*A*). This suppression (averaged across all scalp electrodes) started after rotation onset and reached maximum suppression 1054ms (CW: 1086±79ms, CCW: 1022±63ms) after rotation onset. Alpha band had the largest modulation in spectral power in healthy subjects with respect to other frequency bands when averaged within the pre-selected temporal window of interest, i.e. 650ms to 1300ms (CW=-1.96 ± 0.45dB, CCW=-2.15 ± 0.52dB (mean ± S.E.M.); Fig. 2*A*). Electrodes with the highest magnitude of alpha power suppression in the time window from 650 to 1300ms were clustered around the vertex over bi-parietal scalp regions (Fig. 2*B*).

In BVPs, alpha band power averaged across all electrodes was also significantly suppressed in time bins during rotation (bootstrap t-test, $p<0.05$; Fig. 3*A*). Alpha power suppression in BVPs started after rotation onset and reached maximum suppression 1182ms (CW: 1086±111ms, CCW: 1277±268ms) after rotation onset. Alpha power averaged over the temporal window of interest was also suppressed in BVPs (CW=-1.13±0.24dB, CCW=-1.13±0.24dB; Fig. 3*A*). Electrodes with maximal suppression during this window were not clustered in BVPs, and scattered over parietal, occipital, and frontal scalp regions (Fig. 3*B*). Although alpha band oscillations were also significantly suppressed in the patient group compared to pre-rotation baseline, the alpha suppression during the temporal window of interest was significantly smaller in the BVPs compared to healthy subjects (CW: $p=0.05$, CCW: $p=0.04$; average over all

electrodes). A running bootstrap test comparing alpha band power during rotation in healthy subjects to BVPs at every timeframe revealed that alpha power suppression was significantly greater in healthy subjects (bootstrap t-test, $p<0.05$; cluster-permutation test, $p<0.05$) from 764 ms (CW: 797ms, CCW: 732ms) to 1358ms (CW: 1502ms, CCW: 1213ms; Fig. 4*B*), and thus for a duration of 594ms (CW: 705ms, CCW: 481ms). The power density profile during the temporal window of interest showed a broader pattern of alpha power suppression extending into adjacent lower and higher frequencies as compared to healthy subjects in whom we found a distinct alpha peak (Insets of Fig. 2*A* (healthy), Fig. 3*A* (BVPs), and Fig. 4*A*(difference between healthy and BVP)).

Beta Band. Beta band power was also significantly suppressed during rotation in healthy subjects (bootstrap test, $p<0.05$; Fig. 2*A*). Beta power suppression started after rotation onset and reached maximum suppression at 910ms (CW: 1022±141ms, CCW: 797± 190ms). Healthy subject beta band power averaged across all electrodes within the temporal window of interest was suppressed with respect to baseline (CW=-0.41±0.20dB, CCW=-0.49±0.16dB). Electrodes with the largest suppression were clustered around the vertex in bi-parietal scalp regions (Fig 2*C*). The pattern of suppression we observed for the beta band was primarily at the lower end of the beta range (dark blue shading in Fig. 2*A*, close to the alpha band frequency range) and was weaker or absent in the higher beta band range.

In BVPs, time-frequency bins in the beta band (averaged across all electrodes) were also significantly suppressed during rotation (bootstrap test, $p<0.05$; Fig. 3*A*). Beta power suppression in BVPs started immediately after rotation onset and reached maximum suppression 893ms (CW:988±108ms, CCW:797±206ms; Fig. 3*A*) after rotation onset. BVP beta power during the temporal window of interest was suppressed (averaged across all electrodes: CW=-0.82±0.19dB, CCW=-0.77±0.20dB). Importantly, beta suppression in the temporal window of interest did not differ significantly from that found in healthy subjects (CW: $p=0.08$, CCW: $p=0.14$) and the BVPs scalp electrodes with maximal beta suppression in the BVPs were clustered in the same region as in

healthy subjects (bi-parietal electrodes: Figs. 2*C* and 3*C*). Comparing beta band suppression between healthy subjects and BVPs at every time point during rotation showed beta suppression was significantly greater in BVPs compared to healthy subjects near rotation onset (bootstrap t-test, $p<0.05$; cluster-based permutation test, $p<0.05$), becoming significantly different between 62ms (CW: 94ms, CCW: 29ms) to 734ms (CW: 831ms, CCW: 637ms; Fig. 4*C*), for a duration of 672ms (CW: 737ms, CCW: 608ms). Thus, a significant difference between healthy subjects and BVPs vanishes near peak velocity (Fig. 4*C*).

Gamma Band. Power in the gamma band (>30Hz) was significantly enhanced relative to baseline in both CW and CCW directions in healthy subjects (bootstrap test, $p<0.05$; Fig. 2*A*). Scalp distributions of gamma power in healthy subjects (averaged during the temporal window of interest) differed from those of the alpha and beta bands and revealed that maximal gamma enhancement was centered on fronto-polar electrodes (between the left and right lateral recti). The location of these gamma oscillations suggests that they reflect quick phases of ocular nystagmus induced by whole body rotations. The observed posterior local maxima that are apparent in the CW and CCW scalp topographies are also characteristic of microsaccadic signatures found in previous EEG studies (i.e. Yuval-Greenberg et al., 2008; Yuval-Greenberg et al., 2009). The measures that we implemented to control for ocular artifacts – visual fixation and EEG artifact removal – are unlikely to have a significant impact on very small fixational eye movements. Thus the modulation of gamma-band activity is likely to reflect residual VOR and/or microsaccades.

In BVPs, time-frequency bins in the low gamma range were significantly suppressed relative to baseline, in contrast to the enhancement found in healthy subjects (bootstrap test, $p<0.05$; Fig. 3*A*). This is consistent with the absence of vestibular driven oculomotor reflexes in these patients.

Summary – Study 1

In summary, the data from study 1 show that yaw rotation is associated with a significant suppression of alpha power over a large bi-parietal scalp region that peaks approximately 350ms after peak velocity (1000ms after rotation onset). Comparisons between healthy subjects and BVPs demonstrated that this alpha modulation lacked a clear topography in BVPs, was significantly smaller in amplitude during the temporal window of interest, and was associated with a broader power density profile. Beta suppression did not significantly differ between healthy subjects and BVPs during the temporal window of interest, peaked at a similar latency as the alpha suppression, and had the same scalp topography in both subject groups. Beta oscillations differed at rotation onset, but this effect vanished by peak stimulus velocity. Beta oscillations were also suppressed more strongly in BVPs, while having a similar distribution of scalp electrodes in both healthy subjects and BVPs. This suggests that they reflect extra-vestibular brain processes. Based on the topography and previous EEG findings (Yuval-Greenberg et al., 2008), we presume that significant gamma band enhancement in healthy subjects (and suppression in BVPs) was most likely generated by residual VOR and microsaccades (see discussion). Thus, these EEG data in healthy subjects and BVPs suggest that alpha oscillations reflect VS caused by yaw rotation (Fig. 4*A*). To further investigate the vestibular nature of alpha oscillations we next used a constant velocity rotation protocol.

Study 2- Constant Velocity Vestibular Stimulation

We next studied cortical oscillations during constant velocity rotational VS. We examined spectral modulations during the early period of rotation (the first 5 seconds of constant velocity rotation, immediately after the acceleration pulse) when the vestibular response is maximal, and compared these to two different baseline conditions: 1) the late period of rotation from 100s to 105s after constant velocity had been reached; and 2) an average during the static recording (which compares rotation to static as in the transient profile of study 1). Spectral modulations during the post-rotation period were similarly examined; we compared the first 5 seconds of rest after

rotation with the average of the static baseline condition. As with transient stimulation (study 1), constant velocity experiments were performed in both healthy subjects and BVPs.

Alpha Band. For healthy subjects, alpha band power was significantly suppressed during the early period compared to the late period for both CW and CCW rotations (Fig. 5*A*). We performed a statistical analysis over the entire sensor array, using a cluster-based permutation test to control for multiple comparisons ($p < 0.01$ electrode-wise threshold). This test identified a large cluster of electrodes exhibiting alpha suppression over fronto-parietal regions (CW: 161 electrodes; CCW: 152 electrodes; 141 electrodes in common; cluster-permutation test, $p<0.01$; Fig. 5*B*). Alpha band suppression (averaged across all electrodes: CW=-3.89±0.75dB, CCW=-3.79±0.70dB) in healthy subjects had a similar topography to that obtained in the prior group of healthy subjects subjected to transient rotations (compare Fig. 5*A* and Fig. 2*B*). Electrodes with maximal alpha suppression when comparing early and late rotation were clustered in parietal scalp regions around the vertex in healthy subjects (Fig. 5*B*). The static condition control analysis, in which no rotational stimulus was delivered, did not reveal any electrode that showed a significant difference between the same two periods. Additional analysis confirmed these findings by showing that the difference between early and late alpha suppression during rotation was significantly greater than during the static condition (CW: $p\approx0$, CCW: $p=0.01$, bootstrap t-test; Fig. 5*C*). When analyzing the effects of direction of rotation, no significant electrodes were found based on a comparison of the early periods of CW versus CCW rotation in healthy subjects. Importantly, no electrodes were found to be significantly different when comparing the late period of rotation with the static baseline indicating that alpha power returned to static levels by the end of constant velocity stimulation. These results demonstrate that alpha band suppression found during rotation in healthy subjects did not result from rotation-related artefacts.

We repeated the same analysis using the average power during the entire static, non-rotation recording, as a baseline. We compared alpha band power in the early and

late rotation periods with alpha band power during rest, and thereby matching the extra-vestibular conditions of the transient rotation protocol of study 1. Furthermore, we compared alpha power during the post-rotation period, when subjects were at rest but the vestibular response was maximal, to the same static baseline. Results for both of these cases were similar to those for the early versus late analysis in terms of cluster size, topography, and amplitude for the average across all electrodes (see Table 1).

Alpha suppression was different in BVPs than in healthy subjects. In BVPs, alpha band power was not significantly suppressed (cluster-permutation test, $p<0.01$) at any electrode when comparing early versus late rotation in each direction (average across all electrodes: CW=-1.40 ± 0.84dB, CCW=-0.48 ± 0.74dB; Fig. 6*A*). No significant clusters were found using the cluster-based permutation test even with a more liberal ($p < 0.05$) electrode-wise threshold (Fig. 6*B*). In addition, electrodes showing the largest suppression were scattered over the entire scalp for BVPs, differing from the vertex-clustered topography observed for healthy subjects (Fig. 6*A*). Moreover, early rotation versus late rotation alpha band suppression in BVPs did not differ significantly from early-static versus late-static alpha suppression during the static control condition, when no VS was given (CW: p=0.34, CCW: p=0.08) (Fig. 6*C*). Early rotation versus late rotation alpha band suppression averaged across all electrodes in the BVPs was significantly smaller than that found in healthy subjects (CW: p=0.01, CCW: $p\approx0$, bootstrap t-test; Fig. 7*A*).

We repeated the same analysis of the patient data but with the average alpha power of the static recording as a baseline. Results comparing the early rotation period and post-rotation period to the static baseline condition were similar to the early versus late analysis in BVPs in terms of cluster size, topography, and amplitude across all electrodes (see Table 1). Note that the relatively few significant electrodes identified in the CW rotation condition were distributed at the outer edges of the montage in several small clusters, as opposed to the single, large fronto-parietal clusters found in healthy subjects.

Beta Band. In healthy subjects, clusters of electrodes exhibiting significant beta suppression (CW=-1.51 ± 0.38dB, CCW=-1.09 ± 0.34dB; CW: 78 electrodes; CCW: 39 electrodes; 34 common electrodes) were found in medial fronto-parietal scalp regions (Fig. 5*E*). Electrodes with maximal suppression were clustered near the vertex in the CCW direction and distributed more frontally in the CW direction (Fig. 5*D* and 6*E*). Control analysis of the static condition found no significant electrodes when comparing beta suppression in the early static versus late static periods. Early versus late beta suppression was found to be significantly greater during rotation compared to the static condition, but only in the CW direction (CCW: p=0.15, CW: p=0.03, bootstrap t-test; Fig. 5*F*).

When the analysis was repeated for early rotation and post-rotation periods using average beta power during the static condition as a baseline, similar results were obtained in terms of cluster size, topography, and amplitude across all electrodes (see Table 1). However, electrodes with maximal beta suppression were not spatially clustered in these cases, being widely scattered over the scalp for both rotation directions.

For the BVPs, there were no significant clusters (we found 2 electrodes during CW rotation over the left temporal region that were significantly suppressed and survived the cluster-based permutation test) (Fig. 6*E*) when comparing beta power for early versus late rotation (CW=-1.83 ± 0.65dB, CCW=-1.02 ± 0.60dB) (Fig. 6*D*). Electrodes with the largest beta suppression were clustered in left-frontal regions for CCW rotation and in right-frontal regions in response to CW rotation. Early-rotation versus late-rotation beta suppression did not differ significantly from static-early versus static-late spectral power (CW: p=0.08, CCW: p=0.27, bootstrap t-test; Fig. 6*F*). There was no significant difference in early rotation versus late rotation beta band suppression between healthy subjects and BVPs (CW: p=0.32, CCW: p=0.49, bootstrap t-test; Fig. 7*B*)

Comparing the early and post-rotation periods to the average of the entire static condition in BVPs again revealed similar results to the above early versus late

comparison in terms of number of electrodes exhibiting a significant effect and mean amplitude across all electrodes (see Table 1). However, in these cases electrodes with maximal beta suppression were not clustered.

Gamma Band. There were no significant clusters found in the gamma band (one significant electrode in the BVPs that survived the cluster-based permutation test when comparing early-rotation versus late-rotation in the CCW direction). There were no significant spectral modulations in the gamma band in healthy subjects or BVPs for either direction of rotation (two tailed t-test, $p<0.01$; permutation test, $p<0.01$).

EEG Source Localization (study 2)

Our findings in study 2 reveal a prominent modulation of alpha-band oscillations in healthy subjects during passive whole body yaw rotations. To further analyze the origin of alpha suppression we localized the neural generators of these changes for each of the comparison conditions (early rotation versus late rotation, early rotation versus static and post-rotation versus static) using sLORETA at the voxel level (see Methods). This was done for healthy subjects and for BVPs. In healthy subjects, comparisons localized the generators of alpha suppression to bilateral parietal cortex, which was centered in Brodmann areas 5 and 7 and extended more posteriorly and laterally towards parieto-occipital and temporo-occipital cortex (Fig. 8; see Table 2). The negative F-ratios in these clusters correspond to alpha suppression of the test condition. Additionally, application of sLORETA revealed smaller volume (<10% of supra-threshold voxels) enhanced activation (positive F-ratios) over right fronto-temporal regions during rotation (centered in Brodmann areas 44 and 22; Fig. 8; see Table 2). This enhancement was not present for the post-rotation versus static comparison. No significant voxels were found for the BVPs, consistent with results at the scalp level.

Summary – Study 2

As with transient stimulation, the alpha band exhibited the most prominent and consistent modulation in spectral power compared to all other bands in healthy subjects. Moreover, this effect was absent in BVPs. Alpha suppression was significantly greater in healthy subjects than in the BVPs. Beta suppression was weaker and did not differ between healthy subjects and BVPs. There were no statistically significant modulations in either group in the gamma band during constant velocity stimulation.

Evoked Potential Analysis of Transient Vestibular Stimulation.

We performed two parallel analyses of the evoked potentials during transient VS, in order to compare the results obtained using different pre-processing methods. First we performed the analysis using the same preprocessing method employed in previous vestibular evoked potential studies (i.e. a remote reference in lieu of an average reference, and without removing artefacts with the FASTER algorithm; Hood and Kayan, 1985; Durrant and Furman, 1988; Elidan et al., 1991; Probst et al., 1995). We examined the evoked response at electrode Cz (vertex), as this electrode was reported to have the largest response in previous studies. The evoked response of BVPs and healthy subjects exhibited a similar time course. Both healthy subjects and BVPs exhibited the same previously reported long latency response that lasted the duration of rotation (Fig. 9*A*). We found three distinct positive evoked potential components: 1) one commencing at rotation onset and peaking between 40ms and 200ms, 2) one near peak velocity at 650ms, 3) and one at the end of rotation. Comparison with the acceleration profile (grey line in Fig. 9*A*) demonstrated that these peaks coincided with a zero-crossing, and hence direction change, of stimulus acceleration. This effect was found in both groups and in response to rotation in both directions.

We then repeated the analysis after performing additional pre-processing (average reference, artefact suppression using the FASTER algorithm; see methods), and found that the previously-observed long-latency effect was abolished (Fig. 9*B*). In healthy subjects, the evoked response consisted of an initial negative peak (CW: 100ms, CCW: 47ms), followed by a positive peak 100ms later (CW: 184ms, CCW: 166ms), and

culminating with a negative peak roughly 150ms later (CW: 301ms, CCW: 303ms). We note that as with the first preprocessing method the evoked response in BVPs again had a similar time course to that in healthy subjects. An initial negative peak (CW: 117ms, CCW: 49ms), was followed by a positive peak roughly 100ms later (CW: 201ms, CCW: 180ms), and culminating with a negative peak roughly 150ms later (CW: 328ms, CCW: 328ms). Statistical analysis comparing the healthy subject and BVP response did not reveal any extended periods of significant difference between these cohorts during rotation (bootstrap t-test, $p<0.05$ sample-wise threshold; cluster-based permutation test, $p<0.05$; 100ms temporal threshold). This differs from statistical comparisons of alpha and beta band spectral powers in study 1, which showed long duration (>500ms) significant differences when comparing healthy subject to BVP spectral power.

Earlier EEG studies of the human vestibular system were limited in that only 1 to 20 scalp electrodes were used (Hood and Kayan, 1985; Probst et al., 1995; Durrant and Furman, 1988; Elidan et al., 1991). The majority of these studies demonstrated a long latency vestibular EP, described as a dome-shaped negativity, that was reported to match the rotation profile and to persist for the duration of the stimulus (Hood and Kayan, 1985; Probst et al., 1995). Hood and Kayan (1985) used raised-cosine rotational stimuli and measured full-scalp EEG in a group of healthy subjects and BVPs and reported vestibular EP characterized by a negativity (maximal at Cz) that peaked halfway through the rotation profile (at peak velocity) for both groups. This was confirmed by Probst et al. (1995) using a similar VS protocol across different axes of rotations. The present vestibular EP analysis yielded long latency vestibular EPs consistent with those reported above when signals were referenced to the vertex, with large magnitude negative peaks in response to changes in direction of the acceleration profile. However, these components were absent when recordings were preprocessed (i.e. re-referencing to an average reference and removal of eye movement). High-density 192 electrode recordings and analysis was further improved by independent component analysis, which is part of the FASTER artefact correction method (Nolan and Whelan, 2010), to achieve this and allowed us to minimize VOR and movement related artefacts. Yet,

despite these technical improvements, potentials evoked by transient VS did not differ significantly between healthy subjects and BVPs. This indicates that the evoked potential may originate from extra-vestibular sources (such as somatosensory and/or interoceptive signals; e.g. Vaitl et al., 1997).

Discussion

Transient and constant velocity vestibular stimulation

During transient VS subjects were continuously accelerated and therefore semicircular canal afferents were continuously stimulated. This reliably evoked a change in alpha band power, which was suppressed throughout the VS relative to pre-rotation baseline. Importantly, in BVPs this alpha suppression was significantly smaller in magnitude, had no consistent topography and was more diffuse across frequencies. In healthy subjects the alpha band also exhibited the most prominent and consistent modulation in spectral power compared to all other frequency bands. The temporal evolution further linked alpha suppression to the yaw rotation profile: significant alpha suppression occurred after stimulus onset, was maximal after peak velocity, and started to return to baseline levels after rotation ended, somewhat comparable to phase shifts (Grüsser et al., 1990a) and latencies between neural responses in PIVC and VS (Chen et al., 2011).

The use of a constant velocity VS allowed us to examine whether alpha suppression with similar spectral, topographical, and functional characteristics as described for transient VS is also present for constant velocity VS. Comparing the early and late phases of rotation, and additionally the post-rotation with rest periods, allowed us to examine periods with and without vestibular activation but with identical extra-vestibular cues. This is relevant for excluding the contribution of somatosensory signals (tactile and proprioceptive signals), which are inherent to body rotations and present during transient VS, but not during constant velocity VS (we do not discuss interoceptive signals related to VS; i.e. Vaitl et al., 2002). Accordingly, we argue that the significantly stronger alpha suppression (early vs. late; early vs. rest) in healthy subjects is a correlate of cortical vestibular processing. This finding is strengthened (and extends to different constant extra-vestibular cues present during rotation; Chaudhuri et al., 2013) by analogous results we obtained during the post-rotation period (after constant velocity rotation had ended), and in which subjects were immobile but the vestibular system

was activated. Alpha suppression had the same spectral, topographical, and functional characteristics as during rotation.

Despite motion profile differences, the spectral changes were consistently limited to the alpha band and consistently localized to bilateral parieto-temporal scalp regions. Testing BVPs with the same experimental conditions provides additional arguments that the electrophysiological responses are of vestibular origin. Thus, comparisons between healthy subjects and BVPs in both motion profiles showed that alpha modulation had no consistent topography in BVPs, was absent or significantly weaker in amplitude during the temporal window of interest and associated with a broader power density profile. We adopted the same procedures as previous studies aimed at showing that BVPs have weaker or absent vestibular-evoked myogenic potentials (Watson and Colebatch, 1998) or deficits in perception and spatial cognition (Brandt et al., 2005). Our approach overcame significant technical hurdles of past electrophysiological investigations of the human vestibular system (Hood and Kayan, 1985; Probst et al., 1995; Durrant and Furman, 1988; Elidan et al., 1991). Moreover, these EEG studies were limited to only 1 to 20 scalp electrodes. Compared to previous EEG work in BVP patients, we also performed a group analysis with statistical comparisons that were lacking in previous studies (Hood and Kayan, 1985; Durrant and Furman, 1988; Elidan et al., 1991). Importantly, in our experiments spectral changes across all studies were only seen (and significantly different between healthy subjects and BVPs) in the alpha band, and not in the beta and gamma frequency ranges. Thus, during transient VS and constant velocity VS beta suppression did not significantly differ between healthy subjects and BVPs, and had the same scalp topography in both subject groups.

However, gamma activity did differ between patients and healthy subjects during transient VS suggesting that it either reflects vestibular activation or, alternatively an influence of the VOR on the EEG. Based on the scalp topography and previous EEG findings (Yuval-Greenberg et al., 2008, 2009), we argue that the observed gamma band enhancement in healthy subjects (and suppression in BVPs) was most

likely generated by the VOR and/or microsaccades, whereas this is not the case for the alpha band suppression. Controlling the VOR was central to our experimental design and preprocessing steps. First, we asked subjects to fixate in order to suppress the VOR. Second, analytically removing EOG components strongly diminished the presence of residual eye movements. Third, previous EEG studies investigating the influence and topography of eye movements on electrophysiological studies in humans (Yuval-Greenberg et al., 2008, 2009) reported gamma enhancement as a consequence of microsaccades that gave rise to the same fronto-occipital EEG topography we observed for gamma enhancement. Fourth, despite different VS profiles (and resulting VOR) for the transient and constant velocity studies, results in the alpha band were consistent across studies, whereas results in the gamma band were not. In conclusion, we argue that the spectral, amplitude, temporal, and topographical findings suggest comprehensively that the bilateral parieto-temporal alpha suppression pattern reflects activation of the thalamo-cortical vestibular system during yaw rotation, whereas the gamma band enhancement reflects residual eye movements.

Vestibular alpha

8-13 Hz alpha suppression over posterior and occipital scalp regions has been linked to visual stimulation reflecting activation of the visual thalamo-cortical system (Berger, 1929; Pfurtscheller et al., 1996; Hari et al., 1997), visual spatial attention (Sauseng et al., 2005; Romei et al., 2008), and visual discrimination (Hanslmayr et al., 2005). Prominent 8-13 Hz mu suppression over fronto-parietal scalp regions is traditionally associated with activation of the motor and somatosensory cortex (Gastaut, 1952; Niedermeyer, 2005; Pineda, 2005), and both (posterior and sensorimotor) regions have been shown to harbour vestibular representations (Kahane et al., 2003; for review: Lopez and Blanke, 2011). We argue that the present alpha suppression is a distinct pattern that reflects activation of the multisensory vestibular cortex in bilateral parieto-temporal scalp regions. The sources of this vestibular alpha suppression are in line with the parieto-temporal vestibular cortex previously identified (Lobel et al., 1998; Bense et al., 2001;

Dieterich et al., 2003; Kahane et al., 2003; Hewett et al., 2011; Lopez and Blanke, 2011). The investigation of human vestibular cortex with non-invasive approaches has proven to be technically challenging. Accordingly, high-density EEG investigations seem particularly appropriate to better understand the function, neurophysiology, and location of the human cortical responses during natural VS. Functional neuroimaging studies have used caloric and galvanic VS as well as auditory clicks and short tone bursts to activate vestibular receptors (Lopez et al., 2012; zu Eulenburg et al., 2012). A limitation of these previous approaches is that artificial methods of stimulating vestibular receptors also strongly activate other sensory systems (caloric and galvanic VS activate the tactile, thermoreceptive and nociceptive systems; clicks and short tone bursts activate auditory pathways). Without appropriate controls to exclude extra-vestibular contributions to the activations reported in these studies, it is difficult to establish the exact location and sensory processing in human vestibular cortex.

Linking vestibular processing to alpha band oscillations provides new insights into the human vestibular system and vestibular cortex. The study of cortical rhythms is particularly appropriate to investigate the vestibular cortex, which encompasses a distributed network of multisensory brain areas (Guldin and Grüsser, 1998). Although the contribution of vestibular signals to the modulation of cortical oscillations has not been studied in depth, EEG recordings during space flights (Cheron et al., 2006) revealed alpha/mu enhancement over posterior and sensorimotor scalp regions. Additionally, studies in rats showed that vestibular signals contribute to hippocampal theta oscillations (related to the animal's position in space; Russell et al., 2006; Huxter et al., 2003). Moreover, vestibular signals project to numerous thalamic nuclei and relay and process sensory signals important for cortico-cortical communication and sensorimotor processing (Alitto and Usrey, 2003; Sherman, 2005). This is compatible with the proposal that the 8–13 Hz rhythm is a major neural indicator for sensorimotor integration and "the subject's relationship to the environment" (Hari, 2006) and that it is selectively suppressed by a variety of sensorimotor and multisensory tasks (Klimesch, 1999; Muthukumaraswamy et al., 2004; Pineda, 2005; Del Percio et al., 2007; Babiloni et al.,

2008). These different functions all closely relate to primary vestibular functions such as self-motion and postural control (Angelaki and Cullen, 2008; Angelaki et al., 2009). Accordingly, we propose that alpha suppression in temporo-parietal scalp regions during yaw rotation reflects cortical processing of vestibular signals in vestibular cortex.

References

Alitto HJ, Usrey WM (2003) Corticothalamic feedback and sensory processing. Curr Opin Neurobiol 13:440–445.

Angelaki DE, Cullen KE (2008) Vestibular system: the many facets of a multimodal sense. Annu Rev Neurosci 31:125–150.

Angelaki DE, Klier EM, Snyder LH (2009) A vestibular sensation: probabilistic approaches to spatial perception. Neuron 64:448–461.

Babiloni C, Del Percio C, Iacoboni M, Infarinato F, Lizio R, Marzano N, Crespi G, Dassù F, Pirritano M, Gallamini M, Eusebi F (2008) Golf putt outcomes are predicted by sensorimotor cerebral EEG rhythms. J Physiol 586:131–139.

Bense S, Stephan T, Yousry TA, Brandt T, Dieterich M (2001) Multisensory cortical signal increases and decreases during vestibular galvanic stimulation (fMRI). J Neurophysiol 85:886–99.

Berger H (1929) Über das Elektrenkephalogramm des Menschen. Arch. Psychiatr. Nervenkr. 87:527–570.

Bertolini G, Ramat S, Laurens J, Bockisch CJ, Marti S, Straumann D, Palla A (2011) Velocity storage contribution to vestibular self-motion perception in healthy human subjects. J Neurophysiol 105:209–223.

Bottini G, Sterzi R, Paulesu E, Vallar G, Cappa SF, Erminio F, Passingham RE, Frith CD, Frackowiak RS (1994) Identification of the Central Vestibular Projections in Man: A Positron Emission Tomography Activation Study. Exp Brain Res 99: 164–69.

Brandt T, Schautzer F, Hamilton DA, Bruning R, Markowitsch HJ, Kalla R, Darlington C, Smith P, Strupp M (2005) Vestibular loss causes hippocampal atrophy and impaired spatial memory in humans. Brain 128:2732–2741.

Bremmer F, Klam F, Duhamel JR, Ben Hamed S, Graf W (2002) Visual-Vestibular Interactive Responses in the Macaque Ventral Intraparietal Area (VIP) Eur J Neurosci 16: 1569–86.

Büttner U, Waespe W (1981) Vestibular nerve activity in the alert monkey during vestibular and optokinetic nystagmus. Exp Brain Res 41:310–315.

Chaudhuri SE, Karmali F, Merfeld DM (2013) Whole body motion-detection tasks can yield much lower thresholds than direction-recognition tasks: implications for the role of vibration. J Neurophysiol 110:2764–2772.

Chen A, DeAngelis GC, Angelaki DE (2011) Representation of vestibular and visual cues to self-motion in ventral intraparietal cortex. J Neurosci 31:12036–12052.

Cheron G, Leroy A, De Saedeleer C, Bengoetxea A, Lipshits M, Cebolla A, Servais L, Dan B, Berthoz A, McIntyre J (2006) Effect of gravity on human spontaneous 10-Hz electroencephalographic oscillations during the arrest reaction. Brain Res 1121:104–116.

Del Percio C, Brancucci A, Bergami F, Marzano N, Fiore A, Di Ciolo E, Aschieri P, Lino A, Vecchio F, Iacoboni M, Gallamini M, Babiloni C, Eusebi F (2007) Cortical alpha rhythms are correlated with body sway during quiet open-eyes standing in athletes: a high-resolution EEG study. Neuroimage 36:822–829.

Dieterich M, Bense S, Lutz S, Drzezga A, Stephan T, Bartenstein P, Brandt T (2003) Dominance for vestibular cortical function in the non-dominant hemisphere. Cereb Cortex 13:994–1007.

Durrant JD, Furman JMR (1988) Long-latency rotational evoked potentials in subjects with and without bilateral vestibular loss. Electroencephalogr Clin Neurophysiol 71:251–256.

Elidan J, Leibner E, Freeman S, Sela M, Nitzan M, Sohmer H (1991) Short and middle latency vestibular evoked responses to acceleration in man. Electroencephalogr Clin Neurophysiol 80:140–145.

Evans N, Blanke O (2012) Shared electrophysiology mechanisms of body ownership and motor imagery. Neuroimage 64:216-228.

Fuchs M, Kastner J, Wagner M, Hawes S, Ebersole JS (2002) A standardized boundary element method volume conductor model. Clin Neurophysiol 113:702–712.

Gastaut H (1952) Electrocorticographic study of the reactivity of rolandic rhythm. Rev Neurol 87:176–182.

Goldberg JM, Fernandez C (1971) Physiology of peripheral neurons innervating semicircular canals of the squirrel monkey. I. Resting discharge and response to constant angular accelerations. J Neurophysiol 34:635–660.

Grüsser OJ, Pause M, Schreiter U (1990a) Localization and responses of neurones in the parieto-insular vestibular cortex of awake monkeys (Macaca fascicularis). J Physiol 430:537–557.

Grüsser OJ, Pause M, Schreiter U (1990b) Vestibular neurones in the parieto-insular cortex of monkeys (Macaca fascicularis): visual and neck receptor responses. J Physiol 430:559–583.

Gu Y, Angelaki DE, Deangelis GC (2008) Neural correlates of multisensory cue integration in macaque MSTd. Nat Neurosci 11:1201–1210.

Guldin WO, Grüsser OJ (1998) Is there a vestibular cortex? Trends Neurosci 21:254–259.

Hanslmayr S, Klimesch W, Sauseng P, Gruber W, Doppelmayr M, Freunberger R, Pecherstorfer T (2005) Visual discrimination performance is related to decreased alpha amplitude but increased phase locking. Neurosci Lett 375:64–68.

Hari R (2006) Action-perception connection and the cortical mu rhythm. Prog Brain Res 159:253–260.

Hari R, Salmelin R, Makela JP, Salenius S, Helle M (1997) Magnetoencephalographic cortical rhythms. Int J Psychophysiol 26:51–62.

Hewett R, Guye M, Gavaret M, Bartolomei F (2011) Benign temporo-parieto-occipital junction epilepsy with vestibular disturbance: an underrecognized form of epilepsy? Epilepsy Behav 21:412–416.

Hood JD, Kayan A (1985) Observations upon the evoked responses to natural vestibular stimulation. Electroencephalogr Clin Neurophysiol 62:266–276.

Huxter J, Burgess N, O'Keefe J (2003) Independent rate and temporal coding in hippocampal pyramidal cells. Nature 425:828–832.

Kahane P, Hoffmann D, Minotti L, Berthoz A (2003) Reappraisal of the human vestibular cortex by cortical electrical stimulation study. Ann Neurol 54:615–624.

Klimesch W (1999) EEG alpha and theta oscillations reflect cognitive and memory performance: a review and analysis. Brain Res Rev 29:169–195.

Lenggenhager B, Halje P, Blanke O (2011) Alpha band oscillations correlate with illusory self-location induced by virtual reality. Eur J Neurosci 33:1935–1943.

Liu S, Dickman JD, Angelaki DE (2011) Response Dynamics and Tilt versus Translation Discrimination in Parietoinsular Vestibular Cortex. Cereb Cortex 21:563–573.

Lobel E, Kleine JF, Le Bihan D, Leroy-Willig A, Berthoz A (1998) Functional MRI of galvanic vestibular stimulation. J Neurophysiol 80:2699–709.

Lopez C, Blanke O (2011) The thalamocortical vestibular system in animals and humans. Brain Res Rev 67:119–146.

Lopez C, Blanke O, Mast FW (2012) The human vestibular cortex revealed by coordinate-based activation likelihood estimation meta-analysis. Neuroscience 212:159–179.

Muthukumaraswamy SD, Johnson BW (2004) Changes in rolandic mu rhythm during observation of a precision grip. Psychophysiology 41:152–156.

Nichols TE, Holmes AP (2002) Nonparametric permutation tests for functional neuroimaging: a primer with examples. Hum Brain Mapp 15:1–25.

Niedermeyer E (2005) The normal EEG of the waking adult. In: Electroencephalography. Basic principles, clinical applications, and related fields (Fifth edition)., pp 167–192. Philadelphia: Lippincott Williams & Wilkins.

Nolan H, Whelan R, Reilly RB (2010) FASTER: Fully Automated Statistical Thresholding for EEG artifact Rejection. J Neurosci Methods 192:152–162.

Oberman LM, Hubbard EM, McCleery JP, Altschuler EL, Ramachandran VS, Pineda JA (2005) EEG evidence for mirror neuron dysfunction in autism spectrum disorders. Brain Res Cogn Brain Res 24:190–198.

Pascual-Marqui RD (2002) Standardized low-resolution brain electromagnetic tomography (sLORETA): technical details. Methods Find Exp Clin Pharmacol 24:5–12.

Pfurtscheller G, Stancak A, Neuper C (1996) Event-related synchronization (ERS) in the alpha band-an electrophysiological correlate of cortical idling: a review. Int J Psychophysiol 24:39–46.

Pineda JA (2005) The functional significance of mu rhythms: Translating "'seeing'" and "'hearing'" into "'doing.'" Brain Res Rev 50:57–68.

Probst T, Katterbach T, Wist ER (1995) Vestibularly evoked potentials (VESTEPs) of the horizonal semicircular canals under different body positions in space. J Vestib Res 5:253–263.

Prsa M, Gale S, Blanke O (2012) Self-motion leads to mandatory cue fusion across sensory modalities. J Neurophysiol 108:2282–2291 .

Romei V, Brodbeck V, Michel C, Amedi A, Pascual-Leone A, Thut G (2008) Spontaneous Fluctuations in Posterior alpha-Band EEG Activity Reflect Variability in Excitability of Human Visual Areas. Cereb Cortex 18:2010–2018.

Russell NA, Horii A, Smith PF, Darlington CL, Bilkey DK (2006) Lesions of the vestibular system disrupt hippocampal theta rhythm in the rat. J Neurophysiol 96:4–14.

Sauseng P, Klimesch W, Stadler W, Schabus M, Doppelmayr M, Hanslmayr S, Gruber WR, Birbaumer N (2005) A shift of visual spatial attention is selectively associated with human EEG alpha activity. Eur J Neurosci 22:2917–2926.

Schlindwein P, Mueller M, Bauermann T, Brandt T, Stoeter P, Dieterich M (2008) Cortical Representation of Saccular Vestibular Stimulation: VEMPs in fMRI. Neuroimage 39: 19–31.

Shinder ME, Newlands SD (2014) Sensory Convergence in the Parieto-Insular Vestibular Cortex. J Neurophysiol 111:2445–2464.

Schwarz DWF, Fredrickson JM (1971) Rhesus monkey vestibular cortex: a bimodal primary projection field. Science 172:280–281.

Sherman SM (2005) Thalamic relays and cortical functioning. Prog Brain Res 149:107–126.

Takahashi K, Gu Y, May PJ, Newlands SD, DeAngelis GC, Angelaki DE (2007) Multimodal Coding of Three-Dimensional Rotation and Translation in Area MSTd: Comparison of Visual and Vestibular Selectivity. J Neurosci 27: 9742–56.

Todd NPM, McLean A, Paillard A, Kluk K, Colebatch JG (2014a) Vestibular evoked potentials (VsEPs) of cortical origin produced by impulsive acceleration applied at the nasion. Exp Brain Res.

Todd NP, Paillard AC, Kluk K, Whittle E, Colebatch JG. (2014b) Vestibular receptors contribute to cortical auditory evoked potentials. Hear Res. Mar; 309:63-74.

Todd NP, Paillard AC, Kluk K, Whittle E, Colebatch JG. (2014c) Source analysis of short and long latency vestibular-evoked potentials (VsEPs) produced by left vs. right ear air-conducted 500 Hz tone pips. Hear Res; 312:91-102.

Vaitl D, Mittelstaedt H, Baisch F (1997) Shifts in Blood Volume Alter the Perception of Posture. Int J Psychophysiol 27: 99–105.

Vaitl D, Mittelstaedt H, Saborowski R, Stark R, Baisch F (2002) Shifts in blood volume alter the perception of posture: further evidence for somatic graviception. Int J Psychophysiol 44:1–11.

Waespe W, Henn V (1977) Brain Neuronal Activity in the Vestibular Nuclei of the Alert Monkey during Vestibular and Optokinetic Stimulation. Exp Brain Res 538:523–538.

Watson SR, Colebatch JG (1998) Vestibulocollic reflexes evoked by short-duration galvanic stimulation in man. J Physiol 513:587–597.

Yuval-Greenberg S, Tomer O, Keren AS, Nelken I, Deouell LY (2008) Transient induced gamma-band response in EEG as a manifestation of miniature saccades. Neuron 58:429–441.

Yuval-Greenberg S, Deouell LY (2009) The broadband-transient induced gamma-band response in scalp EEG reflects the execution of saccades. Brain Topogr 22:3–6.

Zu Eulenburg P, Caspers S, Roski C, Eickhoff SB (2012) Meta-Analytical Definition and Functional Connectivity of the Human Vestibular Cortex. NeuroImage 60: 162–169.

Legends.

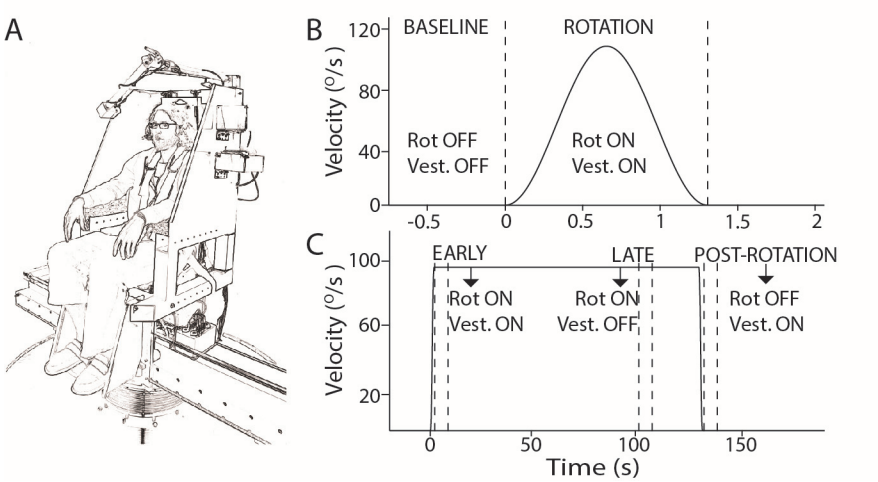

Figure 1. Velocity profiles of vestibular stimulation (VS) delivered by a centrifuge chair. ***A***, Picture of the centrifuge chair, which was housed in a lightproof and soundproof Faraday cage. ***B***, Raised-cosine velocity profile of 1.3s transient VS protocol used in study 1. Baseline and rotation periods are indicated. "Rot. ON/OFF" refers to intervals when the chair is rotating ("ON") or immobile ("OFF"), "Vest. ON/OFF" to periods when the vestibular system is actively encoding VS ("ON") or at baseline activity ("OFF"). ***C***, Velocity profile for constant velocity VS as used in study 2. "Early" and "late" periods are 5s periods when the vestibular system is activated by the rotational stimulus (early) and when it has habituated and returned to baseline levels (late). "Post-rotation" is the first 5s after the rotational stimulus has ended, when rotation is off but the vestibular system is actively encoding the deceleration.

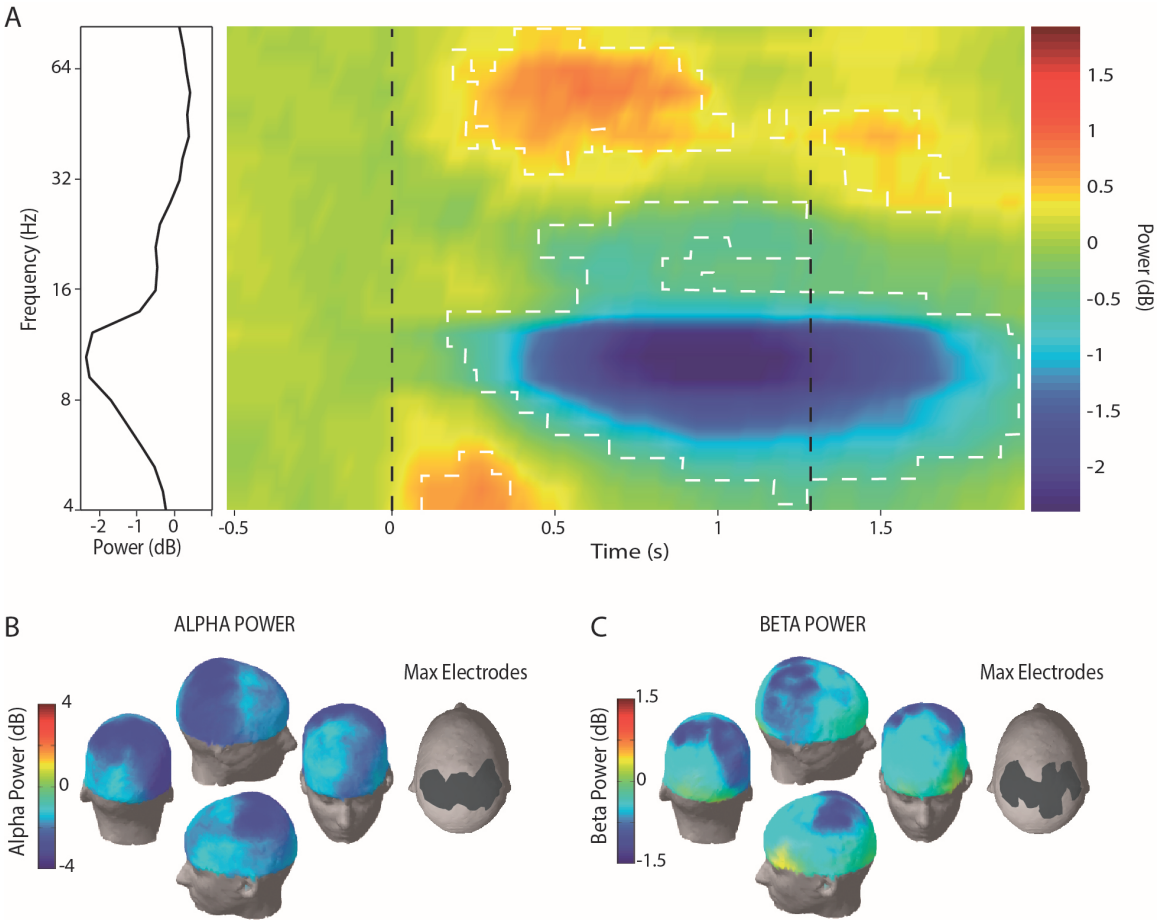

Figure 2. Spectral analysis of healthy subjects during transient VS. *A*, Time-frequency plot for the -0.5 to 2s period relative to counterclockwise rotation onset. Distinct clusters of significant modulation (bootstrap test, $p<0.05$; white dotted contours) of the averaged response (all subjects and 192 electrodes) were found spanning each frequency band of interest; the most prominent spectral suppression (dark blue shading) was in the alpha and beta bands. Inset shows average spectral power across all frequencies (from 650ms after rotation onset until the end of rotation; see methods for further detail). Rotation onset and offset are indicated with black dotted lines. Spectral power at each frequency bin was first normalized to pre-rotation (-0.5 to -0.1s) levels. ***B***, Scalp map (192 electrodes) comparing average alpha band power during the temporal window of interest. Blue represents spectral suppression, red spectral enhancement. The topography of the ten electrodes with the maximal effect (shaded region on scalp map, max electrodes) are also shown. ***C***, Scalp map comparing average beta band power during the temporal window of interest and corresponding topography of maximum effect.

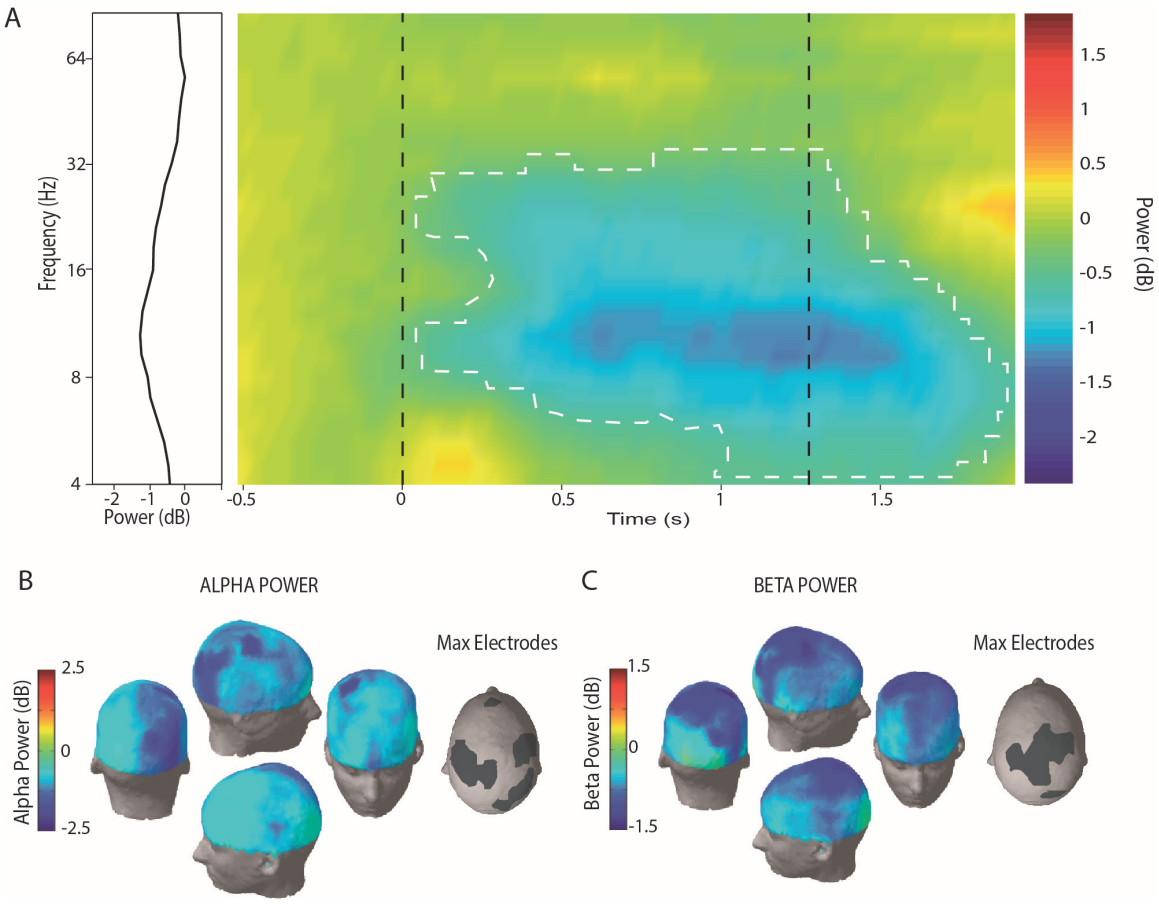

Figure 3. Spectral analysis of bilateral vestibular patients (BVPs) during transient VS. ***A***, Time-frequency plot for the -0.5 to 2s period relative to counterclockwise rotation onset. One large cluster of suppression (bootstrap test, $p<0.05$; white dotted contour) of the averaged response (all BVPs and 192 electrodes) was found spanning the alpha and beta bands. Inset shows average spectral power during the temporal window of interest. Scalp maps of all 192 electrodes and topography of electrodes with maximal effect for ***B,*** alpha band power and ***C***, beta band power during the temporal window of interest are also shown.

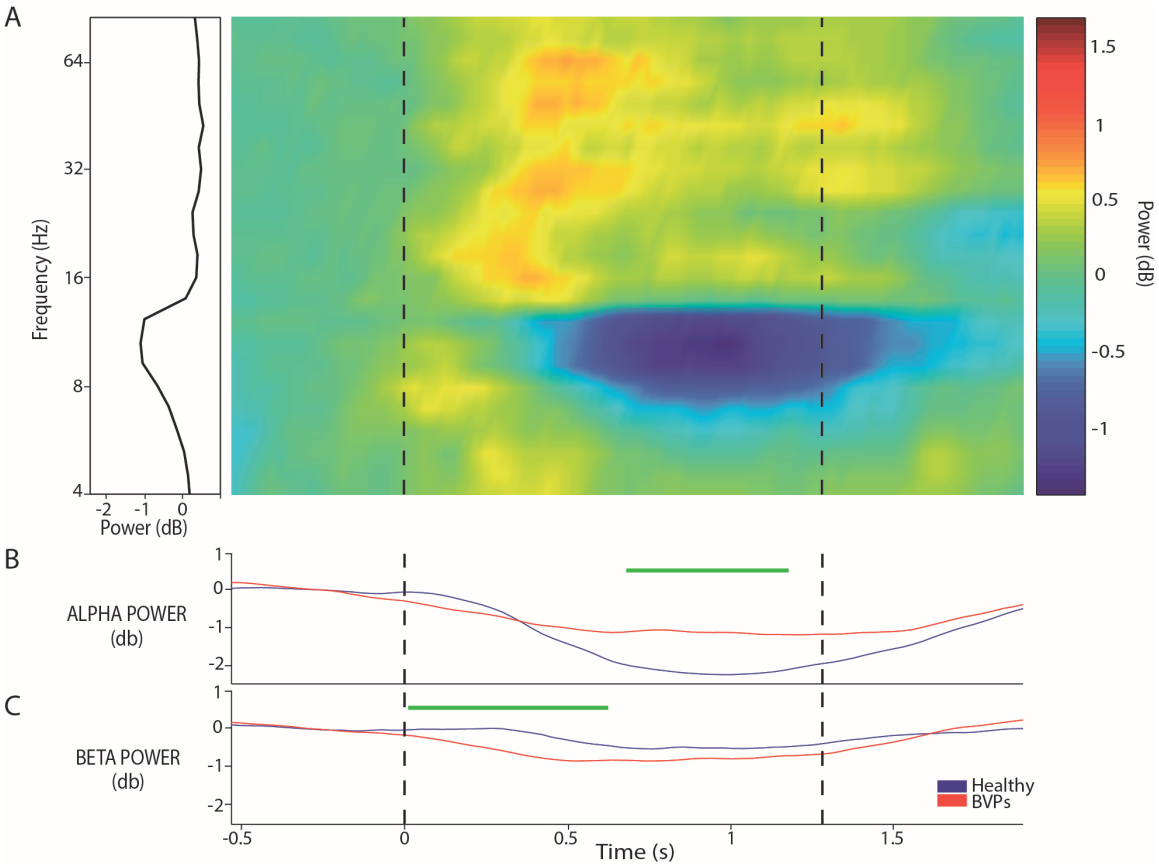

Figure 4. Spectral power difference between healthy subjects and BVPs during transient VS. *A.* Difference plot between healthy subject and BVP spectral power. Time-frequency bins in which spectral power in healthy subjects is more suppressed than BVPs are shaded in blue. Red/yellow shading indicates spectral power is more suppressed than BVPs in that time-frequency bin. Note prominent alpha suppression. ***B***, Alpha band suppression during transient VS in healthy subjects (blue line) and BVPs (red line). Green ticks indicate significantly different time-points between healthy subjects and BVPs (bootstrap test, $p<0.05$; cluster-permutation test, $p<0.05$). ***C***, The same plot for the beta band.

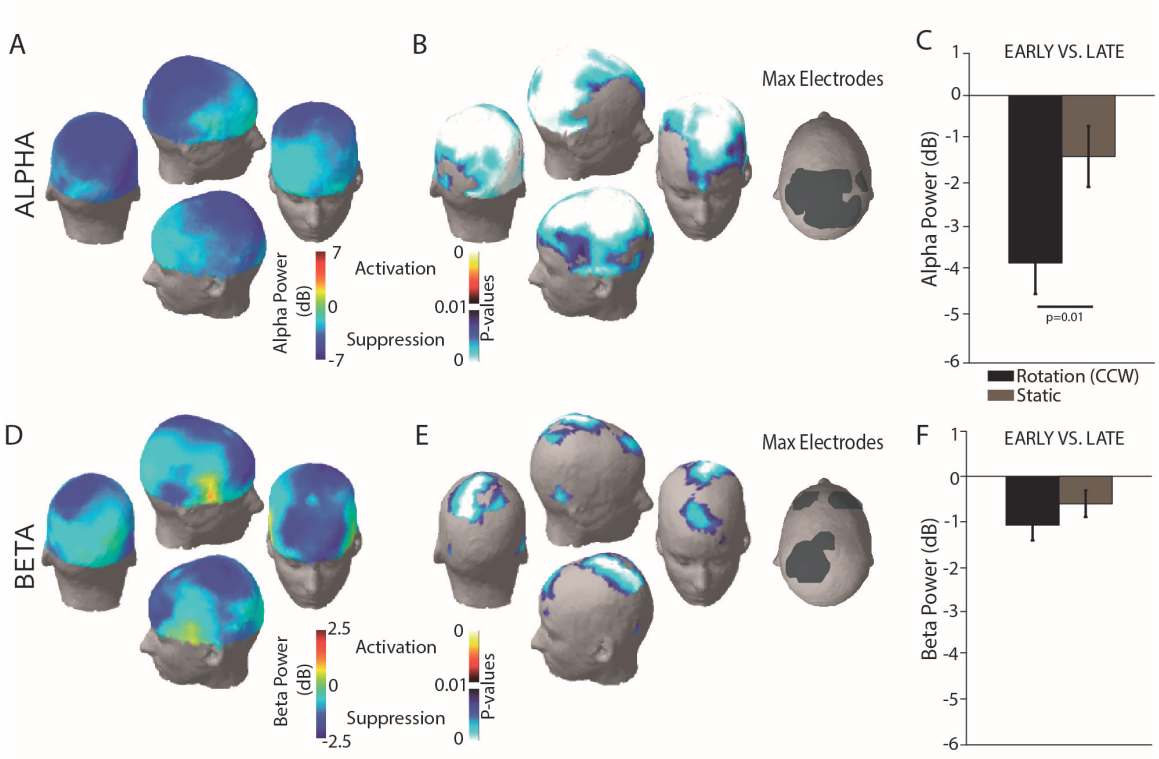

Figure 5. Spectral analysis of healthy subjects during constant velocity VS. *A*, Scalp map of early (first 5s of constant velocity rotation) alpha band power compared to late (5s period commencing 100s later) in response to counterclockwise rotation. Alpha band suppression predominates in posterior scalp regions (blue shading corresponds to spectral suppression). ***B***, Scalp map of p-values showing significant electrodes when comparing early and late alpha band power (two tailed t-test, $p<0.01$; permutation test, $p<0.01$). Shaded regions represent significant differences (blue/white: suppression; red/black: enhancement), un-shaded grey regions electrodes with a p-value>0.01. Topography of max electrodes is also shown. ***C***, Early alpha band power normalized to late period for counterclockwise rotation (black bar) and static baseline (grey bar)(mean ± S.E.M.) for the average of all electrodes. Early alpha band power was significantly suppressed compared to late power during yaw rotation but not for two similar periods during static baseline condition. Suppression during rotation was significantly greater than modulation during the static case (two tailed t-test, $p=0.01$). ***D***, ***E***, ***F*** Same analysis as described for ***A***, ***B***, ***C*** but for the beta band.

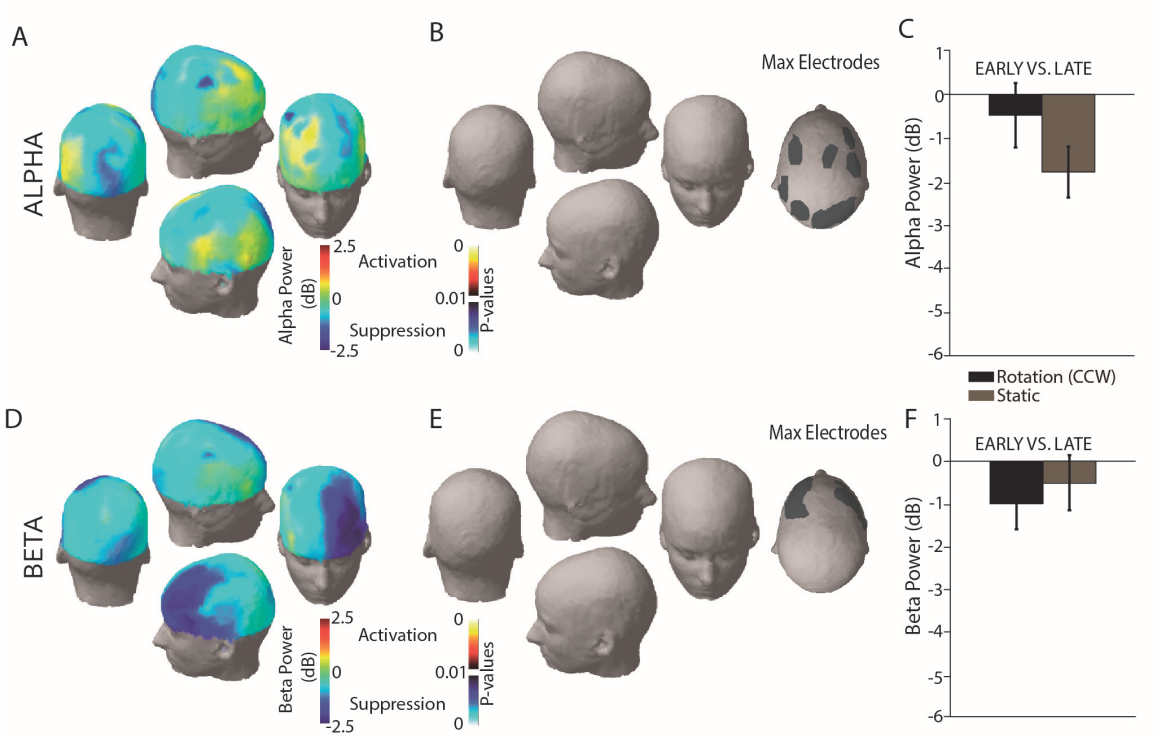

Figure 6. Spectral analysis of BVPs during constant velocity VS. ***A***, Scalp map of early alpha band power compared to late in response to counterclockwise rotation only showed weak alpha band suppression without clear topography. ***B***, Scalp map of p-values showed no significant electrodes when comparing early and late alpha band power as done for healthy subjects. Topography of electrodes with strongest response were not clustered. ***C***, Early alpha band power normalized to late period for counterclockwise rotation (black bar) and static baseline (grey bar) for the average of all electrodes. ***D***, ***E***, ***F*** Same analysis as described for ***A***, ***B***, ***C*** but for the beta band. There were no significant modulations in the alpha or beta bands for the BVPs.

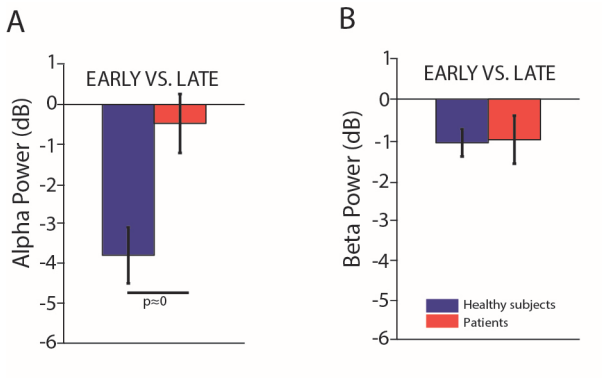

Figure 7. Comparison of spectral modulations between healthy subjects and BVPs in response to constant velocity rotation. ***A***, Early vs. late alpha power during counterclockwise rotation is significantly lower in healthy subjects (blue bar) than in BVPs (red bar). ***B***, The same analysis as in ***A***, but for the beta band. Beta band power in healthy subjects was not statistically different from BVPs.

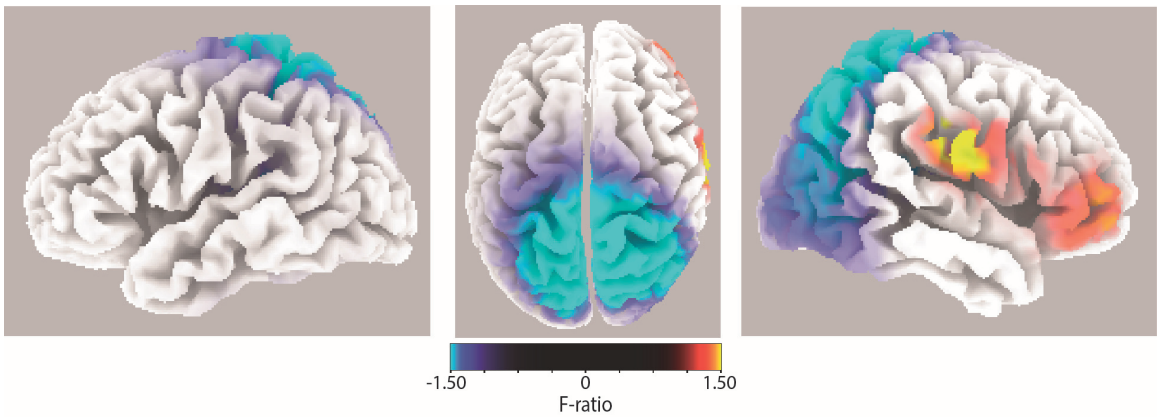

Figure 8. Neural generators of vestibular alpha suppression during constant velocity VS. Linear inverse solution of early versus late alpha band power during counterclockwise rotation in healthy subjects. Voxels are shown in blue for suppression, and red for enhancement.

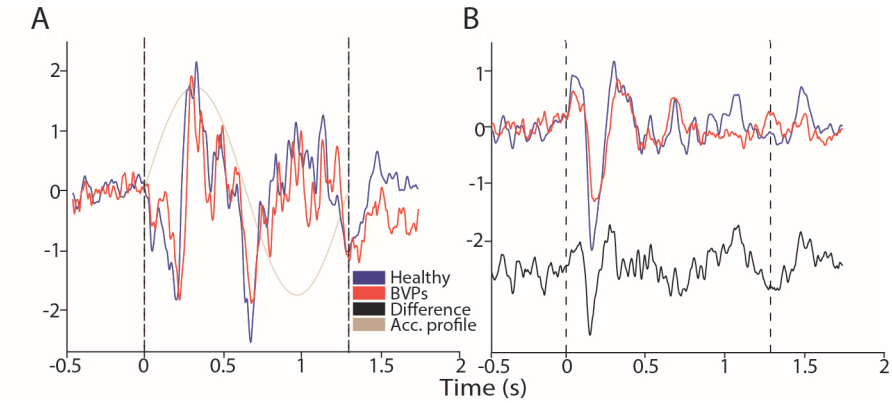

Figure 9. Evoked potentials by transient VS. *A*, Grand average of evoked potentials for healthy subjects (blue trace) and BVPs (red trace) using the same preprocessing regime as previous studies (see results for references). Note that the evoked potentials recorded for healthy subjects and BVPs do not differ. Grey line is the acceleration profile. ***B***, Grand average of evoked potentials after recordings were re-referenced to an average reference and artefact removal using FASTER. Black trace is the difference between healthy subjects and BVPs.

			Healthy		BVPs		Healthy vs. BVP (p-value)	
			CW	CCW	CW	CCW	CW	CCW
Alpha	Early vs. Late	Cluster Size	161	152	0	0		
		Common	141		0			
		Spectral Power	-3.89±0.75	-3.79±0.70	-1.40±0.84	-0.48±0.74	0.01	0
	Early vs. Static	Cluster Size	136	141	26	0		
		Common	125		0			
		Spectral Power	-3.38±0.65	-3.68±0.70	-1.92±0.56	-0.76±0.56	0.02	0
	Post vs. Static	Cluster Size	155	61	24	0		
		Common	60		0			
		Spectral Power	-3.29±0.64	-2.46±0.75	-1.37±0.42	-1.20±0.45	0	0.07
Beta	Early vs. Late	Cluster Size	78	39	2	0		
		Common	34		0			
		Spectral Power	-1.51±0.38	-1.09±0.34	-1.83±0.65	-1.02±0.60	0.32	0.49
	Early vs. Static	Cluster Size	31	48	15	0		
		Common	27		0			
		Spectral Power	-1.35±0.43	-0.94±0.31	-1.36±0.44	-0.91±0.29	0.48	0.46
	Post vs. Static	Cluster Size	39	16	0	0		
		Common	14		0			
		Spectral Power	-1.02±0.36	-0.72±0.37	0.54±0.37	-0.11±0.54	0.2	0.16

Table 1. Results for EEG analysis during constant velocity VS. Results for all groups (healthy subjects and BVPs), directions (CW and CCW), and experimental comparisons for the alpha and beta bands for study 2. Cluster size refers to the size of cluster that survived our cluster-permutation test ($p<0.01$), common refers to the number of electrodes that were significant in both directions, and spectral power the average spectral power in dB for that comparison averaged over all 192 electrodes. P-value is the result of the bootstrap test comparing spectral power between healthy subjects and BVPs.

		Suppression					Enhancement			
		X	**Y**	**Z**	**Brodmann**		**X**	**Y**	**Z**	**Brodmann**
Early vs. Late	**CW**	7	-36	49	5		NA			
	CCW	8	-51	39	31		57	15	15	44
Early vs. Static	**CW**	4	-41	52	5		62	2	5	22
	CCW	4	-43	49	5		58	11	15	44
Post vs. Static	**CW**	9	-54	44	7		NA			
	CCW	23	-47	69	5					

Table 2. Supra-threshold voxel clusters from inverse solution of constant velocity VS conditions. Geographic centers (MNI coordinates) of supra-threshold voxels ($-1.3 \geq F \geq 1.3$) for clusters in each comparison made in study 2. Suppression refers to a lower spectral power in the test case versus baseline, enhancement a higher spectral power in the test case.

3.2

Paper II – Temporal dynamics of cortical oscillations under natural vestibular stimulation.

Temporal dynamics of cortical oscillations under natural vestibular stimulation.

Steven Gale[1,2], Aaron Schurger[1,2], Olaf Blanke[1,2,3]

[1] Center for Neuroprosthetics, École Polytechnique Fédérale de Lausanne, Switzerland

[2] Laboratory of Cognitive Neuroscience, Brain-Mind Institute, École Polytechnique Fédérale de Lausanne, Switzerland

[3] Department of Neurology, University Hospital Geneva, Switzerland

Abstract

The vestibular system encodes movements and orientation of the head in space, and contributes to a wide array of reflexes, as well as sensorimotor and perceptual processes, used throughout our daily lives to process physical motion. However due to technical and physiological barriers, knowledge of the neural correlates of natural vestibular stimuli lags that of the other senses. Recently, studies using electroencephalography (EEG) have shown that cortical oscillations in the alpha band reliably encode passive whole body yaw rotations. Does this supposed cortical marker of vestibular activity share properties with subcortical neurons or the vestibulo-ocular reflex (VOR) at the cortical level? Specifically, does the magnitude of alpha band suppression during constant velocity vestibular stimulation (CVVS) change as velocity is increased? Does it decay exponentially after acceleration/deceleration as the VOR does? If so, is the time constant of this decay physiologically relevant? Here, we measured EEG and VOR in human subjects during CVVS at four different velocities (30º/s, 60º/s, 90º/s, and 120º/s) to see if alpha band oscillations had the same temporal properties as the VOR during CVVS. We found that initial alpha band suppression responded differently than the VOR which increases its magnitude to match an increasing rotation velocity. Importantly, alpha band oscillations decayed exponentially with a similar time constant as the VOR. Oscillations in the beta band were less prominent and gamma band oscillations reflected residual VOR artefacts and microsaccades. These findings open new avenues to understand how natural vestibular stimuli are processed in the cortex.

Introduction

Fundamental work on the brain mechanisms of the vestibular system, and in particular the neural responses to natural vestibular stimuli, has been carried out in non-human primates (Fernandez and Goldberg, 1971; Waespe and Henn, 1977; Guldin and Grüsser, 1998; Gu et al., 2008; Chen et al., 2010). Despite these major insights into the primate vestibular system, the neural mechanisms in humans, especially at the cortical level, remain elusive. Although it is likely that at least some of the identified cortical areas in non-human primates are analogous to those described in humans (Lopez et al., 2011), several methodological and biological factors make such a direct comparison difficult.

Few studies have used electroencephalography (EEG) on human subjects to record cortical activity during natural vestibular stimulation (VS), mainly in the form of evoked potentials in response to short passive whole-body rotations (Hood and Kayan, 1985; Durrant and Furman, 1988; Probst et al., 1995) or high-intensity movements of the head (Elidan et al., 1991; Todd et al., 2014). However it has been difficult to control for artefacts caused by VS such as reflexive eye-movements from the vestibulo-ocular reflex (VOR), and movements of the electrodes/cap relative to the skull (see Gale et al., submitted). Gale et al. (submitted) analyzed cortical oscillations in response to both transient and constant-velocity vestibular stimulation (CVVS) and found suppression of spectral power in the alpha band (8-13Hz) to reliably encode VS in healthy subjects, but not in patients with bilateral vestibular loss.

If spectral power in the alpha band does encode VS, are other features of vestibular processing also present at the cortical level? Exponential decay of vestibular activity in response to CVVS has been demonstrated sub-cortically in the firing rates of neurons in the primate vestibular nerve (Fernandez and Goldberg, 1971; Büttner and Waespe, 1981) and vestibular nuclei (Waespe and Henn, 1977). Importantly, these same temporal dynamics are also present in the slow phase velocity of VOR and perception of rotation in humans, opening a window onto subcortical vestibular activity not otherwise available in human vestibular research (Cohen et al., 1981; Okada et al., 1999; Bertolini et al., 2011). Do oscillations in the alpha band also follow an exponential decay from their initial suppression, and if so how does this temporal evolution compare to that of the VOR? Furthermore, do changes in angular velocity modulate the magnitude of alpha band suppression as the VOR does to

compensate for head movements of different velocities (Bertolini et al., 2011)? Is the time constant of alpha decay fixed and independent of velocity?

Here, we recorded 64-channel EEG while subjects underwent passive whole-body yaw CVVS at four different velocities. We analyzed changes in cortical oscillations at each velocity and compared them to the VOR to see if: 1) the magnitude of initial alpha suppression is modulated by velocity as is the case for the VOR, 2) the time course of alpha suppression is exponential and in the physiological range of the VOR, and 3) if this time course is modulated by velocity.

Methods

Participants.

Data were recorded in 2 separate sessions (one EEG session and one VOR session) from a total of 18 healthy subjects (4 subjects took part both sessions). Sessions were balanced by size and gender (11 subjects with 4 females per session), as well as age (session 1: 23.7±2.69 years, session 2: 25.3±2.94 years). There was a minimum of 8 months between the two recording sessions to control for effects of habituation to the CVVS for subjects that took part in both sessions (Clément et al., 2008). Both studies were approved by the local ethics council and performed in accordance with the Declaration of Helsinki.

Experimental Setup.

Vestibular stimulation was delivered by a cockpit-style centrifuge chair (rotator) centered on the yaw axis (Fig. 1A). The position of the rotator was digitally servo-controlled (PCI-7532) at a rate of 100Hz with a margin of error of ±0.1º.

Subjects' movements were restrained via a 5-point racing harness and foot straps. The subject's head was restrained using a chinrest and forehead fixation. The rotator was inside of a light- and sound-proof Faraday cage. White noise was administered through headphones in order to mask any auditory cues during rotation. Residual light and airflow cues were masked by wrapping the cockpit with a dark blanket. During the EEG session, subjects were instructed to fixate on an LED fixed to the rotator in order to suppress the VOR. An infrared camera monitored subjects during the experiment.

Experimental Procedures.

We investigated the cortical response to different magnitudes of constant velocity vestibular stimulation (CVVS). EEG was recorded (see below) while participants were given 4 rotational stimuli at each of 4 angular velocities (30º/s, 60º/s, 90º/s, and 120º/s for a total of 16 trials) in the counter-clockwise (CCW) direction. The rotation profile was identical for each velocity: a 30s baseline period in which the chair was static was followed by a 1s acceleration pulse, followed by 100s of rotation at constant angular velocity. Subjects were then decelerated to rest (1s deceleration pulse) and recorded for a further 100s during the post-rotation period (Fig. 1B). All

analysis took place during post-rotation to control for any extra-vestibular cues that could be present during rotation. Subjects were instructed to remain immobile and fixate on an LED during EEG recordings in order to reduce the effects of the VOR. During the second session, the fixation LED was removed and the VOR in response to the same vestibular stimuli was recorded.

EEG Recordings.

EEG recordings were performed using a 64-channel system with pre-amplified electrodes (BioSemi Inc., Amsterdam, Netherlands). Recordings were originally sampled at 2048 Hz and referenced to an active electrode pair at the vertex of the skull. Recordings were then downsampled to 512 Hz and re-referenced to the average over all electrodes for offline analysis. Four electro-oculagram (EOG) electrodes (one above and below the right eye, and one each near the left and right lateral canthi) were used to record eye movements.

EEG Data Analysis.

Preprocessing. Natural rotational CVVS will induce a compensatory VOR in healthy subjects. We therefore used the FASTER algorithm (Nolan and Whelan, 2010) to remove eye-movements detected in the EOG signal from the EEG recordings prior to analysis (see: Gale et al., submitted). FASTER was also used to remove and linearly interpolate bad channels.

Power Spectrum Analysis. During CVVS, neurons in the vestibular nuclei respond to the initial acceleration pulse, but encode velocity, and then return to baseline firing rates following an exponential decay at a time constant of ~10-30s (Fernandez and Goldberg, 1971; Waespe and Henn, 1977). Similarly, firing rates in these neurons encode the deceleration from constant velocity to rest following the same time constant. We therefore compared spectral power in the first 2 seconds of the post-rotation period (the “early” period in fig. 1B) when vestibular activity was maximal but the subject was immobile, to the last 2 seconds of the post-rotation period (the “late” period in fig. 1B) when vestibular activity had returned to baseline levels. We also examined the temporal dynamics of spectral power during the entire post-rotation period to see if they followed the classical vestibular temporal dynamics outlined above, and whether this effect was specifically correlated with power in the alpha

band as recently demonstrated (Gale et al., submitted). Analysis was performed on the average of spectral power in different frequency bands (i.e. alpha: 8 to 13Hz, beta: 13 to 30 Hz, and gamma: 30 to 100 Hz), and at discrete frequencies.

After preprocessing, spectrograms (time series of power spectral densities, or PSDs) were calculated for each channel and trial using a custom program written in Matlab (Matlab, Mathworks, Natick, Massachusetts, USA). A 500ms Hanning window with a 250ms time step was used to calculate the PSD at 47 logarithmically scaled frequencies from 4 to 100Hz. To reduce noise the spectrogram for each trial was then baseline corrected via the single-trial normalization method (Grandchamp and Delorme, 2011), i.e. dividing each time-frequency bin in the PSD by the mean over time of the entire trial (including the pre-rotation baseline) at every frequency. Trials were then averaged and normalized by the pre-rotation baseline. The resulting PSDs were converted to decibels to increase their normality (Oberman et al., 2005). We refer to this normalized, log-transformed measure of the PSD as the log-power ratio (LPR).

EEG Statistical Analysis.

The LPRs for the test (early) and baseline (late) conditions were statistically compared using a two-tailed t-test at each electrode (electrode-wise threshold $p<0.01$). A cluster-based permutation test was used to control for multiple comparisons (Lenggenhager et al., 2011). For each comparison, the labels on the data from half of the subjects were randomly permuted and another t-test was performed on this permuted data set. The cluster sizes of contiguous significant electrodes were stored. This process was repeated for every way of selecting half of our subjects. Only clusters of electrodes of the non-permuted dataset larger than 99% of the permuted cluster sizes from the permuted set were deemed to be significant.

A one-way repeated measure ANOVA was used to test for main effects of velocity on early LPRs and early slow-phase velocity of the VOR, as well as the time constants of exponential fits.

Furthermore, a bootstrap test was used to compare the LPR in each frequency band between conditions and experiments. To this end N subjects were chosen, with replacement, from the complete set of N subjects and the LPR was computed on this subset of subjects. This process was repeated 999 times. The p-value for this test

was the percentage of iterations where the test metric was either greater or less than the corresponding comparison metric. This procedure was repeated for analysis of time constants from exponential fits to both EEG and VOR data. Bootstrap standard errors were calculated by creating first creating a bootstrap distribution following the same procedures as described above. The standard error was the standard deviation calculated over this distribution.

VOR Recordings and Preprocessing.

The VOR during CVVS was recorded with an EyeLink 1000 (SR Research Ltd., Mississauga, Ontario, Canada) mounted directly on the rotator and controlled via an Ethernet link and custom coded program written in Python. The EyeLink system was positioned between 50 and 60 cm in from the right eye at an angle of 10 to 45 degrees below eye level. Eye position data were sampled at 1000 Hz and then converted to velocity. The quick-phase of the VOR was removed by a custom program in Matlab leaving only the slow phase for data analysis.

Exponential Fit Procedure.

Both the slow-phase velocity and perception of rotation follow the same temporal dynamics (an exponential decay with a time constant in the range of 10-30s) as the activity of vestibular-nuclei neurons in response to CVVS (Okada et al., 1999; Bertolini et al., 2011). We therefore fit an exponential function to the magnitude of the slow-phase velocity of the VOR or the LPR at a specific frequency or frequency band over the course of an entire trial to see if its time constant followed the same dynamics as vestibular nuclei neurons. The equation used was:

$$Y = ae^{bx}$$

where x is time and a and b are constants. The time constant of decay is therefore the absolute value of 1/b. The fit was exponentially weighted with a time constant of 30s to ensure time-points during epochs of high vestibular activity were accurately fit. We subtracted the average LPR over the last 15s before fitting in order to align our traces and account for any spectral drift. We used the r-squared statistic to test the quality of each fit. An r-squared threshold of 0.1 was used; fits with an r-squared value below this threshold were not included in analysis.

Results

Early and Late LPRs.

To examine the broadband spectral response to CVVS, the spectrogram of the grand average across all velocities, subjects, and electrodes was first studied. Qualitative examination of the grand average spectrogram (Fig. 2A) showed that power in the alpha band exhibited the most prominent modulation. This LPR suppression was maximal immediately after deceleration to rest and decreased in magnitude over time. LPR suppression was also present in the beta band, with a similar in rate of decay, but smaller in magnitude. Gamma-band LPRs had a smaller-magnitude suppression that was constant throughout rotation, differing from the time-decaying responses seen at lower frequencies.

Alpha Band (8-13Hz). Topographical analysis of LPRs comparing the early period of post-rotation to the pre-rotation baseline showed a large, scalp-wide suppression in the alpha band at each velocity. The strongest suppression was found at occipito-parietal electrodes and medial-frontal areas (Fig. 2B; Table 1). Large clusters of significant electrodes at each velocity were found in occipital, parietal, and frontal areas (cluster-based permutation test, $P<0.01$; Fig. 2C; Table 1).

Statistical analysis revealed an effect of velocity on the magnitude of early alpha band LPR (main effect of velocity; $F_{(3,10)}=3.985$; $P=0.02$; one-way ANOVA; Fig. 3A). Post-hoc comparisons of early alpha LPRs showed that spectral suppression in response to 120º/s CVVS was significantly greater than that for 30º/s (bootstrap test, $P=0.05$) and 90º/s (bootstrap test, $P=0.05$), but not different between any other velocity ($P>0.12$).

Late alpha band LPRs did not significantly differ from the pre-rotation baseline.

Beta Band (13-30Hz). Early period beta band LPRs were also suppressed compared to pre-rotation. However, this suppression was less pronounced than in the alpha band (Fig. 2A). Significant clusters of electrodes were found over occipital electrodes in response to CVVS at 30º/s and 120º/s. A sparse cluster of significant electrodes was observed in response to 60º/s CVVS; no electrodes significantly differed during early 90º/s CVVS (Table 1). Statistical analysis did not reveal an effect of velocity on the early period LPR ($F_{(3,10)}=0.828$; $P=0.49$; one-way ANOVA).

For the late- versus pre-rotation comparison no electrodes were significantly different (cluster-based permutation test, P>0.01).

Gamma Band (30-100Hz). No electrodes during the early or late periods significantly differed from baseline (cluster-permutation test, P>0.01). However, early gamma response had two scalp regions with positive LPR, which indicated an increase in spectral power compared to baseline. These occurred over the eyes, and near the vertex, which are consistent with gamma topographies corresponding to microsaccades (Yuval-Greenberg et al., 2008; 2009), and previously linked with VOR (Gale et al., submitted). Late power showed a similar topography.

Early VOR. The early slow-phase velocity of the VOR (i.e. the average of the first 2 seconds of slow-phase VOR velocity, identical to the epoch selected for early LPR) was significantly increased with increasing stimulus velocity (Fig. 3B). Statistical analysis revealed an effect of velocity on the magnitude of slow-phase VOR (main effect of velocity; $F_{(3,10)}$=144.5; P<0.0001; one-way ANOVA). Post-hoc comparisons of early VOR between each velocity of CVVS were significantly different (P<0.0001, bootstrap test), and increased in magnitude as CVVS velocity was increased.

Frequency Response of Early and Late LPR. We calculated early and late LPR at each discrete frequency to better elucidate the frequency response of each (Figs. 5A and 5B). Early LPR had a clear peak within the alpha range (8-13Hz), and this peak increased in magnitude with increasing velocity (Fig. 5A). A second smaller peak was found in the low beta range. Higher frequencies had no salient phenomena. Late power had no obvious tuning with respect to frequency (Fig. 5B).

Temporal Dynamics of LPR.

We fit an exponential function to the LPR for each frequency band in response to CVVS at each velocity. Fits to the alpha band had the highest quality and most physiologically realistic parameters compared to beta and gamma bands. The same fitting procedure was repeated on the VOR at the single trial level and compared with the LPR in each band. The temporal dynamics of alpha LPR decay were statistically identical to that of the VOR.

Alpha Band. Grand average (over all electrodes and subjects) alpha band LPR at each velocity decayed exponentially from initial suppression; model fits were of supra-threshold quality (r-squared>0.1) and time constants within the physiologically pre-determined range (10-30s see refs above; Fig. 4A; Table 2).

Fits were repeated on single-subject data (i.e. the average LPR for each subject at each velocity) and entered into a one-way repeated measures ANOVA in order to test for an effect of velocity on the time constant of alpha LPR decay. No significant effect of velocity was found ($F_{(2,10)}$=0.146; P=0.87; Fig. 3C). Note that rotations at 30º/s were excluded from this per-subject analysis as more than half of the subjects had r-squared values below threshold with time constants outside of the physiological range, indicating a poor fit due to a low signal-to-noise ratio at the single-subject level.

Beta Band. Average beta band LPR at each velocity also decayed exponentially, with r-squared and time-constant values both within our pre-determined physiological ranges (Fig. 4B; Table 2). However, more than half of subjects had r-squared values below our threshold at velocities slower than 120º/s and therefore an ANOVA could not be performed for beta band LPRs at the single-subject level.

Gamma Band. Gamma band LPRs did not rise or decay exponentially, as both the grand average and the per-subject averages were equally well fit by an exponential function or by a line (Fig. 4; Table 2).

VOR. Fits to single-trials of slow-phase velocity of the VOR during CVVS were calculated by following the same fitting procedure as performed on LPRs (Table 2; Fig. 4D). Statistical analysis of extracted per-subject time constants revealed a significant effect of velocity ($F_{(3,10)}$=3.69; P=0.02; Fig. 3D). Post-hoc statistical comparisons showed that the time constant of VOR decay in response to 120º/s CVVS was significantly less than that for 30º/s (bootstrap test, P=0.002) and 60º/s (bootstrap test, P=0.01; Fig. 3D), but not different between any other velocity (P>0.06). Importantly, comparisons between alpha LPR and VOR time-constants were not significantly different in response to VS at 30º/s, 60º/s, and 90º/s (bootstrap test, P>0.18).

Frequency Response of Exponential Fits. The same analysis performed on the average over different frequency bands of LPR was repeated at each discrete frequency (all subjects, channels, and trials). Fit quality peaked for each velocity in the alpha range (Fig. 5C), and decreased rapidly to below threshold within the beta range. Gamma could not be fit to an exponential. Bootstrapped standard errors of LPR time constants were lowest in the alpha range, quickly rising to values greater than 25s, indicating variability was stable inside of alpha and not in other bands (Fig. 5D). We note that 30º/s was excluded from this figure because variability was high in all frequency ranges, indicating a higher signal-to-noise ratio than found in other subjects..

Discussion

Spectral Response to CVVS

Here we have shown that spectral power in the alpha band reliably encodes CVVS. Analysis of the early period of post rotation, when the vestibular response was maximal, revealed that alpha band LPR had the largest magnitude response and largest cluster size of electrodes significantly different from baseline compared to all other frequency bands. This effect was most prominent at occipito-parietal electrodes, extending frontally along the midline. We note that the post-rotation period and pre-rotation baseline are identical in terms of extra-vestibular cues, which effectively controlled for any confounds related to movement. The magnitude of alpha LPR suppression was maximal in response to 120º/s CVVS, and was significantly smaller at slower velocities, but not between other velocities. The magnitude of alpha LPR as a function of velocity of CVVS did not parallel that of the VOR, whose early slow-phase velocity was significantly increased with CVVS velocity. There was no significant alpha LPR suppression during the late period of post-rotation, when vestibular activity had returned to baseline levels, anywhere in the sensor array. Beta band LPR was also significantly suppressed in the early period, but this effect was smaller in magnitude and found at fewer electrodes than for the alpha band. Scalp topographies in the gamma band were indicative of residual VOR and microsaccades as shown previously (Yuval-Greenberg, 2008; 2009). A more continuous spectral analysis, repeated at each recorded frequency without averaging into bands, confirmed these findings as early power clearly peaked within the alpha range of frequencies, and returned to baseline levels outside of this range (Fig. 5A).

Exponential Decay of Alpha Band LPR

LPRs in the alpha band decayed from initial suppression exponentially with the same range of time constants previously found in vestibular nuclei neurons (Waespe and Henn, 1977), perception of rotation, and VOR slow phase velocity (Cohen et al., 1981; Okada et al., 1999; Bertolini et al., 2011). The quality of these fits clearly peaked in the alpha band, and decreased rapidly outside of it (Fig. 5C and 5D); LPRs in the beta range had a lower r-squared, decaying to sub-threshold quality. Gamma band LPR could not be fit to an exponential. Importantly, the time constant of alpha-band LPR decay was not statistically different from the VOR measured with

the same experimental protocols at each velocity. This finding precludes the possibility that alpha suppression was due to the stopping of motion; the VOR is driven by the vestibular system. Finally, LPR time constants converged in the alpha range for all velocities, and quickly diverged outside of physiologically relevant levels at higher frequencies.

Neural Correlate of Vestibular Processing

The similarity of the temporal dynamics of alpha band LPR and the VOR suggests that they may be driven by the same sub-cortical mechanisms. Further work needs to be done to better understand the nature of this vestibular signal in the cortex. Specifically, as signals from vestibular afferents are integrated with other sensory information at the level of the first synapse in the brainstem and cerebellum (Angelaki and Cullen, 2008), what aspect of vestibular processing is this signal encoding in the cortex? Alpha band oscillations have been shown to vary in response to a wide array of sensorimotor, cognitive, and multisensory tasks (Pfurtscheller et al., 1996; Klimesch, 1999; Muthukumaraswamy et al., 2004; Pineda, 2005; Del Percio et al., 2007; Babiloni et al., 2008). Evidence from human behavioural studies suggests that visual and vestibular cues are fused at the perceptual level (Prsa et al., 2012). Indeed, the multisensory and distributed nature of both the vestibular representation and alpha band oscillations in the cortex makes understanding the exact function of alpha LPR suppression challenging.

What is the utility of an EEG correlate of vestibular stimulation? Strong evidence of a connection between alpha LPR in occipito-parietal cortical regions opens up new avenues for studying how cognitive factors and sensory processing are affected by vestibular stimuli, and how this type of processing impacts vestibular encoding in the brain, and particularly in the cortex where the loci and/or networks involved in vestibular processing remain elusive. For example, how is this signal changed when a visual stimulus is present during rotation, and does this affect the magnitude of alpha LPR suppression or the time-constant of spectral or VOR decay? Can visual stimulation during rotation be used to examine the neural correlates of optimal visuo-vestibular integration in humans, similar to work done in non-human primates (Waespe and Henn, 1977)? Can this signal be changed by adaptation, expectation,

or mental imagery? Does this signal encode a higher level sensation of rotation? And if so, under what conditions would alpha LPR and the VOR respond differently to CVVS? This newly established signal can thus serve as a tool for addressing these questions and better understanding cortical sensory processing in general.

References

Angelaki DE, Cullen KE (2008) Vestibular system: the many facets of a multimodal sense. Annu Rev Neurosci 31:125–150.

Babiloni C, Del Percio C, Iacoboni M, Infarinato F, Lizio R, Marzano N, Crespi G, Dassù F, Pirritano M, Gallamini M, Eusebi F (2008) Golf putt outcomes are predicted by sensorimotor cerebral EEG rhythms. J Physiol 586:131–139.

Bertolini G, Ramat S, Laurens J, Bockisch CJ, Marti S, Straumann D, Palla a (2011) Velocity storage contribution to vestibular self-motion perception in healthy human subjects. J Neurophysiol 105:209–223

Büttner U, Waespe W (1981) Vestibular nerv activity in the alert monkey during vestiublar and optokinetic nystagmus. Exp Brain Res:310–315.

Chen A, DeAngelis GC, Angelaki DE (2010) Macaque parieto-insular vestibular cortex: responses to self-motion and optic flow. J Neurosci 30:3022–3042

Clément G, Tilikete C, Courjon J-H (2008) Retention of habituation of vestibulo-ocular reflex and sensation of rotation in humans. Exp Brain Res 190:307–315

Cohen B, Henn V, Raphan T, Dennett D (1981) Visual-Vestibular Interactions in Humans. Annals New York Academy of Sciences. New York 00157:421–433.

Del Percio C, Brancucci A, Bergami F, Marzano N, Fiore A, Di Ciolo E, Aschieri P, Lino A, Vecchio F, Iacoboni M, Gallamini M, Babiloni C, Eusebi F (2007) Cortical alpha rhythms are correlated with body sway during quiet open-eyes standing in athletes: a high-resolution EEG study. Neuroimage 36:822–829.

Durrant JD, J.M.R. Furman (1988) Long-latency rotational evoked potentials in subjects with and without bilateral vestibular loss. Electroencephalogr Clin Neurophysiol:251–256.

Elidan J, Leibner E, Freeman S, Sela M, Nitzan M, Sohmer H (1991) Short and middle latency vestibular evoked responses to acceleration in man. Electroencephalogr Clin Neurophysiol 80:140–145.

Fernandez C, Goldberg JM (1971) Physiology of peripheral neurons innervating semicircular canals of the squirrel monkey. I. Resting discharge and response to constant angular accelerations. J Neurophysiol 34:635–660

Gale S, Prsa M, Schurger A, Gay A, Paillard A, Herbelin B, Guyot JP, Lopez C, Blanke O (submitted) Oscillatory neural responses evoked by natural vestibular stimuli in humans.

Gastaut H (1952) Electrocortographic study of the reactivity of rolandic rhythm. Rev Neurol 2:176–182.

Gu Y, Angelaki DE, Deangelis GC (2008) Neural correlates of multisensory cue integration in macaque MSTd. Nat Neurosci 11:1201–1210.

Guldin WO, Grusser O-J (1998) Is there a vestibular cortex? Trends Neurosci 21:254–259.

Hood JD, Kayan A (1985) Observations upon the evoked responses to natural vestibular stimulation. Electroencephalogr Clin Neurophysiol 62:266–276.

Klimesch W (1999) EEG alpha and theta oscillations reflect cognitive and memory performance: a review and analysis. Brain Res Rev 29:169–195.

Lenggenhager B, Halje P, Blanke O (2011) Alpha band oscillations correlate with illusory self-location induced by virtual reality. Eur J Neurosci 33:1935–1943

Lopez C, Blanke O (2011) The thalamocortical vestibular system in animals and humans. Brain Res Rev:119–146.

Lopez C, Blanke O, Mast FW (2012) The human vestibular cortex revealed by coordinate-based activation likelihood estimation meta-analysis. Neuroscience 212:159–179

Muthukumaraswamy SD, Johnson BW (2004) Changes in rolandic mu rhythm during observation of a precision grip. Psychophysiology 41:152–156.

Nolan H, Whelan R, Reilly RB (2010) FASTER : Fully Automated Statistical Thresholding for EEG artifact Rejection. J Neurosci Methods 192:152–162

Oberman LM, Hubbard EM, McCleery JP, Altschuler EL, Ramachandran VS, Pineda J a (2005) EEG evidence for mirror neuron dysfunction in autism spectrum disorders. Brain Res Cogn Brain Res 24:190–198

Okada T, Grunfeld E, Shallo-Hoffmann J, Bronstein a M (1999) Vestibular perception of angular velocity in normal subjects and in patients with congenital nystagmus. Brain 122 7:1293–1303

Pfurtscheller G, Stancak A, Neuper C (1996) Event-related synchronization (ERS) in the alpha band-an electrophysiological correlate of cortical idling: a review. Int J Psychophysiol 24:39–46.

Pineda JA (2005) The functional significance of mu rhythms: Translating “‘seeing’” and “‘hearing’” into “‘doing.’” Brain Res Rev 50:57–68.

Prsa M, Gale S, Blanke O (2012) Self-motion leads to mandatory cue fusion across sensory modalities. J Neurophysiol 108:2282–2291.

Probst T, Katterbach T, Wist ER (1995) Vestibularly evoked potentials (VESTEPs) of the horizonal semicircular canals under different body positions in space. J Vestib Res 5:253–263.

Waespe W, Henn V (1977) Brain Neuronal Activity in the Vestibular Nuclei of the Alert Monkey during Vestibular and Optokinetic Stimulation *. Exp Brain Res 538:523–538.

Yuval-Greenberg S, Deouell LY (2009) The broadband-transient induced gamma-band response in scalp EEG reflects the execution of saccades. Brain Topogr 22:3–6

Yuval-Greenberg S, Tomer O, Keren AS, Nelken I, Deouell LY (2008) Transient induced gamma-band response in EEG as a manifestation of miniature saccades. Neuron 58:429–441

Legends

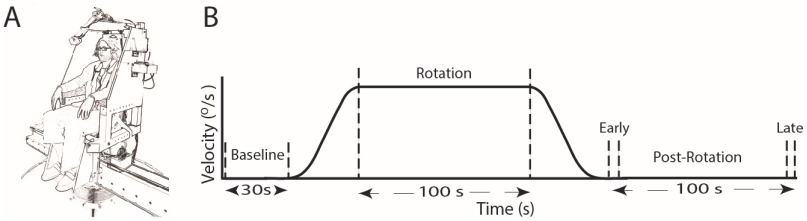

Figure 1. Rotator and velocity profile of CVVS. ***A*****,** Picture of the rotator platform that delivered the CVVS. ***B*****,** Velocity profile of CVVS. Subjects were rotated for a total of 100s at four different constant velocities. An equally long post-rotation period was analyzed, with the first 2 seconds labelled as “early”, and the last 2 “seconds as late.

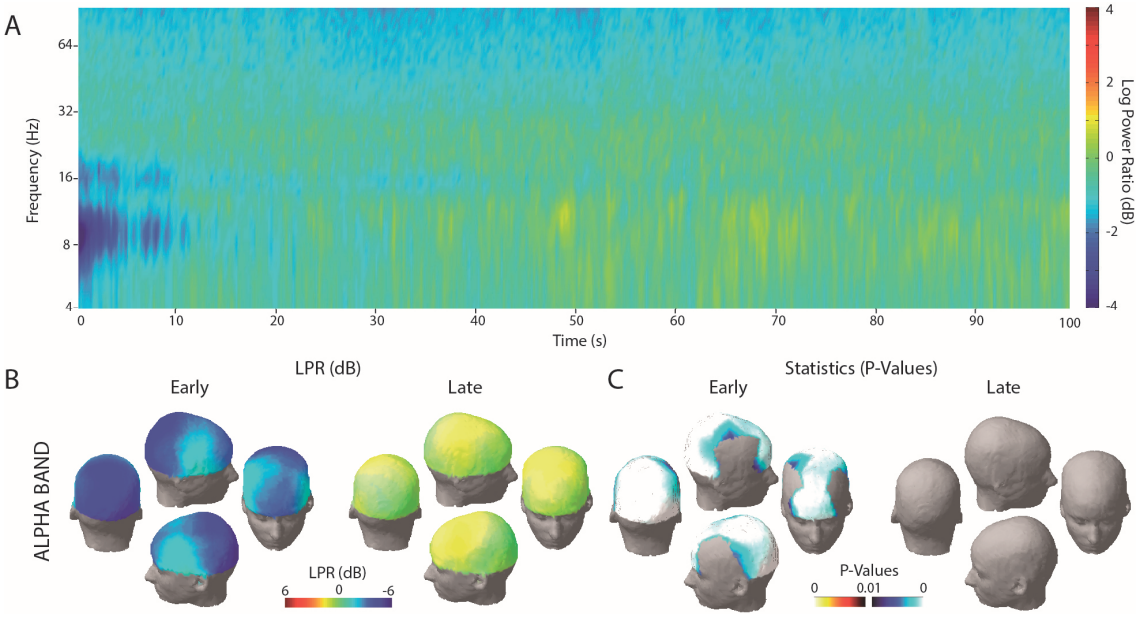

Figure 2. Spectral response to constant velocity vestibular stimulation. ***A,*** Grand average spectrogram of post-rotation LPR. Blue values denote negative LPRs, which correspond to spectral suppression compared to baseline, and red values positive LPRs, which correspond to enhanced spectral activity with respect to baseline. Note the logarithmic scale for frequency. ***B,*** Scalp map of alpha band early and late LPR (left and right, respectively). ***C,*** Corresponding statistical maps for early (left) and late (right) LPR showing significant clusters of electrodes with respect to the pre-rotation baseline.

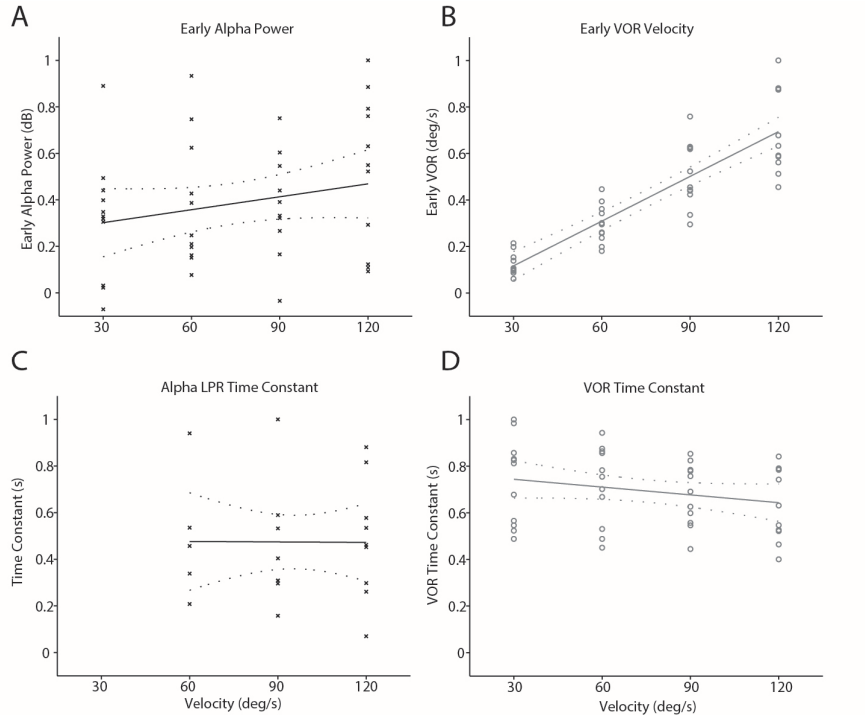

Figure 3. Subject averages for alpha LPRs and VOR. ***A***, Early alpha band power (LPR average over the first 2 seconds of the post-rotation period) for each subject and velocity. ***B***, Early slow-phase velocity of the VOR averaged over the same period as for alpha LPR. ***C***, Time constant of exponential fit on alpha LPR, and ***D***, VOR. Data shown is the average per subject (NOTE: alpha LPR time constants for fits in response to 30º/s were not included as more than half of individual subjects could not be fit with an exponential). For all panels, the line of best fit (solid line) and corresponding 95% confidence intervals are shown.

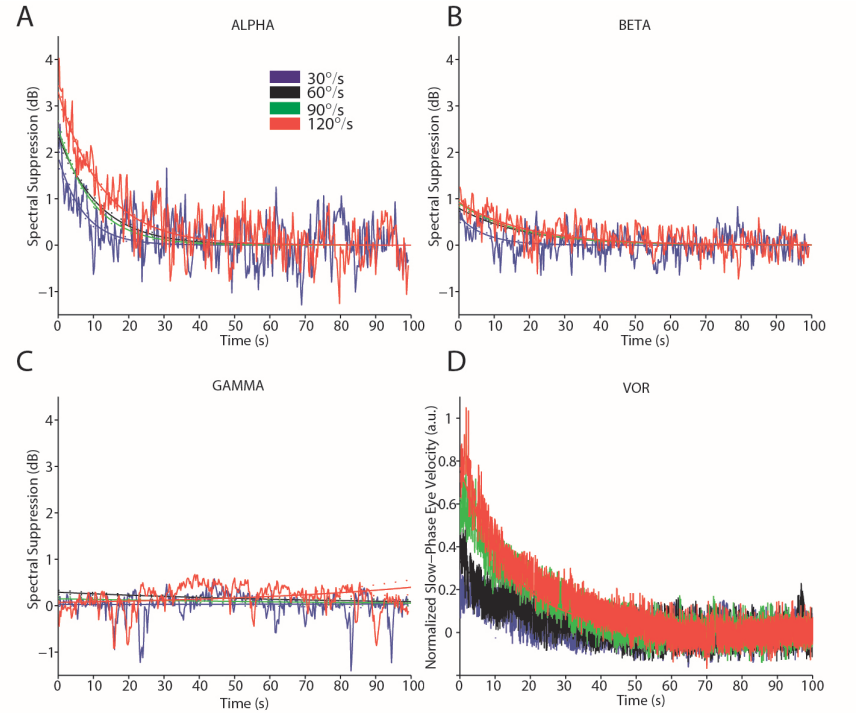

Figure 4. Temporal dynamics of LPRs during post-rotation. Spectral suppression at each velocity (30º/s: blue, 60º/s: black, 90º/s: green, 120º/s: red) and band (***A***, alpha; ***B*** beta; ***C***, gamma) during the post-rotation period. Solid lines are the exponential fit, dotted lines the 95% confidence interval of each fit. For clarity, only raw data for 30º/s and 120º/s are shown. ***D***, Fits on representative traces and exponential fits on single-trial VOR data for one subject.

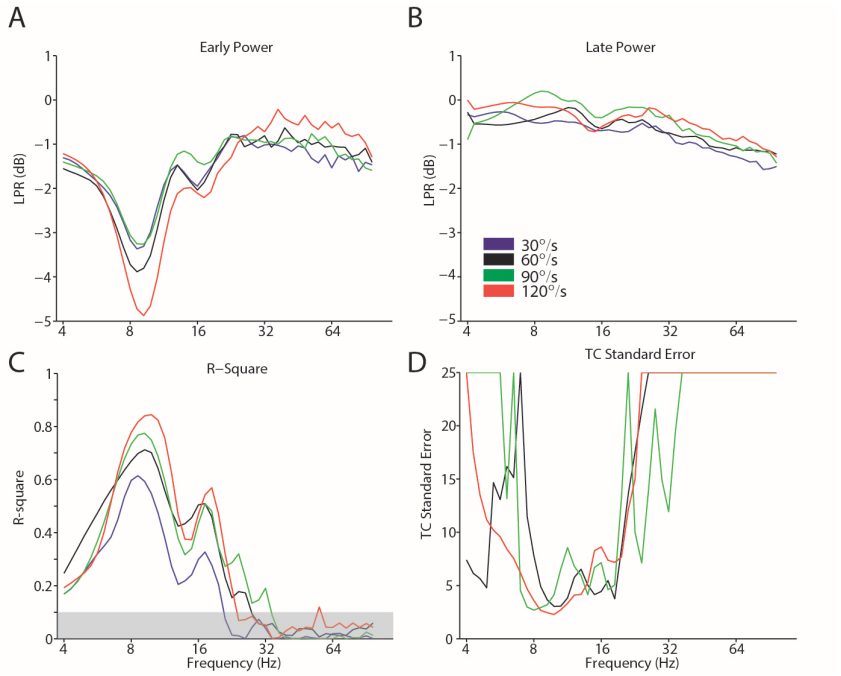

Figure 5. Frequency tuning of LPR and exponential fit. Early (***A***) and late (***B***) period LPRs at each frequency for each velocity. R-squared (***C***) and the standard error of time constants for LPR data (***D***) of exponential fits of the average (over all trials, electrodes, and subjects) LPR at each velocity. The grey bar in C represents our self-imposed r-squared threshold. (NOTE: 30º/s was omitted from panel D due to high variability between subjects).

		30˚/s	60˚/s	90˚/s	120˚/s
Early Alpha	**Cluster Size**	35	42	35	49
	LPR (dB)	-1.96±0.47	-2.33±0.49	-1.98±0.50	-3.22±0.58
Early Beta	**Cluster Size**	21	8	0	25
	LPR (dB)	-0.68±0.18	-0.69±0.22	-0.51±0.25	-0.85±0.15
Early Gamma	**Cluster Size**	0	3	0	0
	LPR (dB)	-0.62±0.37	-0.36±0.19	-0.46±0.41	-0.03±0.22

Table 1. Significant cluster sizes and LPR magnitude by velocity in response to CVVS. Significant electrode cluster sizes (cluster-permutation test, P>0.01) and LPR magnitude for the early period of post-rotation for alpha, beta, and gamma LPR. LPRs are reported as mean ± SEM.

		30˚/s	60˚/s	90˚/s	120˚/s
Alpha	**TC (s)**	7.22	11.43	9.75	12.64
	RSQ	0.51	0.7	0.73	0.83
Beta	**TC (s)**	7.62	18.45	17.5	19.22
	RSQ	0.29	0.54	0.56	0.52
Gamma	**TC (s)**	NA	NA	NA	NA
	RSQ	0	0.06	0.01	0.07

Table 2. Time constants and R-squared values for exponential fits. Time constants and R-squared values for fits on average LPRs by band and velocity of CVVS. All times are in seconds, NA means a fit was below quality threshold and therefore no time constant was recorded.

3.3

Paper III – Self-motion leads to mandatory cue fusion across sensory modalities.

First published July 25, 2012; doi:10.1152/jn.00439.2012.

Self-motion leads to mandatory cue fusion across sensory modalities

Mario Prsa,[1,2] Steven Gale,[1,2] and Olaf Blanke[1,2,3]

[1]*Laboratory of Cognitive Neuroscience, Brain Mind Institute, Ecole Polytechnique Fédérale de Lausanne, Lausanne, Switzerland;* [2]*Center for Neuroprosthetics, Ecole Polytechnique Fédérale de Lausanne, Lausanne, Switzerland; and* [3]*Department of Neurology, University Hospital Geneva, Geneva, Switzerland*

Submitted 25 May 2012; accepted in final form 20 July 2012

Prsa M, Gale S, Blanke O. Self-motion leads to mandatory cue fusion across sensory modalities. *J Neurophysiol* 108: 2282–2291, 2012. First published July 25, 2012; doi:10.1152/jn.00439.2012.— When perceiving properties of the world, we effortlessly combine multiple sensory cues into optimal estimates. Estimates derived from the individual cues are generally retained once the multisensory estimate is produced and discarded only if the cues stem from the same sensory modality (i.e., mandatory fusion). Does multisensory integration differ in that respect when the object of perception is one's own body, rather than an external variable? We quantified how humans combine visual and vestibular information for perceiving own-body rotations and specifically tested whether such idiothetic cues are subjected to mandatory fusion. Participants made extensive size comparisons between successive whole body rotations using only visual, only vestibular, and both senses together. Probabilistic descriptions of the subjects' perceptual estimates were compared with a Bayes-optimal integration model. Similarity between model predictions and experimental data echoed a statistically optimal mechanism of multisensory integration. Most importantly, size discrimination data for rotations composed of both stimuli was best accounted for by a model in which only the bimodal estimator is accessible for perceptual judgments as opposed to an independent or additive use of all three estimators (visual, vestibular, and bimodal). Indeed, subjects' thresholds for detecting two multisensory rotations as different from one another were, in pertinent cases, larger than those measured using either single-cue estimate alone. Rotations different in terms of the individual visual and vestibular inputs but quasi-identical in terms of the integrated bimodal estimate became perceptual metamers. This reveals an exceptional case of mandatory fusion of cues stemming from two different sensory modalities.

mandatory fusion; metamers; multisensory integration; self-motion; vestibular

SENSORY CUES either within (Hillis et al. 2004; Knill and Saunder 2003) or across senses (Alais and Burr 2004; Butler et al. 2010; Ernst and Banks 2002; Fetsch et al. 2009; Gu et al. 2008; Mendonca et al. 2011; van Beers et al. 1996, 1999) are often combined to produce the final percept according to statistical optimality. Until recently, this framework has been exclusively tested in situations where the object of perception is external to the body of the observer. However, the observer's body is also a multisensory object subjected to perceptual processes (Ionta et al. 2011). This is particularly apparent in passive whole body displacements that are perceived using mainly vision and the vestibular organs (Butler et al. 2010; Buttner and Henn 1981; Fetsch et al. 2009; Gu et al. 2008; Young et al. 1973). The associated cues are said to be idiothetic in nature because they are derived from the observer's own displacements. Does the brain process and integrate two idiothetic signals differently from two externally generated signals? For example, an observer can simultaneously and independently use vision and audition to estimate the position of two different objects. In other words, sensory cues making the same physical measurement are often attributed to different causes and are not integrated (Koerding et al. 2007; Parise et al. 2012; Shams and Beierholm 2010). It seems that such dissociations cannot be made in the case of idiothetic cues in most ecological conditions. Visual and vestibular information relevant for perceiving self-motion are necessarily redundant and therefore always integrated. Optic flow incongruent with vestibular input does indeed arise but is in such cases caused by constituents of the visual surrounding that are not world-stationary. These visual cues are not idiothetic; they are attributed to external objects and thus most likely vetoed when estimating self-motion. Even in the presence of eye movements, optic flow information corresponding to the actual motion of the body is extracted to guarantee perceptual stability (Haarmeier et al. 1997, 2001; Royden et al. 1992). Because, for the purpose of estimating self-motion, visuovestibular integration involves sensory cues providing two ecologically nondissociable signals, its neural underpinnings must in some respect differ from those underlying nonidiothetic cue integration.

Extending recent work in heading perception involving linear translation stimuli (Butler et al. 2010; Fetsch et al. 2009; Gu et al. 2008) as well as theoretical models of the optimal use of vestibular signals in general (Laurens and Droulez 2007; MacNeilage et al. 2007; Zupan et al. 2002), we first show that the statistically optimal model of multisensory integration also applies to visual and vestibular cues when perceiving passive self-rotation. Crucially, we subsequently test whether the associated cues are subjected to mandatory fusion. Mandatory fusion entails that once integrated to produce a more reliable bisensory percept, perceptual access to unisensory estimates is lost and has been claimed not to occur across different sensory modalities (Hillis et al. 2002). However, we demonstrate that cross-modal mandatory fusion can ensue from idiothetic sensory input. When that situation arises, different cue combinations can theoretically give rise to the same fused percept, since they would differ only in terms of information that is lost. For example, a perceived rotation size S borne out by a whole body rotation of size $S + \Delta$ paired with an equally reliable visual cue simulating a rotation of size $S - \Delta$ can be indistinguishable from a true rotation size S produced by both stimuli. Such physically different but perceptually indistinguishable stimuli have been called metamers (Richards 1979) and can be compared to lights of the same color but different spectral compo-

Address for reprint requests and other correspondence: M. Prsa, Laboratory of Cognitive Neuroscience, Brain-Mind Institute, Ecole Polytechnique Fédérale de Lausanne, Station 19, AI 2101, 1015 Lausanne, Switzerland (e-mail: mario.prsa@mail.mcgill.ca).

sition. We argue that cues providing two ecologically nondissociable signals about own-body displacements account for this phenomenon.

MATERIALS AND METHODS

The optimal observer model. Based on how probable perceiving an own-body rotation of a certain size is given the visual and vestibular stimuli individually, the multisensory estimate can be predicted from probability theory. To this end, we describe each perceptual estimate in the form of a probability distribution (likelihood). The likelihood provides a probabilistic measure of the estimate: its most likely value and the uncertainty associated with this value. Bayesian statistics then formalize the optimal strategy for combining likelihoods arising from multiple sensory cues (and prior beliefs) to form the a posteriori estimate, the end result of the perceptual process. We describe an optimal observer model, show how it predicts both the variance and the mean of the posterior when human subjects integrate visual and vestibular cues for perceiving whole body rotations, and finally describe within the same framework how to test whether a mandatory fusion of the two cues occurs.

When the body is passively rotated around its yaw axis, both the visual and vestibular senses provide independent information (I_{vi} and I_{ve}) about the rotatory stimulus S. Probabilistic descriptions of the subjects' ensuing perception of rotation $\hat{S}$ can be derived from visual and vestibular cues only [i.e., the likelihoods $P(I_{vi}|S)$ and $P(I_{ve}|S)$] and from the bimodal pairing [i.e., the posterior $P(S|I_{vi}, I_{ve})$]. Each distribution recounts how likely it is to perceive any given rotation size. The value corresponding to the peak of the distribution is the most likely estimate, and its standard deviation captures how uncertain/reliable the estimate is (small values indicate low uncertainty and high reliability) (Fig. 1).

Maximum likelihood estimation (MLE), derived from Bayes' rule (Landy et al. 1995; Yuille and Bulthoff 1996), predicts that the optimal way for the brain to combine sensory cues will result in the posterior distribution being a normalized product of the visual and vestibular likelihoods

$$P(S|I_{vi}, I_{ve}) \propto P(I_{vi}|S)P(I_{ve}|S) \quad (1)$$

given the assumed Gaussian distributions are produced by independent sources of visual and vestibular noise. The predicted variance of $\hat{S}_p$, the value of S that maximizes $P(S|I_{vi}, I_{ve})$, is then

$$\sigma_p^2 = \frac{\sigma_{vi}^2 \sigma_{ve}^2}{\sigma_{vi}^2 + \sigma_{ve}^2}, \quad (2)$$

where σ_{vi}^2 and σ_{ve}^2 are the variances of rotation estimates that maximize $P(S|I_{vi})$ and $P(S|I_{ve})$, respectively. $P(S|I_{vi})$ and $P(S|I_{ve})$ are the single-cue posteriors and are equal to the respective likelihoods under the assumption that all sensory signals are equally likely to occur. The maximum a posteriori estimate (value corresponding to the peak of

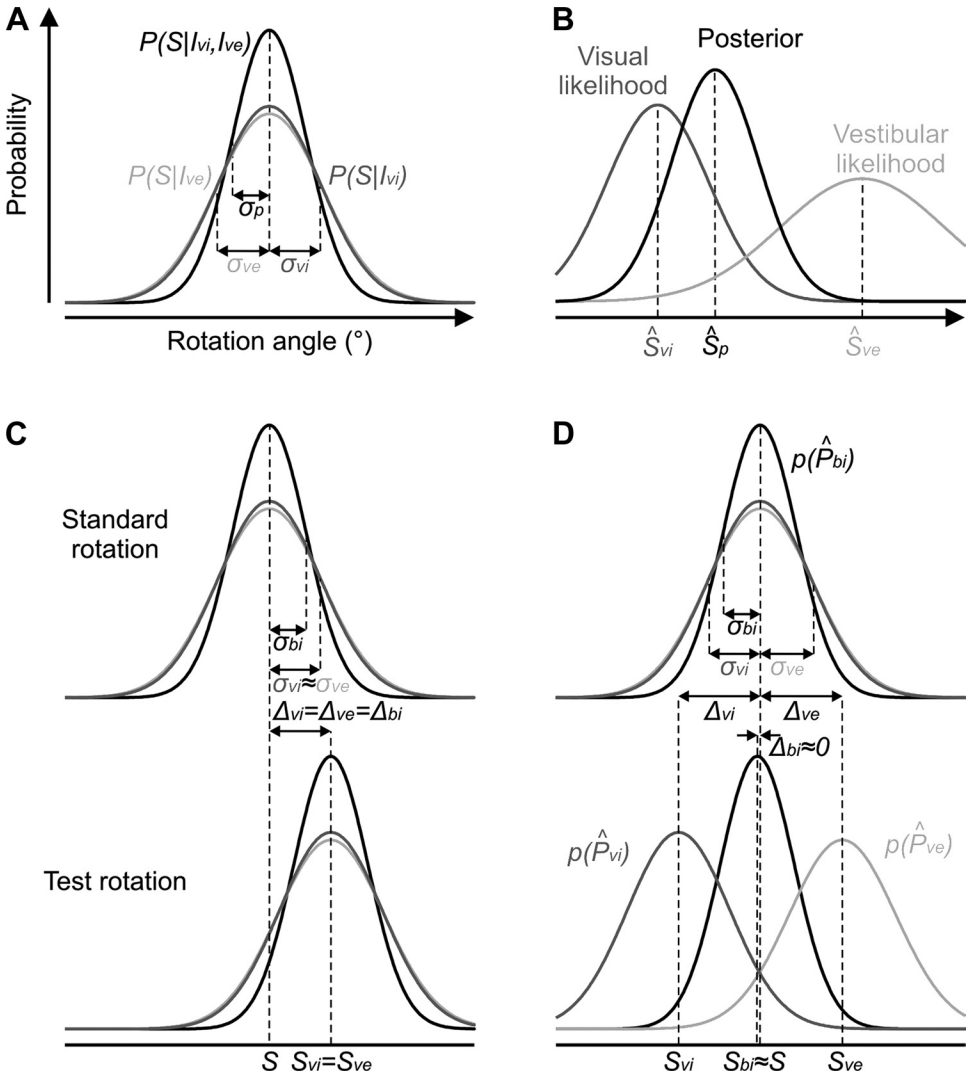

Fig. 1. Predictions of the optimal observer framework. *A* and *B*: a statistically optimal integration of sensory likelihoods results in a reduction of perceptual uncertainty according to *Eq. 2* (*A*) and a reliability-based cue reweighting according to *Eq. 3* (*B*). *C* and *D*: for rotations comprising both stimuli, optimal integration of the visual and vestibular likelihoods results in the posterior estimate according to *Eq. 1*. Discrimination between a standard and a test rotation can be based on either the single-cue estimators $\hat{P}_{vi}$ and $\hat{P}_{ve}$ (light and dark traces) or the bisensory estimator $\hat{P}_{bi}$ (black trace). Traces symbolize the distribution of the estimates over trials. Successful discrimination is achieved when the physical difference between the estimates of the 2 rotations (Δ_{vi}, Δ_{ve}, and Δ_{bi}) is greater than the respective discrimination thresholds (defined as σ_{vi}, σ_{ve}, and σ_{bi}). Use of the bisensory estimator can either improve discriminability, as in *C*, or not, as in *D*. Empirical discrimination thresholds can therefore reveal which estimators the subjects have access to for making perceptual judgments. See MATERIALS AND METHODS for definition of all symbols and terms.

the posterior) will be a weighted average of the two most likely single-cue estimates

$$\hat{S}_p = w_{vi}\hat{S}_{vi} + w_{ve}\hat{S}_{ve}, \quad (3)$$

where the weights are equal to the normalized reliabilities (inverse of variance)

$$W_{vi} = \frac{1/\sigma_{vi}^2}{1/\sigma_{vi}^2 + 1/\sigma_{ve}^2} \quad W_{ve} = \frac{1/\sigma_{ve}^2}{1/\sigma_{vi}^2 + 1/\sigma_{ve}^2} \quad (4)$$

It follows that optimal integration always reduces the variability of the posterior relative to the individual likelihoods (Fig. 1*A*), and the estimate of the more reliable likelihood weighs more heavily on the posterior estimate (Fig. 1*B*).

To discriminate between a standard rotation of size S and a test rotation of size $S + \Delta$, the probabilistic observer can compare their visual and vestibular estimates $\hat{P}_{vi}$ and $\hat{P}_{ve}$ on any given trial. We refer to the two as the single-cue estimators, and we define the single-cue discrimination thresholds (T_{vi} and T_{ve}) as equal to one standard deviation over trials of $\hat{P}_{vi}$ and $\hat{P}_{ve}$ (i.e., σ_{vi} and σ_{ve}). When the rotations are composed of both stimuli, sensory integration produces an additional bisensory estimator $\hat{P}_{bi}$ with discrimination threshold T_{bi}, estimated as in *Eq. 2*. Mandatory fusion can be tested by assessing which of the three estimators the subjects use to perceive the bimodal pairs ($S_{vi} = S$, $S_{ve} = S$) and ($S_{vi} = S + \Delta_{vi}$, $S_{ve} = S + \Delta_{ve}$) as different (Fig. 1, *C* and *D*). If all three estimators are available for perceptual judgments, then the two rotations can be perceived as different if either of the following inequalities is satisfied:

$$|\Delta_{vi}| > T_{vi} \quad (5)$$

$$|\Delta_{ve}| > T_{ve} \quad (6)$$

$$|w_{vi}\Delta_{vi} + w_{ve}\Delta_{ve}| > T_{bi} \quad (7)$$

where the cue weights are estimated as in *Eq. 4*. The left-hand side of *Eq. 7* corresponds to the size difference Δ_{bi} between the bisensory estimates of the two rotations. Therefore, if all three estimators are accessible, successful discrimination can be achieved whenever the estimated difference between the two rotations using any of the estimators reaches its own discrimination threshold $\pm T_{vi}$, $\pm T_{ve}$, or $\pm T_{bi}$. When the visual and vestibular stimuli rotate by the same amount ($\Delta_{vi} = \Delta_{ve}$), an optimal observer can achieve better discrimination performance if using the bisensory estimator (Fig. 1*C*). However, with different combinations of Δ_{vi} and Δ_{ve}, the two rotations can be close to metamers (e.g., if $\Delta_{vi} = -\Delta_{ve}$, Fig. 1*D*), indistinguishable in terms of $\hat{P}_{bi}$ (the estimated difference using $\hat{P}_{bi}$ will not reach $\pm T_{bi}$), and successful discrimination can be achieved only if access to the unimodal estimators is still available. Empirical assessments of the subjects' discrimination thresholds and a comparison with theoretical predictions for different Δ_{vi}/Δ_{ve} values can therefore reveal which estimators the subjects have access to and use for perceiving the two rotations as different.

Experimental setup. Vestibular stimuli were delivered in complete darkness by a centrifuge cockpit-style chair digitally servo-controlled (PCI-7352) with highly precise positioning (±0.1°). The chair was centered on the rotation axis so that only angular and no linear stimuli were provided to the vestibular organs. Subjects were comfortably restrained with a five-point racing harness, feet straps, and additional cushioning. Head movements were minimized by using a head pillow and face paddles pressed against the cheek bones. Rotation profiles were precomputed and specified the chair's instantaneous angular position at a rate of 100 Hz. The rotations' velocity profile $v(t)$ was a single cycle of a 0.77-Hz raised cosine function (Fig. 2*B*)

$$v(t) = \frac{A}{T}\left[1 - \cos\left(\frac{2\pi t}{T}\right)\right], \quad (8)$$

where A is rotation size and T is its duration ($T = 1.3$ s in this case). Instantaneous angular position $p(t)$ is then specified as

$$p(t) = A\left[\frac{t}{T} - \frac{1}{2\pi}\sin\left(\frac{2\pi t}{T}\right)\right]. \quad (9)$$

Such transient stimuli fall into the pass-band range of the transfer function describing the cascade of semicircular canal dynamics and the velocity storage mechanism (Bertolini et al. 2011). The signal encoding the rotation at the first stage of neural processing is therefore quasi-identical to actual head velocity in this case. Visual-only stimuli were simulated by a moving stereoscopic random dot pattern presented on a 22-in. display fixed to the chair and facing the subject at a distance of ~29 cm (Fig. 2*A*). The limited visual field therefore covered ~80° of horizontal and 56° of vertical visual angle. The subject and the display were physically enclosed to eliminate any visual cues that might emanate from the stationary surroundings during rotations. The visual scene was constructed as an almost infinite three-dimensional volume of randomly distributed dots of different size. Rotations were then simulated by having the observer's point of view placed in the middle of this space and rotated around the yaw axis. The generated scene therefore simulated retinal optic flow information that would ensue from actual rotation. The stereoscopic stimulus was generated by the Nvidia Quadro FX 3800 graphics card using the OpenGL quad-buffer mechanism. The stimulus was programmed with the Python language and viewed with the Nvidia 3D Vision kit (active shutter glasses) paired with a Samsung Syncmaster 2233RZ display (120-Hz refresh rate) via an infrared transmitter. Subjects were required to maintain visual fixation on a stationary target in the middle of the display in all conditions, and masking white noise was delivered over earphones at all times. The fixation dot was of different color than the random dot pattern and appeared with zero binocular disparity.

Participants. Eight healthy adults (MP, SG, and 6 subjects naive to the aims of the experiment) with normal or corrected vision and no history of inner ear disease participated in each experiment (optimal integration: 1 female, mean age 27 ± 5.8 yr; mandatory fusion: 4 females, mean age 24 ± 4.2 yr). In both experiments, an additional subject completed the task but had to be discarded because the performance did not surpass chance level in a number of conditions. All participants gave informed consent and received monetary retribution at 20 CHF/h. The studies were approved by a local ethics committee and were conducted in accordance with the Declaration of Helsinki.

Experimental paradigms. To test for optimal integration, subjects judged the relative size of two successive rotations (the standard and the test) in a two-alternative forced-choice task (Fig. 2*C*). The size of the standard was 15°, and the test was any of 7 equally spaced angles in the interval 10°-20° tested using the method of constant stimuli. These values were chosen on the basis of preliminary tests conducted on two subjects and such that they would include one point on each end of the psychometric fitting curve where size discrimination could be achieved with nearly 100% certainty. The two rotations were preceded, followed, and separated by an interval of 0.5 s. A 2-s period followed during which the subject had to answer, via a button press, whether the second rotation was bigger or smaller than the first. The standard rotation was randomly assigned to come either first or second, but measured responses were always those comparing the test with the standard. Each comparison was repeated 10 times per subject, and no feedback was given. Trials in which the subjects failed to give an answer were discarded; this constituted 0.2% of all trials. The relative reliability of the visual and vestibular cues was manipulated by changing the coherence of the visual motion (number of dots simulating rotation/number of dots moving randomly) from trial to trial between four different levels. The random motion varied in both direction and speed, but the stereoscopic depth of the individual dots did not change during the motion. The four coherence levels used were 100%, 75% (for 2 subjects) or 65% (for 6 subjects), 50%, and 25%. For bimodal comparisons, visual and vestibular stimuli were temporally synchronized and occurred simultaneously in congruent

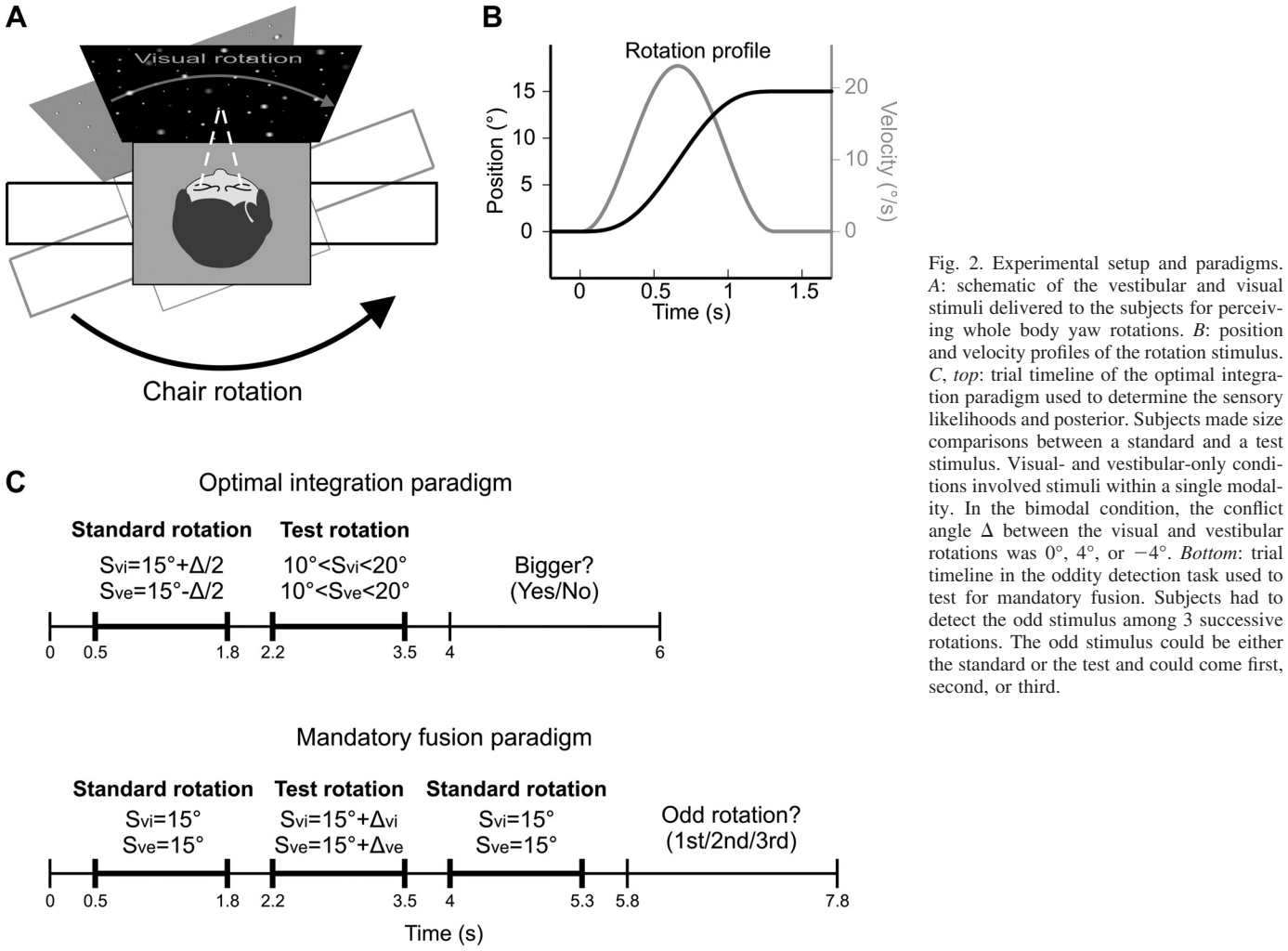

Fig. 2. Experimental setup and paradigms. *A*: schematic of the vestibular and visual stimuli delivered to the subjects for perceiving whole body yaw rotations. *B*: position and velocity profiles of the rotation stimulus. *C*, *top*: trial timeline of the optimal integration paradigm used to determine the sensory likelihoods and posterior. Subjects made size comparisons between a standard and a test stimulus. Visual- and vestibular-only conditions involved stimuli within a single modality. In the bimodal condition, the conflict angle Δ between the visual and vestibular rotations was 0°, 4°, or −4°. *Bottom*: trial timeline in the oddity detection task used to test for mandatory fusion. Subjects had to detect the odd stimulus among 3 successive rotations. The odd stimulus could be either the standard or the test and could come first, second, or third.

(i.e., opposite) directions. Three conflict angles were tested in the bimodal case ($S_{vi} - S_{ve} = 0°$, 4°, or −4°) and were applied to the standard rotation. This produced 17 conditions in total (1 vestibular, 4 visual, and 12 bimodal) giving rise to 1,190 trials per subject (7 angles × 10 repetitions × 17 conditions). The experiment was divided into 14 sessions of 10 min each during which all the conditions were randomly intermingled with an intertrial interval of 0.9 s. Visual-only, vestibular-only, and bimodal stimuli were therefore alternated on a trial-by-trial basis, and predicting the nature of the stimulus was impossible. The subjects took regular breaks between sessions and completed the entire experiment in ~4 h. The direction of rotation (left or right) was randomly chosen on each trial.

To test for mandatory fusion, subjects had to pick out the odd stimulus among three successive rotations in a three-alternative forced-choice task (Fig. 2*C*). The same standard rotation size and the same trial timings were used as in the first experiment. The test rotation sizes were 7 equally spaced angles in the interval 9°-21°. The sizes were again chosen on the basis of preliminary tests conducted on two subjects and such that they would include one point on each end of the fitting curve where size discrimination could be achieved with nearly 100% certainty. Two of the rotations were the test and one the standard (or vice versa), and all were presented in random order. For bimodal stimuli, the test rotation included conflicting visual and vestibular cue pairs ($S_{vi} = S + \Delta_{vi}$, $S_{ve} = S + \Delta_{ve}$). We tested eight conditions of bimodal pairings, each corresponding to a different Δ_{vi}/Δ_{ve} ratio (1, 0.5, 2, 0, ∞, −1, −0.5, and −2) (see RESULTS for details). The different ratios yield different amounts of conflict between S_{vi} and S_{ve}, with no conflict in the 1 condition and maximum conflict in the −1 condition. For the 1 ratio, S_{vi} and S_{ve} were always equal and therefore correspond to the easiest condition for picking out the odd stimulus (tested Δ_{ve} and Δ_{ve} values were 0, ±1.71, ±3.43, and ±5.14). For the −1 ratio, the average of S_{vi} and S_{ve} was always equal to the standard rotation size S and, in the case of equal cue reliabilities, makes the identification of the odd stimulus theoretically impossible if single cues remain inaccessible. For the ∞ ratio, $\Delta_{ve} = 0$, meaning that S_{ve} was always equal to the standard rotation size, whereas S_{vi} took on the 7 equally spaced angles in the interval 9°-21°. The opposite was true for the 0 condition. For the 2 and −2 ratios, tested Δ_{vi} values were 0, ±1.71, ±3.43 and ±5.14 and the Δ_{ve} values were calculated from the Δ_{vi}/Δ_{ve} ratio. The opposite was true for the −0.5 and 0.5 ratios. The subject had to answer whether the first, second, or third rotation was different from the other two on any basis. Each comparison was repeated 10 times across the 10 conditions (2 unimodal and 8 bimodal), producing a total of 700 trials per subject, randomly intermixed in 10 sessions of 10 min each. In both experiments, subjects initially underwent multiple short training sessions to familiarize themselves with the task and to ensure better than chance performance. Data collected on these sessions were not used for analysis.

Data analysis. All data analyses were performed off-line with custom programs compiled in MATLAB (The MathWorks). For each test angle, individual answers were pooled across all subjects to obtain a probabilistic measure of the response and yield a sufficient sample set for the statistical comparisons. This consisted of calculating the proportion of "bigger" (see Fig. 3) or "incorrect" responses (see Fig. 6) based on 80 answers (10 from each subject) for every test angle.

Using the method of least squares, the proportions of "bigger" responses in the first experiment were fit with a cumulative Gaussian function and the proportions of incorrect responses in the second experiment were fit with a Gaussian. Measures of the mean, variance, and discrimination threshold were then extracted from the obtained fits in each condition. A bootstrap analysis provided standard errors for each measure and allowed statistical comparison between the experimentally measured values and model predictions. This consisted of repeating the data fit for each condition 9,999 times on a different subset of responses each time. The different subsets were formed by taking at random, with replacement, N trials from the total set of N for each test angle (for $N = 80$, 10^{23} such combinations are possible). The standard deviation of 9,999 repeated measures is then the standard error of the measure obtained using the original data set. Statistical tests were made by assessing the amount of overlap between the bootstrap iterations of two measures. If the measure of interest is σ, and σ^j_{ex} and σ^j_{pr} are its experimental and predicted estimates obtained from the jth bootstrap sample, then the one-tailed bootstrap probability of $(\sigma_{ex} > \sigma_{pr})$ is

$$p = \frac{1}{B}\sum_{j=1}^{B} I\left(\sigma^j_{ex} - \sigma^j_{pr} > 0\right),$$

where $B = 9{,}999$ and $I()$ is the indicator function, which is equal to 1 when its argument is true and 0 otherwise. The inequality would be reversed for the probability of $(\sigma_{ex} < \sigma_{pr})$. The one-tailed bootstrap P value is therefore simply the proportion of $(\sigma^j_{ex} - \sigma^j_{pr})$ values that are more extreme than 0. We prefer this approach to parametric testing because it provides a direct computation of the cumulative distribution of a test statistic instead of having to use an asymptotic approximation.

RESULTS

Optimal integration of visual and vestibular cues. To experimentally obtain the visual and vestibular likelihoods and the posterior resulting from their integration when perceiving own-body rotations, subjects made relative judgments about the size of two consecutive rotations: a standard rotation of fixed angular displacement and a test rotation of variable size (Fig. 2*C* and MATERIALS AND METHODS). The probabilities of perceiving the test rotation as bigger than the standard were fit by a cumulative Gaussian function for the tested range of angles, and the Gaussian likelihoods and posterior can be derived for each condition by taking the mathematical derivative of the fits.

Variance measures extracted from the experimentally obtained sensory likelihoods were used to predict the variance of the posteriors according to MLE and *Eq. 2* (see MATERIALS AND METHODS). Because these were evaluated by comparing the size of two successive rotations, they actually correspond to the true likelihood variances scaled by a factor of 2. The variances measured experimentally using the bimodal stimuli (means ± SE: $\sigma_p = 2.7 \pm 0.2, 3.1 \pm 0.24, 3.3 \pm 0.26, 3.9 \pm 0.35$ for the 4 coherence levels) were reduced relative to using either single cue alone ($\sigma_{ve} = 5.1 \pm 0.54$; $\sigma_{vi} = 3.5 \pm 0.28, 3.7 \pm 0.3, 5.0 \pm 0.53, 7.3 \pm 1.1$) and closely matched the predictions for all four visual coherence levels (Fig. 3*A*). The result was readily reproducible across individual participants. The standard deviations of the psychometric fits to the bimodal data of individual subjects across coherence levels were not statistically different between the measured and MLE-predicted values (paired t-test, $P = 0.56$) and are shown in Fig. 4*A*. The same bimodal thresholds were, however, significantly reduced relative to the smallest single-cue thresholds (paired t-test, $P < 0.001$), confirming that integrating information from visual and vestibular senses reduces perceptual uncertainty in a statistically optimal manner when estimating rotatory self-motion. As the critical test for demonstrating cue integration, we furthermore provide a comparison between the bimodal and single-cue thresholds for each subject in the case where the visual and vestibular weights were closest to being equal (Fig. 4*B*).

To test for the predictions of *Eq. 3*, size comparisons were made against a standard stimulus in which the chair and the visual scene rotated by different amounts so that $\hat{S}_{vi} \neq \hat{S}_{ve}$. When $\hat{S}_{ve}$ signaled a bigger rotation than $\hat{S}_{vi}$, the subjects' most

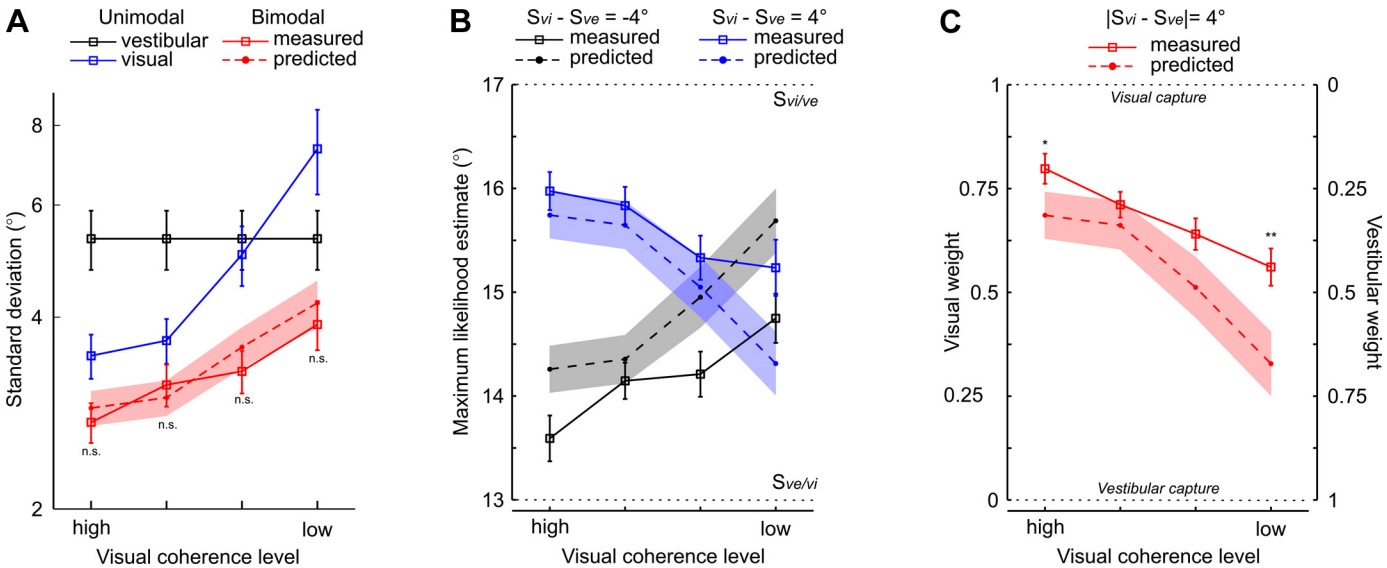

Fig. 3. Optimal integration of visual and vestibular cues. *A*: standard deviations obtained from the measured visual, vestibular, and bisensory likelihoods for 4 different levels of visual coherence. The empirical bisensory values were not significantly different (n.s.: $P > 0.2$, 1-tailed bootstrap test) from the maximum likelihood estimation (MLE) predictions. *B*: MLEs extracted from the measured posterior distributions and compared with the MLE predictions for the 2 conflicting visual and vestibular stimuli ($S_{vi} = 13°$, $S_{ve} = 17°$) and ($S_{vi} = 17°$, $S_{ve} = 13°$). *C*: averaged data from the 2 conditions in *B* and expressed in terms of weights show a suboptimal cue reweighting compared with model predictions (*$P < 0.05$, **$P < 0.01$, 1-tailed bootstrap test). All delimiters correspond to bootstrap standard error.

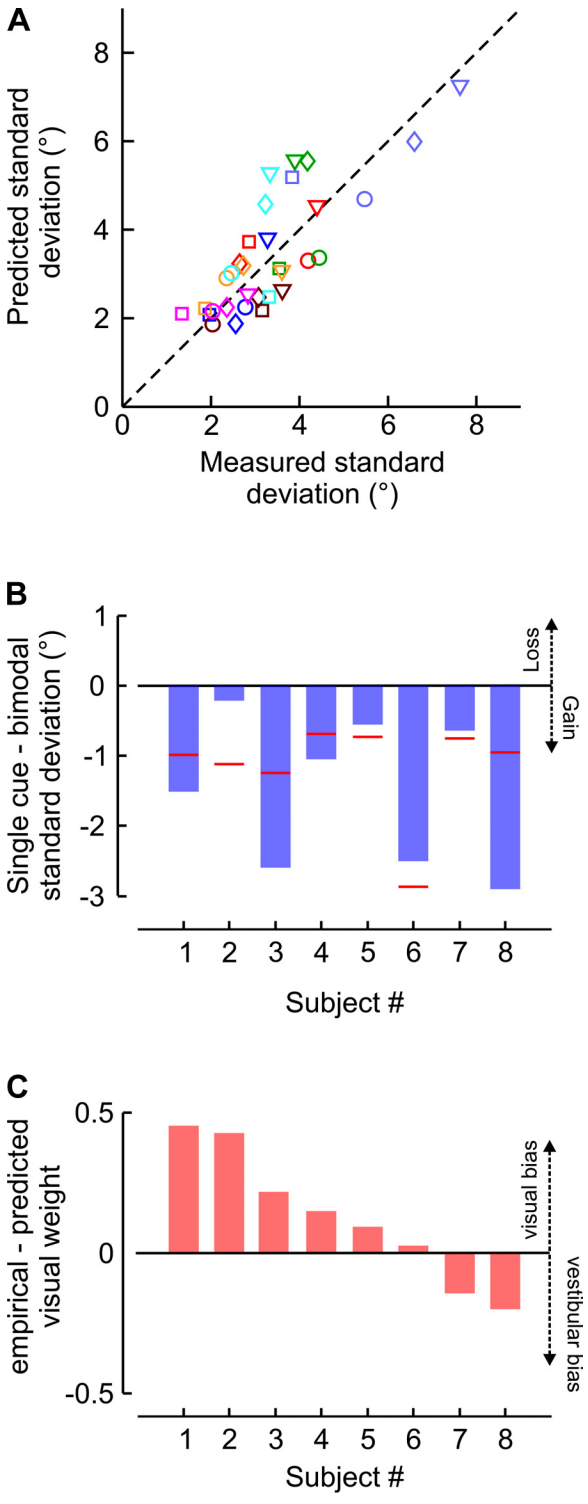

Fig. 4. Individual subject data. *A*: similarity between the predicted and measured standard deviations of the posterior across all subjects and for all 4 coherence levels. Colors denote different subjects, and symbols correspond to the different coherence levels. *B*: difference between the lowest single-cue standard deviation and the measured (blue bars) and predicted (red lines) bimodal standard deviations for the coherence level yielding best-matched visual and vestibular weights for each subject. *C*: difference between predicted and empirical visual weights averaged across the 4 coherence levels and sorted in descending order for the 8 subjects.

likely posterior estimate $\hat{S}_p$ increased with decreasing visual coherence level (black trace in Fig. 3*B*). The opposite was observed when $\hat{S}_{vi} > \hat{S}_{ve}$ (blue trace in Fig. 3*B*). This is what is predicted if the subjects dynamically attribute more weight to the vestibular cue than the visual, according to *Eqs. 3* and *4*, as the reliability of the latter is reduced (dotted lines in Fig. 3*B*). Pooling the data from the two conflict conditions and expressing it in terms of visual and vestibular weights (Fig. 3*C*) shows that cue reweighting occurs and follows the MLE-predicted trend but deviates from optimality because subjects tended to significantly overweigh the visual cue. The extent of the visual bias was, however, variable across individuals (Fig. 4*C*).

Mandatory fusion. We next addressed the issue of mandatory cue fusion by adopting a paradigm (Hillis et al. 2002) measuring an observer's ability to perceive two rotations as different. Subjects were asked to detect the odd stimulus among three successive rotations, two of which were the standard and one the test (or vice versa) (Fig. 2*C* and MATERIALS AND METHODS). This oddity task is advantageous to outright asking the subjects whether two rotations are different, because it forces them to adopt the same decision criterion and thus eliminates response bias from the observer's actual discriminability (Swets 1961) (i.e., the subjects stay unaware of the task's real purpose; perceptual responses are not contaminated by higher level cognitive strategies).

In the unimodal cases, comparisons were made between a standard rotation of size S and a test of size $S + \Delta$. The proportions of incorrect responses for each Δ were fit by a Gaussian function (Fig. 5*A*). The fits symbolize the distribution over trials of visual and vestibular estimators $\hat{P}_{vi}$ and $\hat{P}_{ve}$, the probabilistic descriptions of the observer's discrimination ability using each sense alone, and the associated single-cue discrimination thresholds T_{vi} and T_{ve} that we define here as equal to one standard deviation of the Gaussian fits. The coherence level used for the visual stimulus was the one that yielded $\sigma_{vi} \approx \sigma_{ve}$ for the average subject when optimal integration was tested in the first experiment (see Fig. 3*A*). In the bimodal case, discriminability between the pairs ($S_{vi} = S$, $S_{ve} = S$) and ($S_{vi} = S + \Delta_{vi}$, $S_{ve} = S + \Delta_{ve}$) was assessed. We tested eight conditions of bimodal pairings, each corresponding to a different Δ_{vi}/Δ_{ve} ratio. A ratio of 1 generates visual and vestibular stimuli that always rotate by the same amount, and the bisensory estimator $\hat{P}_{bi}$ should provide better discrimination ability than either single-cue estimator in that case (Fig. 1*C*). A ratio of -1 produces conflicting visual and vestibular cues but identical bisensory estimates between the standard and the test according to *Eq. 3* when $w_{vi} \approx w_{ve}$. Theoretically, the ability to discriminate the two metameric stimuli will be compromised if the observer only uses $\hat{P}_{bi}$ and does not retain the unimodal estimators $\hat{P}_{vi}$ and $\hat{P}_{ve}$ (Fig. 1*D*). The remaining six conditions corresponded to Δ_{vi}/Δ_{ve} values (0.5, 2, 0, ∞, -0.5, -2) that produce bimodal stimuli with varying amounts of cue conflict that lie between the latter two extremes.

If all three estimators are accessible, in the cue space depicted in Fig. 5*B*, the predicted discrimination thresholds (blue dots) would lie on the contour defined by the red (*Eqs. 5* and *6*) and green lines (*Eq. 7*). That is the case if the subjects do not make an additive use of all three estimators. Probability summation is actually unrealistic, because it assumes that the three estimators can be used independently. Given the fact that $\hat{P}_{bi}$ is a weighted average of $\hat{P}_{vi}$ and $\hat{P}_{ve}$, the independence

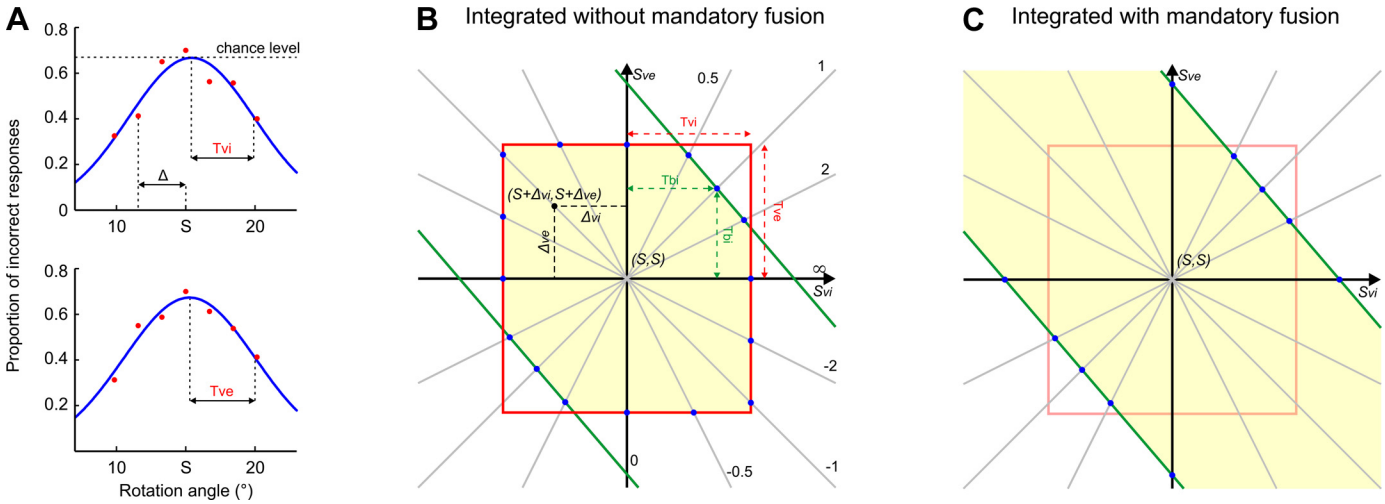

Fig. 5. Theoretical predictions for rotation size discrimination. *A*: mean responses for choosing the odd visual or vestibular stimulus (i.e., perceiving S + Δ as different from *S*) obtained by pooling raw choices from all subjects. The Gaussian fits symbolize the visual and vestibular estimators and provide the unimodal discrimination thresholds T_{vi} and T_{ve}. *B*: cue space where each point corresponds to a bimodal pairing (abscissas and ordinates indicate rotation sizes signaled by the visual and vestibular stimuli, respectively). When perceiving $(S + \Delta_{vi}, S + \Delta_{ve})$ as different from (S, S), if the cues are integrated without mandatory fusion, discrimination thresholds (blue dots) are predicted to lie on the contour defined by the red (*Eqs. 5* and *6*) and green lines (*Eq. 7*). Gray lines and main axes each correspond to a Δ_{vi}/Δ_{ve} value representing one of the tested conditions. The yellow area comprises data points theoretically indistinguishable from (*S*, *S*). *C*: predictions in the case of mandatory fusion.

assumption is clearly invalid. The probability summation model will thus not be considered further and in any case makes a less conservative prediction than the model in Fig. 5*B*. If mandatory fusion was to occur, perceptual access to $\hat{P}_{vi}$ and $\hat{P}_{ve}$ would be lost and discrimination performance would uniquely be based on the bisensory estimator. (S, S) can be perceived as different from $(S + \Delta_{vi}, S + \Delta_{ve})$ only if *Eq. 7* is satisfied, giving rise to the theoretical prediction shown in Fig. 5*C*.

The prediction depicted in Fig. 5*B* was compared with the mandatory fusion prediction (Fig. 5*C*) to see which best accounts for the discrimination thresholds obtained experimentally in the eight tested conditions. The predicted contours were constructed using the measured T_{vi} and T_{ve} (means ± SE: 4.54 ± 0.42 and 4.74 ± 0.45, respectively) and the estimated T_{bi}. Our results show that the subjects' discrimination thresholds (again defined as equal to 1 standard deviation of the obtained Gaussian fits) for perceiving (S, S) as different from $(S + \Delta_{vi}, S + \Delta_{ve})$ were in many cases larger than those predicted from an independent use of all three estimators (Fig. 6*A*). Individual subjects indeed showed consistent losses in discrimination performance compared with prediction with the use of single-cue estimators, even without adding probabilistic responses (Fig. 6*B*). Threshold predictions were derived for each subject individually from the corresponding measured single-

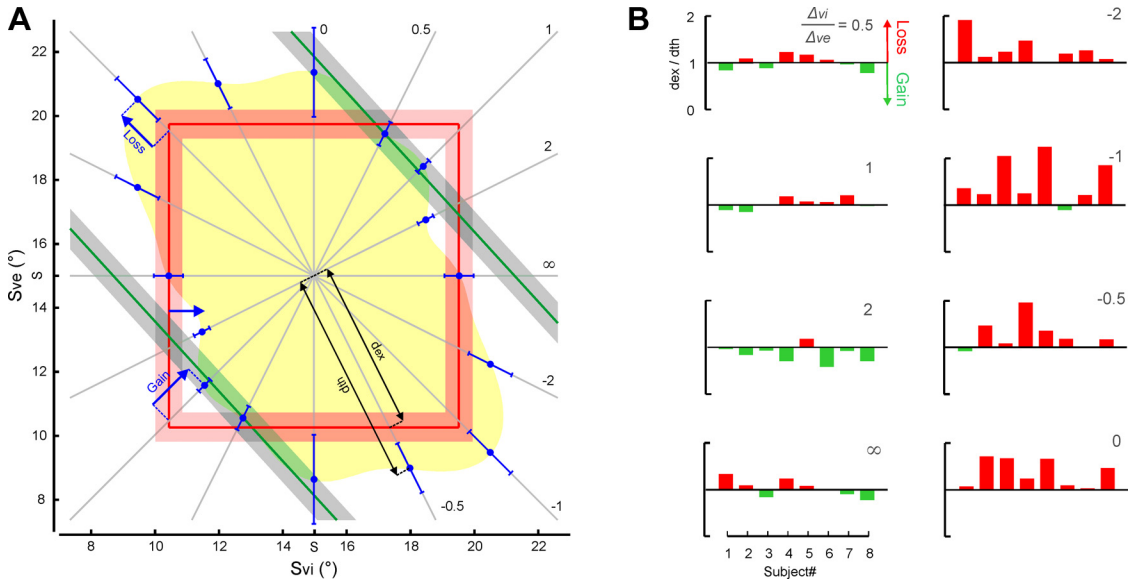

Fig. 6. Comparison between predicted and measured discrimination thresholds. *A*: compared with single-cue thresholds (red), pooled data from all subjects show improved discrimination ability ("gain") when using the bisensory estimator (green) is advantageous (0.5, 1, and 2 conditions) and worse discrimination ("loss") when it is not (∞, −2, −1, −0.5, and 0 conditions). *B*: loss or gain in discrimination ability compared with the theoretical prediction of Fig. 5*B* for individual subject data as measured by the d_{ex}/d_{th} ratio, where d_{ex} is the distance between the cue space origin and experimental data (blue), and d_{th} is the distance between the origin and the theoretical limits (red or green), as depicted in *A*. All shadings and delimiters correspond to bootstrap standard error.

cue thresholds. For Δ_{vi}/Δ_{ve} ratios (0.5, 1 and 2) where the use of $\hat{P}_{bi}$ leads to a gain in performance over the use of $\hat{P}_{vi}$ and $\hat{P}_{ve}$, single subject thresholds (Fig. 6*B*) were not statistically different ($P > 0.05$, *t*-test) from the identical predictions of Fig. 5, *B* and *C*. On the other hand, in the remaining conditions where mandatory fusion leads to a worse performance, subjects showed losses in discrimination ability (Fig. 6*B*) relative to use of the single-cue estimators ($P < 0.05$, for $\Delta_{vi}/\Delta_{ve} = -2, -1, -0.5$ and 0, average power = 0.81, and $P > 0.3$ for ∞, 1-tailed *t*-test). The results are therefore best accounted for by assuming that only the bisensory estimator stemming from sensory fusion is available for making perceptual judgments. Conditions where very large, even infinite, discrimination thresholds are predicted ($\Delta_{vi}/\Delta_{ve} = -0.5, -1, -2$) are those that involve stimuli with the largest conflict angles between the visual and vestibular cues. Because the subjects were free to detect the odd stimulus on any basis, it is reasonable to assume that detection was based on sometimes perceiving the conflict in trials corresponding to the biggest Δ values. The absence of optimal cue integration in those cases explains the noninfinite or lower than theoretically expected thresholds. Also, a perceptual aspect other than rotation size or conflict detection might have transpired in cases of large conflict and been used by the subjects to do the task. We finally note that visuovestibular integration resulted in overweighing of the visual cue (Fig. 3*C*): including a visual bias in the model would increase w_{vi} and decrease w_{ve} in *Eq. 7*, translate into the green lines being rotated clockwise in Fig. 6*B*, and therefore yield an even better correspondence between experimental results and the mandatory fusion prediction.

DISCUSSION

When perceiving properties of the world, observers combine redundant information from different sensory modalities. Perceptual estimates derived from each of these sensory cues will naturally exhibit variability across repeated observations of the same stimulus. It has been repeatedly shown that the variability is reduced in a statistically optimal manner if cues are combined to produce the final percept. The neural mechanism underlying multisensory integration is therefore likely to be a process of probabilistic inference seeking to reduce perceptual uncertainty (Knill and Pouget 2004). Our results demonstrate, and extend what has recently been reported for the perception of heading (Butler et al. 2010; Fetsch et al. 2009), that the central nervous system integrates multisensory idiothetic information according to the same laws of probability. Indeed, the same optimal reduction of variance and cue reweighting in proportion to relative reliability occurs as for nonidiothetic cues (Fig. 3). When perceiving whole body rotations, however, subjects tended to overweigh the visual cue (Figs. 3*C* and 4*C*), which is in contrast with heading perception, where an excessive reliance on the vestibular cue is observed (Butler et al. 2010; Fetsch et al. 2009). A selective overweighting of otolith signals and an underweighting of semicircular canal signals might thus be occurring when integrated with vision. Similarly suboptimal cue weights have been observed for other sensory modalities as well (Battaglia et al. 2003; Knill and Saunders 2003), and why such deviations from optimality occur is not fully understood. One possibility is that the biases might be reflective of a recalibration mechanism, where one estimate is remapped and realigned with the other in an attempt to internally correct the inconsistencies in multisensory input. Such a process is indeed known to occur when the observer is constrained to integrate conflicting information (Adams et al. 2001; Block and Bastian 2011), even after only a very short exposure (in the milliseconds range) to the conflict (Wozny and Shams 2011).

When sensory cues are combined, perception is governed by the posterior, the product of their integration. Because they are individually less reliable, neural signals underlying the two isolated sensory likelihoods are therefore not used at the perceptual level. It has been demonstrated that when the two cues originate from different sensory modalities (vision and touch, for example), observers still have access to this unused unimodal information (Hillis et al. 2002). Why might the ability to access these "useless" signals be preserved? In laboratory settings, experimental conditions can be constructed where the use of individual likelihoods, if available, is advantageous in terms of better task performance, even in the presence of a more reliable estimate (Fig. 1*D*). Such conditions, however, have little ecological validity. They can only serve as a useful experimental tool for testing whether likelihood signals are accessible but do not provide a valid explanation for their accessibility. The reasons might instead be rooted in the causal inference process (Koerding et al. 2007; Parise et al. 2012; Shams and Beierholm 2010) since observers often effortlessly attribute separate causes to simultaneously received cross-modal cues. The dissociated cues are not integrated, and each gives rise to an independent percept. Preserving unused information when cues are integrated might thus be reflective of a neural organization sculptured by the experience that most cues simply do not have the same cause in everyday life. Actually, the MLE model of *Eq. 1* is a simplification, under the common cause assumption, of a more generalized hierarchical causal inference (HCI) model (Shams and Beierholm 2010). In the full HCI model, the a posteriori estimate is a weighted average of the MLE estimate of *Eq. 3* and one of the single-cue estimates, the one that dominates when separate causes are inferred. The weighting is determined by the probability of the common cause scenario. Therefore, whenever the latter probability is not equal to one, the individual likelihoods must remain accessible for one of them to be combined with the product of their initial integration.

Our results show that this generalization does not apply to cross-modal integration when the object of perception is the perceiver's own body. Visual and vestibular idiothetic cues are individually discarded after being fused into a single percept (Fig. 6) similarly to nonidiothetic cues within the same sense. Indeed, mandatory fusion has so far only been observed for the integration of unimodal cues: binocular disparity and texture gradients when perceiving the slant of a surface (Hillis et al. 2002; Nardini et al. 2010). These two cases share the characteristic of cues not being dissociable in natural conditions; they are necessarily redundant and always integrated. The probability of the common cause scenario is therefore never different from unity. Even when observers are instructed to actively attend either the visual or vestibular stimulus and ignore the other, providing the cue conflicts go unnoticed, they seem incapable of weighing the two cues independently (Berger and Buelthoff 2009). Because there is a cost, in terms of brain resources, associated with carrying two neural representations

of the same rotation stimulus, mandatory fusion likely results from the absence of an evolutionary pressure to preserve the individual channels for stimuli including both information sources. Sensory signals for perceiving self-motion thus seem to be processed more like unimodal cues rather than as originating from separate senses. In addition, the particular rotations we used (Fig. 2*B*) are faithfully encoded by both visual and vestibular systems. For a broader range of stimuli, however, both systems are individually deficient. Low-frequency, low-acceleration vestibular stimuli and high-frequency, high-acceleration visual stimuli are inaccurately encoded at early stages of neural processing (Waespe and Henn 1977, 1979). Only neural signals generated by rotations including both sensory inputs give a truthful account of the actual motion of the body over the entire operating range (Dichgans et al. 1973; Waespe and Henn 1977, 1979). A loss of inaccurate unisensory information might be incurred for the benefit of a more accurate bisensory signal, thus providing a potential neurophysiological basis for the mandatory fusion that we observed. We postulate that the same is also likely to be true for heading perception (Butler et al. 2010; Fetsch et al. 2009) but not in other instances where optimal cross-modal cue integration has been previously demonstrated (Alais and Burr 2004; Ernst and Banks 2002; Mendonca et al. 2011). This also applies to own hand position perception using visual and proprioceptive cues (van Beers et al. 1996, 1999), despite the idiothetic nature of the latter, because it is identical, in all things that matter, to estimating the position of an external object held in that hand.

It follows that passive whole body rotations can be simulated by combinations of visuovestibular stimuli that, like color metamers, differ physically but "look" the same. Our result is also akin to examples of visual metamers such as, for instance, two verniers with opposite offsets flashed in quick succession that are fused and become indistinguishable from a single, almost aligned vernier (Scharnowski et al. 2009). Color metamers occur because spectral information is lost by cone photoreceptors in the retina (Wandell 1995) and therefore cannot be recovered in the brain. In the case of visual and visuovestibular metamers, information loss necessarily occurs at a neural level upstream of where the metameric stimuli would yield identical neural responses. We envision that our findings might guide future electrophysiology and modeling approaches to elucidate where and how visuovestibular metamers are formed, similar to recent attempts at explaining visual metamerism (Freeman and Simoncelli 2011) and at examining the dynamics of the fusion process (Scharnowski et al. 2009). Finally, mandatory fusion of visual and vestibular signals can explain why neurons in cortical and subcortical vestibular centers are highly multimodal (Akbarian et al. 1988; Bremmer et al. 2002; Buttner and Buettner 1978; Butter and Henn 1976; Dichgans et al. 1973; Duffy 1998; Grusser et al. 1990; Henn et al. 1974; Meng and Angelaki 2010; Page and Duffy 2003; Schlack et al. 2002; Takahashi et al. 2007; Waespe et al. 1981; Waespe and Henn 1977, 1979) and most often visually responsive, and it hints at developmental reasons for the absence of a centralized vestibular cortex (Fukushima 1997; Guldin and Grusser 1998).

ACKNOWLEDGMENTS

We thank Bruno Herbelin for technical assistance and Danilo Jimenez Rezende for advice on data analysis, as well as Michael Herzog and Wulfram Gerstner for comments on an earlier version of the manuscript.

GRANTS

This study was supported by Swiss National Science Foundation Grant SINERGIA CRSII1-125135/1.

DISCLOSURES

No conflicts of interest, financial or otherwise, are declared by the authors.

AUTHOR CONTRIBUTIONS

M.P. and O.B. conception and design of research; M.P. and S.G. performed experiments; M.P. analyzed data; M.P., S.G., and O.B. interpreted results of experiments; M.P. prepared figures; M.P. drafted manuscript; M.P., S.G., and O.B. edited and revised manuscript; M.P., S.G., and O.B. approved final version of manuscript.

REFERENCES

Adams WJ, Banks MS, van Ee R. Adaptation to three-dimensional distortions in human vision. *Nat Neurosci* 4: 1063–1064, 2001.

Akbarian S, Berndl K, Grusser OJ, Guldin W, Pause M, Schreiter U. Responses of single neurons in the parietoinsular vestibular cortex of primates. *Ann NY Acad Sci* 545: 187–202, 1988.

Alais D, Burr D. The ventriloquist effect results from near-optimal bimodal integration. *Curr Biol* 14: 257–262, 2004.

Battaglia PW, Jacobs RA, Aslin RN. Bayesian integration of visual and auditory signals for spatial localization. *J Opt Soc Am A* 20: 1391–1397, 2003.

Berger DR, Buelthoff HH. The role of attention on the integration of visual and inertial cues. *Exp Brain Res* 198: 287–300, 2009.

Bertolini G, Ramat S, Laurens J, Bockisch CJ, Marti S, Straumann D, Palla A. Velocity storage contribution to vestibular self-motion perception in healthy human subjects. *J Neurophysiol* 105: 209–223, 2011.

Block HJ, Bastian AJ. Sensory weighting and realignment: independent compensatory processes. *J Neurophysiol* 106: 59–70, 2011.

Bremmer F, Klam F, Duhamel JR, Ben Hamed S, Graf W. Visual-vestibular interactive responses in the macaque ventral intraparietal area (VIP). *Eur J Neurosci* 16: 1569–1586, 2002.

Butler JS, Smith ST, Campos JL, Buelthoff HH. Bayesian integration of visual and vestibular signals for heading. *J Vis* 10: 2010.

Buttner U, Buettner UW. Parietal cortex (2v) neuronal-activity in alert monkey during natural vestibular and optokinetic stimulation. *Brain Res* 153: 392–397, 1978.

Buttner U, Henn V. Circularvection—psychophysics and single-unit recordings in the monkey. *Ann NY Acad Sci* 374: 274–283, 1981.

Buttner U, Henn V. Thalamic unit-activity in alert monkey during natural vestibular stimulation. *Brain Res* 103: 127–132, 1976.

Dichgans J, Schmidt CL, Graf W. Visual input improves speedometer function of vestibular nuclei in goldfish. *Exp Brain Res* 18: 319–322, 1973.

Duffy CJ. MST neurons respond to optic flow and translational movement. *J Neurophysiol* 80: 1816–1827, 1998.

Ernst MO, Banks MS. Humans integrate visual and haptic information in a statistically optimal fashion. *Nature* 415: 429–433, 2002.

Fetsch CR, Turner AH, DeAngelis GC, Angelaki DE. Dynamic reweighting of visual and vestibular cues during self-motion perception. *J Neurosci* 29: 15601–15612, 2009.

Freeman J, Simoncelli EP. Metamers of the ventral stream. *Nat Neurosci* 14: 1195–U1130, 2011.

Fukushima K. Corticovestibular interactions: anatomy, electrophysiology, and functional considerations. *Exp Brain Res* 117: 1–16, 1997.

Grusser OJ, Pause M, Schreiter U. Vestibular neurons in the parieto-insular cortex of monkeys (*Macaca fascicularis*)—visual and neck receptor responses. *J Physiol* 430: 559–583, 1990.

Gu Y, Angelaki DE, DeAngelis GC. Neural correlates of multisensory cue integration in macaque MSTd. *Nat Neurosci* 11: 1201–1210, 2008.

Guldin WO, Grusser OJ. Is there a vestibular cortex? *Trends Neurosci* 21: 254–259, 1998.

Haarmeier T, Bunjes F, Lindner A, Berret E, Thier P. Optimizing visual motion perception during eye movements. *Neuron* 32: 527–535, 2001.

Haarmeier T, Thier P, Repnow M, Petersen D. False perception of motion in a patient who cannot compensate for eye movements. *Nature* 389: 849–852, 1997.

Henn V, Young LR, Finley C. Vestibular nucleus units in alert monkeys are also influenced by moving visual-fields. *Brain Res* 71: 144–149, 1974.

Hillis JM, Ernst MO, Banks MS, Landy MS. Combining sensory information: mandatory fusion within, but not between, senses. *Science* 298: 1627–1630, 2002.

Hillis JM, Watt SJ, Landy MS, Banks MS. Slant from texture and disparity cues: optimal cue combination. *J Vis* 4: 967–992, 2004.

Ionta S, Heydrich L, Lenggenhager B, Mouthon M, Fornari E, Chapuis D, Gassert R, Blanke O. Multisensory mechanisms in temporo-parietal cortex support self-location and first-person perspective. *Neuron* 70: 363–374, 2011.

Knill DC, Pouget A. The Bayesian brain: the role of uncertainty in neural coding and computation. *Trends Neurosci* 27: 712–719, 2004.

Knill DC, Saunders JA. Do humans optimally integrate stereo and texture information for judgments of surface slant? *Vision Res* 43: 2539–2558, 2003.

Koerding KP, Beierholm U, Ma WJ, Quartz S, Tenenbaum JB, Shams L. Causal inference in multisensory perception. *PLoS One* 2: 2007.

Landy MS, Maloney LT, Johnston EB, Young M. Measurement and modeling of depth cue combination: in defense of weak fusion. *Vision Res* 35: 389–412, 1995.

Laurens J, Droulez J. Bayesian processing of vestibular information. *Biol Cybern* 96: 389–404, 2007.

MacNeilage PR, Banks MS, Berger DR, Buelthoff HH. A Bayesian model of the disambiguation of gravitoinertial force by visual cues. *Exp Brain Res* 179: 263–290, 2007.

Mendonca C, Santos JA, Lopez-Moliner J. The benefit of multisensory integration with biological motion signals. *Exp Brain Res* 213: 185–192, 2011.

Meng H, Angelaki DE. Responses of ventral posterior thalamus neurons to three-dimensional vestibular and optic flow stimulation. *J Neurophysiol* 103: 817–826, 2010.

Nardini M, Bedford R, Mareschal D. Fusion of visual cues is not mandatory in children. *Proc Natl Acad Sci USA* 107: 17041–17046, 2010.

Page WK, Duffy CJ. Heading representation in MST: sensory interactions and population encoding. *J Neurophysiol* 89: 1994–2013, 2003.

Parise CV, Spence C, Ernst MO. When correlation implies causation in multisensory integration. *Curr Biol* 22: 46–49, 2012.

Richards W. Quantifying sensory channels - generalizing colorimetry to orientation and texture, touch, and tones. *Sens Processes* 3: 207–229, 1979.

Royden CS, Banks MS, Crowell JA. The perception of heading during eye-movements. *Nature* 360: 583–587, 1992.

Scharnowski F, Rueter J, Jolij J, Hermens F, Kammer T, Herzog MH. Long-lasting modulation of feature integration by transcranial magnetic stimulation. *J Vis* 9: 2009.

Schlack A, Hoffmann KP, Bremmer F. Interaction of linear vestibular and visual stimulation in the macaque ventral intraparietal area (VIP). *Eur J Neurosci* 16: 1877–1886, 2002.

Shams L, Beierholm UR. Causal inference in perception. *Trends Cogn Sci* 14: 425–432, 2010.

Swets JA. Is there a sensory threshold? *Science* 134: 168–177, 1961.

Takahashi K, Gu Y, May PJ, Newlands SD, DeAngelis GC, Angelaki DE. Multimodal coding of three-dimensional rotation and translation in area MSTd: comparison of visual and vestibular selectivity. *J Neurosci* 27: 9742–9756, 2007.

van Beers RJ, Sittig AC, Denier van der Gon JJ. Localization of a seen finger is based exclusively on proprioception and on vision of the finger. *Exp Brain Res* 125: 43–49, 1999.

van Beers RJ, Sittig AC, Denier van der Gon JJ. How humans combine simultaneous proprioceptive and visual position information. *Exp Brain Res* 111: 253–261, 1996.

Waespe W, Buttner U, Henn V. Visual-vestibular interaction in the flocculus of the alert monkey. 1. Input activity. *Exp Brain Res* 43: 337–348, 1981.

Waespe W, Henn V. Neuronal activity in vestibular nuclei of alert monkey during vestibular and optokinetic stimulation. *Exp Brain Res* 27: 523–538, 1977.

Waespe W, Henn V. Velocity response of vestibular nucleus neurons during vestibular, visual, and combined angular-acceleration. *Exp Brain Res* 37: 337–347, 1979.

Wandell BA. *Foundations of Vision*. Sunderland, MA: Sinauer Associates, 1995.

Wozny DR, Shams L. Recalibration of auditory space following milliseconds of cross-modal discrepancy. *J Neurosci* 31: 4607–4612, 2011.

Young LR, Dichgans J, Murphy R, Brandt T. Interaction of optokinetic and vestibular stimuli in motion perception. *Acta Otolaryngol* 76: 24–31, 1973.

Yuille AL, Bulthoff HH. Bayesian decision theory and psychophysics. In: *Perception as Bayesian Inference*, edited by Knill DC and Richards W. Cambridge: Cambridge University Press, 1996.

Zupan LH, Merfeld DM, Darlot C. Using sensory weighting to model the influence of canal, otolith and visual cues on spatial orientation and eye movements. *Biol Cybern* 86: 209–230, 2002.

4. GENERAL DISCUSSION

4.1 Summary of Main Findings

In **chapter 3.1** I showed that cortical oscillations in the alpha band reliably encoded natural rotational VS. Analysis of spectral power during transient and constant velocity rotations showed significant spectral suppression in the alpha band for healthy subjects, but not for patients with bilateral vestibular loss (BVPs). This effect was strongest over temporo-parietal scalp regions. Beta oscillations did not differ between healthy subjects and BVPs, and gamma band oscillations reflected residual VOR and microsaccades. This novel finding demonstrated that cortical oscillations in the alpha band respond to VS in the same manner as for other sensory stimuli, such as visual and somatosensory (Niedermeyer, 2005). Furthermore, this study overcame numerous technical/analytical challenges that have limited previous vestibular EEG studies. Firstly, as demonstrated by the evoked potential analysis of the same data, our preprocessing regime removed rotation-related artefacts that may have contaminated past vestibular evoked potential studies (Hood and Kayan, 1985; Durrant and Furman, 1988; Probst et al., 1995). Secondly, we demonstrated the validity of spectral analysis as a tool for mapping cortical vestibular function, bringing it in line with other sensory modalities such as vision and touch that are also modulate alpha band power (Niedermeyer, 2005). Thirdly, spectral analysis offers advantages over time domain evoked responses by isolating the vestibular response to the alpha band and eye movement artefacts to gamma band (Yuval-Greenberg et al., 2008).

In **chapter 3.2** I expanded on the results of paper 1, demonstrating that alpha band suppression in response to constant velocity VS had the same properties and temporal dynamics as subcortical vestibular processes. Specifically, spectral power was compared to the VOR to see if: 1) spectral power was modulated by velocity in the same manner as the slow-phase of the VOR, and 2) the temporal dynamics of initial spectral modulation matched that of the VOR, which decays exponentially. Our results confirmed that alpha band power followed the same trajectory as the VOR. However early alpha band power, when vestibular activity was maximal, was not significantly increased with velocity in a manner predicted by the VOR. Importantly, alpha band power decayed back to baseline levels exponentially from maximum suppression with a time constant equal to the VOR, and in the range of previous studies of subcortical neurons in monkeys and VOR in humans (Waespe

and Henn, 1977; Okada et al., 1999; Bertolini et al., 2011). This finding further cemented alpha band oscillations as a marker of vestibular activity in the human cortex. Oscillations in the beta band had a lower quality fit than alpha, and gamma band oscillations did not decay exponentially.

In **chapter 3.3** we explored the perceptual nature of visual-vestibular integration. We demonstrated that visual and vestibular information are optimally integrated at the perceptual level according to the MLE model. Importantly, we showed that we discard individual visual and vestibular cues and rely only on a "fused" cue to make perceptual judgements. Does the neural correlate of this multisensory percept also fuse, or are visual and vestibular cues represented separately in the cortex? The research in paper 3 gives us a foothold to begin answering such questions about how vestibular information is processed and integrated at the cortical level.

4.2 Ongoing Work

4.2.1 Effects of Long-Term Sensory Adaptation on Visuo-Vestibular Integration

Certain specially trained sub-groups of the population (e.g. athletes, video-game players, etc…) train specific senses over long periods of time. Do these specialized populations integrate sensory information in the same way as untrained subjects? Here, we studied the effect of long-term sensory adaptation on visuo-vestibular sensory integration.

We recruited from two highly trained groups in disciplines relying on visual and vestibular senses: experienced competitive figure skaters and regular video game players of first person shooter (FPS) games. Experimental protocols were identical to those previously presented in paper 3, which studied integration in normal, non-specialized subjects. Participants made relative judgements about the size of two consecutive yaw rotations comprised of visual-only, vestibular-only, or a combined visual-vestibular bimodal stimulus.

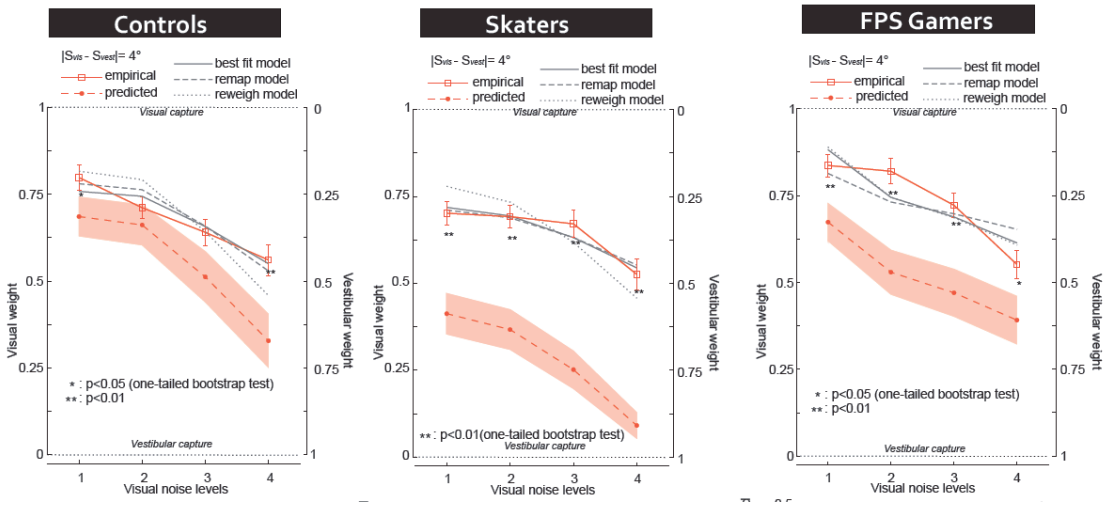

Figure 4.1: Empirical and MLE predicted results for control subjects (LEFT), figure-skaters (MIDDLE), and FPS gamers (RIGHT). Note the significant visual bias for the skaters and FPS gamers at each visual noise level.

Our results demonstrated that all three groups integrated visual and vestibular cues in a statistically optimal manner that was predicted by our model, suggesting that long-term sensory adaptation to visual-only (FPS group) or visual-vestibular (figure skaters) rotational stimuli does not compromise optimal reduction of uncertainty in the integrated percept. However, both groups exhibited a significant visual bias in the conflict cases as demonstrated by significantly higher-than-predicted weighting of the visual cue at each level of visual noise. The smaller visual bias in control subjects was only significant for the highest level of visual noise. We account for this visual bias using our model and show that its origin is different for each group; a re-mapping of the visual cue for control and figure skaters, and a re-weighting of the visual cue for the FPS group (Fig. 4.1).

4.2.2 Visuo-Vestibular Integration in Patients with Vestibular Deficits

We tested the visuo-vestibular integration paradigm presented in chapter 3.3 on groups of patients with vestibular deficits. The first group of patients was diagnosed with unilateral vestibular loss. Here we asked three research questions: 1) is visuo-vestibular integration present in unilateral patients, 2) if present, is this integration optimal, 3) is sensory integration equal on the healthy and deficit sides.

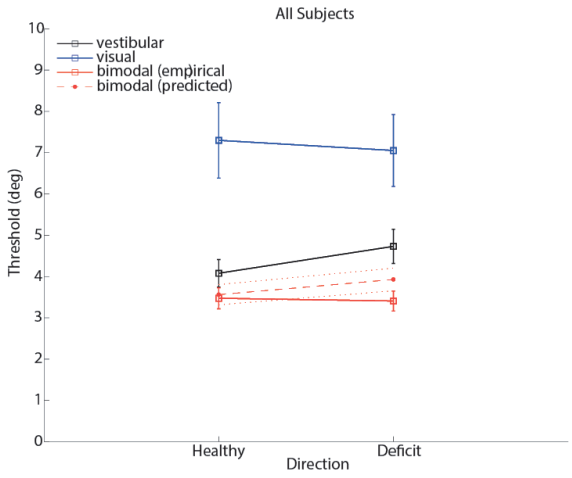

Figure 4.2: Perceptual thresholds for unilateral vestibular patients for rotations in their healthy and deficit directions. Blue line represents the vestibular cue, black line the visual cue, solid red line the empirically measured bimodal cue, and dashed red line the predicted MLE bimodal cue.

Results showed that unilateral patients also integrate optimally when turning in both directions; performance did not differ from the MLE prediction for test conditions in the healthy or deficit directions. However, note that empirical bimodal and visual cues were significantly different in the deficit direction, but not statistically different in the healthy direction. This indicates that unilateral patients integrate visuo-vestibular cues differently on their healthy and deficit sides (Fig. 4.2).

The second group was composed of patients with “mystery” vertigo. All of these subjects suffered from vertigo episodes, but presented clinically with no neurological or vestibular deficits. We hypothesized that that the source of these episodes was irregular or deficient integration of visual and vestibular cues, and therefore our analysis technique might help clinicians with diagnosis and treatment. However the results of this study were inconclusive, probably due to the wildly different causes of the vertigo spells.

4.3 Outlook

The work presented in this thesis shines new light on vestibular processing in humans. Chapters 3.1 and 3.2 showed that power in the alpha band reliably encodes natural vestibular stimulation of the horizontal semicircular canals, which allows a new line of research connecting an extensive literature on alpha band modulations in response to sensory, motor, and cognitive tasks and vestibular processing. This effect should be studied in greater depth for the other organs of the vestibular

labyrinth. Specifically, do alpha band oscillations respond to stimulation of the posterior or anterior canals in the same manner as found for the horizontal canals? Does this alpha response change if more than one canal is stimulated simultaneously? Furthermore, stimulation of the otolithic organs through linear whole body accelerations, which would presumably suppress alpha in the same manner that angular VS does, needs to be examined. This work is crucial to elucidate whether or not modulation of alpha band oscillations is a universal response to VS of any kind.

Another new avenue might be the exploration of vestibular processing and multisensory integration in the cortex. As Waespe and Henn (1977) showed with recordings in monkey vestibular nuclei neurons during vestibular, visual, and visual-vestibular stimulation, interesting non-linear processing occurs that alters the temporal dynamics of the neuronal response when visual stimulation is combined with CVVS. According to these important results, visual and vestibular information complement each other to reliably encode the velocity of rotation *without* the exponential decay observed in response to VS alone. Do alpha band oscillations respond in the same manner when visual stimuli are present, cancelling the exponential decay reported here? Does this effect change when there is a conflict between the visual and vestibular stimuli? The research presented in this thesis facilitates answering these questions and other important facets of multisensory integration in the human cortex.

Could this neural correlate be of clinical value? As outlined in chapter 4.2 of this thesis, we have already attempted to use perceptual multisensory integration tasks to understand and perhaps diagnose patients with vestibular deficits. Is the alpha suppression weaker, as demonstrated for the BVPs in chapter 3.1, during VS for patients with other types of vestibular deficits? More work needs to be done in order to better understand how alpha oscillations are affected by concurrent visual-vestibular stimulation before it can be used as a diagnosis tool, but it remains an intriguing possibility.

The work presented in this thesis represents a step forward in understanding vestibular processing. While more research needs to be carried out in order to bring

knowledge of vestibular processing in line with other sensory modalities, the work in this thesis offer new avenues to tackle this important question.

5. BIBLIOGRAPHY

Angelaki DE, Cullen KE (2008) Vestibular system: the many facets of a multimodal sense. Annu Rev Neurosci 31:125–150.

Angelaki DE, Klier EM, Snyder LH (2009) A vestibular sensation: probabilistic approaches to spatial perception. Neuron 64:448–461.

Berger H (1929) Über das Elektrenkephalogramm des Menschen. Arch. Psychiatr. Nervenkr. 87:527–570.

Bertolini G, Ramat S, Laurens J, Bockisch CJ, Marti S, Straumann D, Palla a (2011) Velocity storage contribution to vestibular self-motion perception in healthy human subjects. J Neurophysiol 105:209–223.

Brandt T, Dieterich M (1999) The Vestibular Cortex: Its Locations, Functions, and Disorders. Ann N Y Acad Sci 871:293–312.

Butler JS, Smith ST, Campos JL, Bülthoff HH (2010) Bayesian integration of visual and vestibular signals for heading. 10:1–13.

Buttner U, Waespe W (1981) Vestibular nerv activity in the alert monkey during vestiublar and optokinetic nystagmus. Exp Brain Res:310–315.

Cohen B, Henn V, Raphan T, Dennett D (1981) Visual-vestibular interactions in humans. Annals New York Academy of Sciences. New York 00157:421–433.

Cullen KE, Sadeghi S (2008) Vestibular system. Scholarpedia, 3(1):3013.

Dieterich M, Brandt T (2000) Brain activation studies on visual-vestibular and ocular motor interaction. Curr Opin Neurol 13:13–18.

Durrant JD, J.M.R. Furman (1988) Long-latency rotational evoked potentials in subjects with and without bilateral vestibular loss. Electroencephalogr Clin Neurophysiol:251–256.

Fernandez C, Goldberg JM (1971) Physiology of peripheral neurons innervating semicircular canals of the squirrel monkey. I. Resting discharge and response to constant angular accelerations. J Neurophysiol 34:635–660.

Fetsch CR, Turner AH, Deangelis GC, Angelaki DE (2009) Dynamic Reweighting of Visual and Vestibular Cues during Self-Motion Perception. J Neurosci 29:15601–15612.

Gastaut H (1952) Electrocorticographic study of the reactivity of rolandic rhythm. Rev Neurol 87:176–182.

Guldin WO, Grusser O-J (1998) Is there a vestibular cortex? Trends Neurosci 21:254–259.

Haegens S, Händel BF, Jensen O (2011) Top-Down Controlled Alpha Band Activity in Somatosensory Areas Determines Behavioral Performance in a Discrimination Task. J Neurosci 31:5197–5204.

Haegens S, Luther L, Jensen O (2012) Somatosensory Anticipatory Alpha Activity Increases to Suppress Distracting Input. J Cogn Neurosci 24:677–685.

Hari R, Salmelin R (1997) Human cortical oscillations: a neuromagnetic view through the skull. Trends Neurosci 20:44–49.

Hillis JM, Ernst MO, Banks MS, Landy MS (2002) Combining sensory information: mandatory fusion within, but not between, senses. Science 298:1627–1630.

Hood JD, Kayan A (1985) Observations upon the evoked responses to natural vestibular stimulation. Electroencephalogr Clin Neurophysiol 62:266–276.

Klimesch W (1999)" EEG alpha and theta oscillations reflect cognitive and memory performance: a review and analysis. Brain Res Brain Res Rev 29:169–195.

Knill DC, Pouget A (2004) The Bayesian brain: the role of uncertainty in neural coding and computation. Trends Neurosci 27:712–719.

Lopez C, Blanke O (2011) The thalamocortical vestibular system in animals and humans. Brain Res Rev:119–146.

Lopez C, Blanke O, Mast FW (2012) The human vestibular cortex revealed by coordinate-based activation likelihood estimation meta-analysis. Neuroscience 212:159–179.

Niedermeyer E (2005) The normal EEG of the waking adult. In: Electroencephalography. Basic principles, clinical applications, and related fields (Fifth edition)., pp 167–192. Philadelphia: Lippincott Williams & Wilkins.

Okada T, Grunfeld E, Shallo-Hoffmann J, Bronstein a M (1999) Vestibular perception of angular velocity in normal subjects and in patients with congenital nystagmus. Brain 122:1293–1303.

Pineda JA (2005) The functional significance of mu rhythms: Translating "'seeing'" and "'hearing'" into "'doing.'" Brain Res Rev 50:57–68.

Probst T, Katterbach T, Wist ER (1995) Vestibularly evoked potentials (VESTEPs) of the horizonal semicircular canals under different body positions in space. J Vestib Res 5:253–263.

Prsa M, Gale S, Blanke O (2012) Self-motion leads to mandatory cue fusion across sensory modalities. J Neurophysiol 108:2282–2291.

Purves D, Augustine GJ, Fitzpatrick D, Hall WC, LaMantia AS, McNamara JO, White LE (2007) Neuroscience (Fourth edition).,pp 343-362. Sunderland: Sinauer Associates, Inc.

Raphan T, Matsuo V, Cohen B (1979) Velocity Storage in the Vestibulo-Ocular Reflex Arc. Exp brain Res 35:229–248.

Romei V, Brodbeck V, Michel C, Amedi A, Pascual-Leone A, Thut G (2008) Spontaneous Fluctuations in Posterior alpha-Band EEG Activity Reflect Variability in Excitability of Human Visual Areas. Cereb Cortex 18:2010–2018.

Sauseng P, Klimesch W, Stadler W, Schabus M, Doppelmayr M, Hanslmayr S, Gruber WR, Birbaumer N (2005) A shift of visual spatial attention is selectively associated with human EEG alpha activity. Eur J Neurosci 22:2917–2926.

Waespe W, Henn V (1977) Brain Neuronal Activity in the Vestibular Nuclei of the Alert Monkey during Vestibular and Optokinetic Stimulation. Exp Brain Res 538:523–538.

Yuval-Greenberg S, Tomer O, Keren AS, Nelken I, Deouell LY (2008) Transient induced gamma-band response in EEG as a manifestation of miniature saccades. Neuron 58:429–441.

6. APPENDIX

6.1

Paper IV – Visuo-neural discrepancies modulate the sense of agency for brain-machine actions.

Learning to integrate contradictory multisensory self-motion cue pairings

Mariia Kaliuzhna[1,2], Mario Prsa[1,2], Steven Gale[1,2], Stella J. Lee[1,2,4], Olaf Blanke[1,2,3]

[1] Center for Neuroprosthetics, School of Life Science, Ecole Polytechnique Fédérale de Lausanne, Lausanne, Switzerland

[2] Laboratory of Cognitive Neuroscience, Brain Mind Institute, School of Life Science, Ecole Polytechnique Fédérale de Lausanne, Lausanne, Switzerland

[3] Department of Neurology, University Hospital, Geneva, Switzerland

[4]Harvard-MIT Division of Health Sciences and Technology, Harvard Medical School

Olaf Blanke

Center for Neuroprosthetics & Brain Mind Institute

Faculty of Life Sciences

Ecole Polytechnique Fédérale de Lausanne

1015 Lausanne

Switzerland

Tel: + 41 21 693 18 22

e-mail: olaf.blanke@epfl.ch

Abstract

Humans integrate multisensory information to reduce perceptual uncertainty when perceiving the world and self. Integration however fails if a common causality is not attributed to the sensory signals, as would occur in conditions of spatio-temporal discrepancies. In the case of passive self-motion, visual and vestibular cues are integrated according to statistical optimality, yet the extent of cue conflicts that do not compromise this optimality are currently underexplored. Here, we investigate whether human subjects can learn to integrate two arbitrary, but co-occurring, visual and vestibular cues of self-motion.

Participants made size comparisons between two successive whole body rotations using only visual, only vestibular, and both modalities together. The vestibular stimulus provided a yaw self-rotation cue, the visual – a roll (Experiment 1) or pitch (Experiment 2) rotation cue. Experimentally measured thresholds in the bimodal condition were compared with theoretical predictions derived from the single cue thresholds.

Our results show that human subjects combine and optimally integrate vestibular and visual information, each signalling self-motion around a different rotation axis (yaw vs. roll and yaw vs. pitch). This finding suggests that the experience of two temporally co-occurring but spatially unrelated self-motion cues leads to inferring a common cause to these two initially unrelated sources of information about self-motion. We discuss our results in terms of specific task demands, cross-modal adaptation and spatial compatibility. The importance of these results for understanding of bodily illusions is also discussed.

Key words: multisensory integration, multisensory conflict, self-motion, vestibular.

Introduction

During passive self-motion (be it heading or rotation), an observer derives the direction, speed and the distance travelled from an optimal combination of redundant information provided by different sensory cues: visual, vestibular, auditory, and tactile sensations (Gibson, 1950; Kapralos, Zikovitz, Jenkin, & Harris, 2004; Warren & Wertheim, 2014). To date, in order to account for such processes Bayesian statistics of sensory cue combination are used, which describe how the perceptual uncertainty associated with the sensory cues (due to noisy sensory and neural processing) is reduced according to statistical optimality when multiple uncertain estimates of the same physical property are probabilistically combined (Ernst and Banks 2002).

Computational theories of multisensory integration posit integration when a common cause is assumed for the sensory cues (Körding et al. 2007; Parise, Spence, and Ernst 2012; Shams and Beierholm 2010). The probability of a common cause depends on how similar/correlated these cues are and on the observer's prior beliefs/knowledge about the possible common cause. In daily life under normal conditions visual and vestibular stimuli signalling self-motion are most likely congruent and highly correlated, which results in their integration and mandatory fusion even in the presence of slight conflicts between them (Butler et al., 2010; Fetsch et al., 2009; Jürgens & Becker, 2006; Prsa et al., 2012). Accordingly, it is also assumed that integration should break down if the conflict between the stimuli is too large, implying that they relate to different sources. Such latter conflicts could also mean that that there is no correlation between stimuli. In the present study we address the limits of visuo-vestibular integration by testing spatially conflicting multisensory (visuo-vestibular) cues.

Previous work has shown that large degrees of directional conflict (that are consciously detected by the participant) do not lead to integration of visual, vestibular, and proprioceptive self-motion cues (Ohmi 1996) (similar results have been obtained for conflicting cues about external objects (Bertelson & Radeau, 1981; Gebhard & Mowbray, 1959; Gepshtein et al., 2005; Lunghi, Morrone, & Alais, 2014; Pick, Warren, & Hay, 1969; Recanzone, 2003; Welch & Warren, 1980). Specifically for small degrees of conflict it has been found that integration occurs, whereas for larger degrees of conflict such

interactions between the two modalities are no longer observed (Gepshtein et al., 2005; Roach et al., 2006; Wallace et al., 2004)).

However, it has also been shown that multisensory cues can influence one another despite the absence of perceptual unification. Also, participants who initially do not integrate arbitrary cue pairings, may learn to combine them when these stimuli temporally co-occur over time (i.e. arbitrary but correlated stimuli) (Bresciani et al., 2005; M. O. Ernst, 2007; Wozny & Shams, 2011). Additionally, the particular demands of the task an observer has to perform might also influence the integration process (Roach, Heron, & McGraw, 2006). Thus, it appears possible that multiple parameters of conflicting stimuli could be taken into account which will determine whether integration occurs: the amount of conflict, the task at hand, the amount of correlating characteristics of the stimuli. The exact contribution of each of these parameters to the integration process remains, however, unknown.

In our previous work, we have demonstrated that human observers integrate congruent yaw visual and vestibular rotation cues according to statistical optimality (Prsa et al., 2012). Here, with an identical experimental apparatus and task design, we address whether repeated exposure to overtly spatially incongruent (but correlated on other dimensions) multisensory self-motion stimuli (visual and vestibular) results in optimal cue integration. Our participants were simultaneously exposed to whole body yaw rotations in conjunction with synchronised optic flow rotation around a different axis (roll, Experiment 1). We asked participants to compare the sizes of two successively experienced rotation angles and determined probabilistic descriptions of their perceptual estimates. Our data revealed that the variance associated with these incongruent visual-vestibular cue pairings decreased over time and approached the statistically optimal predictions derived from the variances of the single cue estimates. We argue that our results be accounted for by a progressively increasing probability of attributing a common cause to the two incongruent stimuli. Further evidence for such integration was found when simultaneously exposing participants to whole body yaw rotations in conjunction with synchronized optic flow rotation around the pitch axis (Experiment 2), which resulted in optimality right from the onset. We discuss the

implications of our finding in the context of multisensory integration, own-body perception, and vestibular symptoms in neurological patients.

Materials and Methods

Participants

Eight healthy adults naïve to the purpose of the study with normal or corrected vision and no history of inner ear disease participated in each experiment (Experiment 1: 2 females, mean age 24 ± 2.7 yr; Experiment 2: 3 females, mean age 22 ± 3.9 yr). Three participants from experiment 1 also participated in experiment 2. All participants gave informed consent and received monetary compensation at 20 CHF/hour. The studies were approved by a local ethics committee and were conducted in accordance with the Declaration of Helsinki.

The optimal observer model (OBE)

When perceiving a whole-body rotation of size S each sensory modality provides an independent estimate of S. Perceptual uncertainty is naturally associated with each of the unimodal estimates, the visual and the vestibular in our case, and can be measured as their trial-by-trial variance σ_{vi}^2 and σ_{ve}^2, respectively. Maximum likelihood estimation (derived from Bayes' rule) dictates that if the two unimodal cues are integrated according to statistical optimality, the uncertainty associated with the bimodal estimate σ_{bi}^2 is reduced relative to unimodal uncertainties according to:

$$\sigma_{bi}^2 = \frac{\sigma_{vi}^2 \sigma_{ve}^2}{\sigma_{vi}^2 + \sigma_{ve}^2} \qquad (1)$$

Experimental setup

Subjects were seated in a centrifuge cockpit-style chair which delivered passive whole body rotational stimuli (Figure 1). After adopting a comfortable position, the subjects were restrained by a five-point racing harness, feet-straps and extra cushioning. To prevent the subject's head from moving, a chinrest and a head-fixation at the forehead were used.

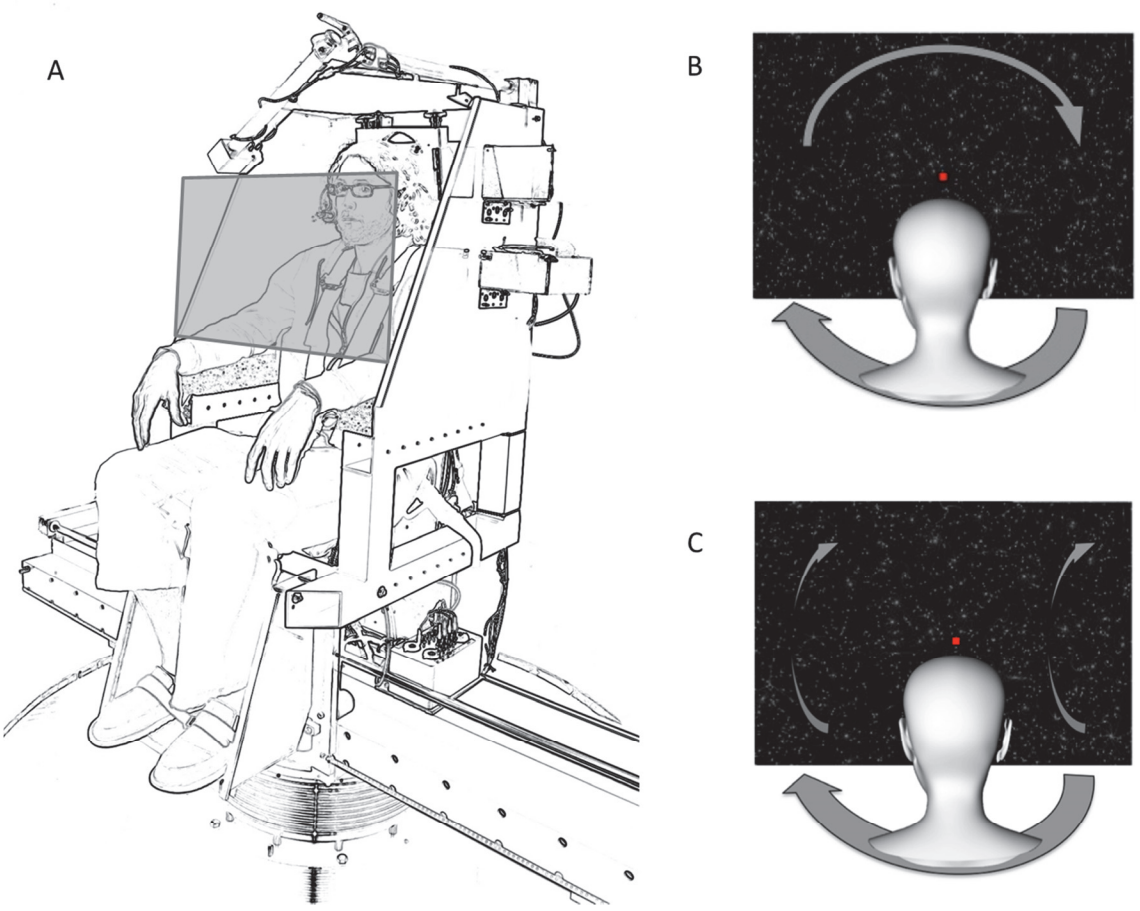

Figure 1. Experimental setup and experimental conditions

A. Experimental setup. Participants were seated in a human motion platform that delivered yaw whole body rotations. A 3D monitor was positioned in front of the participant and showed a pattern of stereoscopic moving dots that simulated either roll (B, experiment 1) or pitch (C, experiment 2) self-motion.

The chair was digitally servo-controlled (PCI-7352) and had very precise positioning of around 0.1°. The chair always rotated in the yaw plane and was centred on the rotation axis, restraining the vestibular stimuli to angular accelerations only. The rotation profiles of the chair were pre-set and designated the immediate angular position of the chair at a rate of 100 Hz. The velocity profile *v(t)* of the rotations was a single cycle of 0.77 – Hz raised cosine function

$$v(t) = \frac{A}{T}\left[1 - \cos\left(\frac{2\pi t}{T}\right)\right] \qquad (2)$$

where A is rotation size and T is its duration (T = 1.3 s in this case). Instantaneous angular position $p(t)$ is then specified as

$$p(t) = A\left[\frac{t}{T} - \frac{1}{2\pi}\sin\left(\frac{2\pi t}{T}\right)\right] \qquad (3)$$

The visual stimuli were presented on a 22 inch display, which was fixed to the chair in front of the subject at a distance of about 29cm. The limited visual field covered ~80° of horizontal and 56° of vertical visual angle. The visual image consisted of a stereoscopic pattern of randomly distributed moving dots of different size. The dots were two dimensional symmetric greyscale Gaussian blobs with a minimum and maximum standard deviation of 0.5 and 3 pixels respectively. For each blob, the standard deviation was drawn from an exponential distribution with a rate parameter of 2 and the peak pixel intensity from a uniform distribution between 0.1 and 0.3 (1 denotes maximum intensity, i.e. white). The binocular disparity was a linear function of blob standard deviation, and yielded minimum and maximum values of 0 (for the maximum sized dots) and 50 (for the minimum sized dots) pixels, respectively. All dots had therefore zero or positive stereoscopic depth. The dot density was set to 0.002 dots/pixel producing roughly 3500 dots in any given frame of the 1680 by 1050 resolution display. Their lifetime was not limited and their initial position reset at the start of every trial. Rotation was simulated by placing the subject's view-point in the middle of the scene and rotating it either around the roll axis (Experiment 1) or the pitch axis (Experiment 2). These patterns simulated the actual optic flow that would result from physically rotating the subject around these axes in congruent directions. During the rotations in all conditions subjects were instructed to fixate a stationary central point, which was a filled red circle with a radius of 3 pixels, 0.5 intensity level and was presented at zero binocular disparity. The stereoscopic stimulus was generated by the Nvidia Quadro FX 3800 graphics card using the OpenGL quad-buffer mechanism. The stimulus was programmed with the Python language and viewed with the Nvidia 3D Vision kit (active shutter glasses) paired with a Samsung Syncmaster 2233RZ display (120-Hz refresh rate) via an infrared transmitter. The velocity of the optic flow matched that of the rotating chair. While subjects performed the task masking white noise was presented over headphones.

Experimental paradigm

Subjects were seated in the rotating chair with a computer screen in front of them. On every trial they experienced two successive rotations (a standard and a test) and had to judge their relative size. The rotations were either delivered by the chair alone, simulated by the motion of the visual field on the display, or were a combination of both (on every trial the two rotations were of the same kind). The size of one of the two rotations was always 20° (i.e. the standard rotation) and the size of the second (i.e. the test rotation) was one of 7 equally spaced angles in the interval of 12°-27° tested using the method of constant stimuli (see Prsa et al., 2012 for a similar procedure). The two rotations were preceded, followed, and separated by an interval of 0.5 s. A 2-s period followed during which the subjects had to answer, via a button press, whether the second rotation was bigger or smaller than the first. The standard rotation was randomly assigned to come either first or second.

Subjects came in on two different days. On the first day we determined their unimodal discrimination thresholds (see Data analysis below) for the vestibular and the visual modalities separately. In Experiment 1, participants performed the same task as described above for vestibular yaw rotations and visual roll rotations. In Experiment 2, the same task was performed, but with vestibular yaw and visual pitch rotations. They first completed several blocks of vestibular-only stimuli, where the different test angles were presented in a randomised order. Each block contained 35 trials and lasted for about 5 minutes. Participants performed a minimum of 280 trials (in total) amounting to 40 trials per test angle. After extracting participants' thresholds for the vestibular modality we used the same procedure for the visual modality. In order to match participants' visual threshold to their vestibular threshold we manipulated the reliability of the visual stimulus by changing the coherence of the visual motion (number of dots simulating rotation/number of dots moving randomly). The random dots moved in a straight line with the identical displacement velocity profile as the rotation. The overall displacement size was limited to 200 pixels in horizontal and vertical directions and was drawn from a uniform distribution. The radial motion direction was randomly chosen for each dot between -180° and 180° (uniform distribution). The random dots were also Gaussian blobs with identical parameters and therefore visually

indistinguishable (when stationary) from the blobs simulating rotation. Their initial positions were also reset at the start of each trial. Participants performed a minimum of 4 visual-only blocks (140 trials, 20 trials per test angle) with a given level of coherence; if their performance matched that of the vestibular modality this level of coherence was retained, otherwise it was changed and the procedure continued as described before until a matched level was obtained. The experimentally established levels of visual coherence corresponding to matched discrimination thresholds in the two single modalities were then used for Experiment 1; they were 100% for four subjects, 95% for 1 subject, 85% for 2 subjects and 80% for 1 subject. Analogously, for Experiment 2 the used levels were 100% for 3 subjects, 95% for 3 subjects and 85% for 2 subjects. Overall, subjects performed a mean of 557.5 trials for each modality (about 40 repetitions of each test angle for each modality).

On the second day, subjects performed the task, but were now exposed to the three conditions: unimodal vestibular, unimodal visual, and both modalities together. For bimodal comparisons, visual and vestibular stimuli were temporally synchronized and occurred simultaneously (e.g. Prsa et al., 2012). The experiment was divided into sessions of approximately 5 minutes that we grouped into 6 blocks (the comparisons between these blocks allowed to test for progressive learning of the visuo-vestibular association). Every session contained trials of each of the three conditions presented in a randomised order, which made it impossible to predict which condition will occur next. Subjects performed a total of 420 trials for each of the three conditions, 70 trials per block per condition, 10 trials per test angle per condition (i.e. 60 trials per test angle for each of the conditions). The direction of rotation (left or right for vestibular yaw and visual roll; up or down for pitch) was randomly chosen on each trial. In Experiment 1, left yaw rotations were always arbitrarily paired with right visual roll rotations (i.e. simulating a left roll self-rotation) and right yaw rotations with left visual roll rotations. In Experiment 2, left yaw was always arbitrarily paired with down visual pitch rotations (and right yaw rotations with up pitch rotations).

Data analysis

The data analysis was done using custom programs compiled in MATLAB (MathWorks). During the pre-test, in order to match the performance between the two modalities, we

pooled the answers obtained for each test angle separately for the vestibular and visual conditions. For the analysis, the test angle was always compared to the standard angle, regardless of their order of occurrence in a trial. The proportion of "bigger" responses was calculated and fit with a cumulative Gaussian function. From this fit we obtained discrimination thresholds for the two modalities. In order to match these thresholds we manipulated the reliability of the visual cue as described earlier.

The analysis for the actual experiments was run in a similar fashion. Answers obtained for each test angle were pooled across all subjects to obtain a probabilistic measure and create a sufficient sample set for statistical comparisons. From the variance of the Gaussian fits to the proportion of "bigger" answers we obtained the measure of the discrimination threshold for each of the three conditions. We next conducted a bootstrap analysis to compare the predictions of the optimal observer model to the experimentally obtained values. To this end, we repeated the data fit for each condition 9999 times using a different subset of responses every time. The different subsets were formed by taking at random, with replacement, *N* trials from the total set of *N* for each test angle. The standard deviation of 9999 repeated measures is then the standard error of the measure obtained using the original data set. Statistical tests were made by assessing the amount of overlap between the bootstrap iterations of two measures. If the measure of interest is σ, and σ_{ex}^{j} and σ_{pr}^{j} are its experimental and predicted estimates obtained from the *j*th bootstrap sample, then the one tailed bootstrap probability of ($\sigma_{ex} > \sigma_{pr}$) is

$$p = \frac{1}{B}\sum_{j=1}^{B} I\left(\sigma_{ex}^{j} - \sigma_{pr}^{j} > 0\right),$$

where B = 9,999 and $I()$ is the indicator function, which is equal to 1 when its argument is true and 0 otherwise. The inequality would be reversed for the probability of ($\sigma_{ex} < \sigma_{pr}$). The one-tailed bootstrap *P* value is therefore simply the proportion of ($\sigma_{ex}^{j} - \sigma_{pr}^{j}$) values that are more extreme than 0. We prefer this approach to parametric testing because it provides a direct computation of the cumulative distribution of a test statistic instead of having to use an asymptotic approximation.

The threshold values obtained through the bootstrapping were also analysed using repeated measures ANOVAs. In the group analysis (see Results section) the threshold

values pooled across subjects were used in a 6 x 3 ANOVA (with 6 blocks and 3 conditions as factors). For the single subject analysis the ANOVAs were performed on the bootstrapped values of single subjects for each block and condition. Bonferroni post-hoc comparisons were used to explore the result of the interactions.

Results

For both experiments the same analyses were performed. We first explored the results of our subjects as a group and then conducted more detailed analyses on single subject data.

Experiment 1. Vestibular yaw and visual roll: Group analysis.

A 6 x 3 repeated measures ANOVA with blocks (6) and conditions (3) as factors yielded significant main effects and interaction (all $p<0.0001$). All Bonferroni post-hoc comparisons were significant, (all $p<0.0001$; except for block 5 visual unimodal threshold not being different from block 2 vestibular unimodal threshold). Next, we performed a one-tailed bootstrap analysis collapsing all blocks for all participants, which revealed a significant difference between the two single cues (vestibular threshold 6.0, visual threshold 5.3; $p=0.004$). The bimodal threshold was significantly different form the best single cue, i.e. visual (bimodal threshold 4.6; $p=0.0001$) as well as from the threshold predicted by the OBE (predicted threshold 3.97; $p=0$).

We further divided the data (pooled across subjects, as described in the Data analysis section) according to the six experimental blocks that our participants performed. Figure 2 summarises the experimentally obtained and predicted discrimination thresholds for each of the six experimental blocks. In the first four blocks the difference between the best single cue thresholds and the bimodal thresholds did not differ significantly (all $p>0.1$). Bimodal thresholds – measured experimentally and those predicted by the OBE model – also differed significantly (one-tailed bootstrap test, $p<0.03$), compatible with the absence of statistically optimal visual-vestibular integration. A significant difference between the best single cue thresholds and the empirically measured bimodal thresholds emerged only in the last two blocks ($p<0.02$), signalling integration. In these last two blocks participants' bimodal thresholds also became not statistically different from the predicted thresholds ($p>0.05$) (Figure 2).

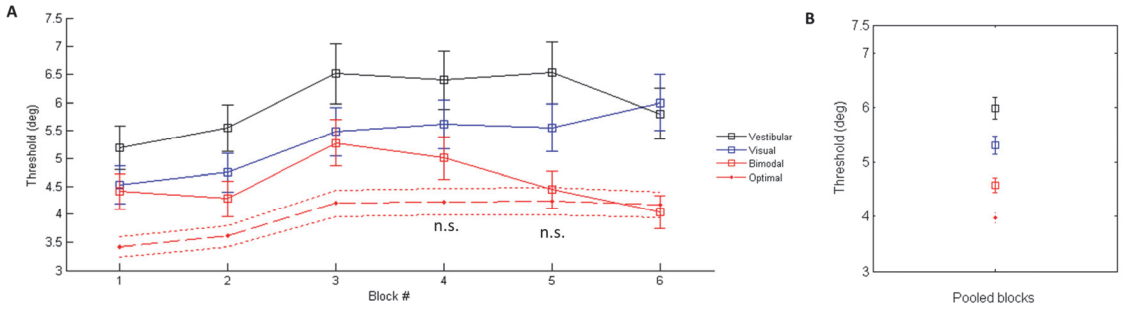

Figure 2. Experiment 1 (vestibular yaw + visual roll stimulation).

A. Integration of vestibular and visual cues in experiment 1 is shown across the six blocks. The difference between the predicted and the experimentally measured threshold becomes non-significant in the last two blocks, compatible with optimal visual-vestibular integration. Blocks, where the bimodal threshold is not significantly different from the predicted one (i.e. optimal integration) are marked by "n.s." ($p>0.05$, one-tailed bootstrap test). Error bars represent bootstrap standard error. **B**. The same analysis performed collapsing across blocks and participants.

We next conducted a more detailed analysis of each condition separately (visual, vestibular and visual-vestibular) over the six blocks. Table 1 contains the results of the linear regression analysis for each condition over the experimental blocks as well as the p-values of the bootstrap test comparing the thresholds of the first and last blocks. For the unimodal vestibular condition, no significant changes of the discrimination thresholds were observed over time (r^2 =0.31, p=0.25). The same analysis for the unimodal visual condition showed a significant difference between the first and last experimental blocks (p=0.005) due to a linear increase of the threshold values (r^2=0.89, p=0.005). Finally, the bootstrap test for the bimodal condition showed that the thresholds did not significantly change between the initial and final blocks (p=0.19) (a linear change was not observed, r^2=0.03, p=0.73). There was no significant difference between the vestibular and the visual unimodal threshold values in any of the blocks indicating well-matched single cue reliabilities between the two sensory modalities. This suggests that the emergence of optimal multisensory integration for incongruent but temporally co-occurring visual-vestibular stimuli is in our case revealed by a stable bimodal threshold which did not accompany a progressive increase in the visual

threshold, thereby exposing a relative reduction of perceptual variance when cues are combined.

Table 1

Between-block comparisons for each condition in both experiments

Condition	Linear regression		Bootstrap *p-value*
	R^2	*p-value*	Block 1 to 6
Experiment 1(yaw + roll)			
vestibular	0.31	0.25	0.15
visual	0.89	0.01	0.01
bimodal	0.03	0.73	0.19
Experiment 2(yaw + pitch)			
vestibular	0.90	0.00	0.02
visual	0.01	0.88	0.45
bimodal	0.04	0.71	0.25

R^2 and p-values of the linear regression and bootstrap analysis within each condition for the two experiments. Values in red represent a significant change in threshold values across blocks.

Experiment 1. Vestibular yaw and visual roll: Single subject analysis

We performed 6 x 3 (block by condition) repeated measures ANOVAs on the values for each subject generated by the bootstrap procedure. Bonferroni post-hoc comparisons between the bimodal and the best unimodal cue showed integration for four subjects: for subject 3 in block 6, for subject 4 in all blocks except block 4, for subject 5 – integration only in block 5 and for subject 6 in all blocks except block 3 and 6. To quantify the extent of overall integration for each subject we performed a within subject test comparing the bimodal threshold to the predicted threshold values (Figure 4 and Table 2). The tests were performed by pooling all blocks together per subject in order to yield enough data points for a statistical comparison. Four subjects out of eight in Experiment 1 show optimal integration. Out of the four remaining subjects for whom

this analysis showed no optimal integration, subject 1 showed integration in the last two blocks (optimal in block 6), subject 3 showed integration only in block 6, subject 5 – only in block 5, and subject 8 – in blocks 4 and 6 (see Figure 4). The differences between this analysis and the results of the ANOVA are due to the latter results being skewed by high threshold values in one of the conditions in one of the blocks for some subjects.

To assess inter-subject variability we analysed the performance of individual subjects in each of the six experimental blocks (Figure 5). To quantify the extent of integration, we subtracted the bimodal threshold values (white bars) and the values predicted by the OBE model (red lines) from the best single cue thresholds. Positive values represent cue integration, which might or might not be optimal (the latter can be assessed by the proximity of the white bars and the red lines: white bars at the level of or above the red lines suggest optimality). Subject 1 is an example participant who learns to integrate the two cues only in the two last experimental blocks (negative white bars in all blocks but 5 and 6), the integration moreover seems to reach optimality in block 6.

Table 2

Single subject analysis. P-value of the bootstrap comparison

	Experiment 1 (Yaw+ Roll)		Experiment 2 (Yaw + Pitch)	
Subject	bimodal to optimal	bimodal to best single cue	bimodal to optimal	bimodal to best single cue
1	0.05	0.27	0.34	0.22
2	**0.39**	**0.05**	**0.27**	**0.02**
3	0.00	0.11	**0.31**	**0.03**
4	**0.05**	**0.00**	0.04	0.09
5	0.00	0.01	**0.14**	**0.00**
6	**0.39**	**0.01**	0.15	0.15
7	**0.44**	**0.02**	**0.21**	**0.02**
8	0.00	0.37	0.20	0.19

P-values of the one-tailed bootstrap analysis testing a) whether the bimodal thresholds are greater than the theoretically predicted values and b) whether the bimodal thresholds are lower than the best single cue for each subjects for all experimental

blocks pooled together. Numbers in bold indicate the subjects who integrated (optimally).

The results of experiment 1 indicate that it is possible to learn to integrate visuo-vestibular cue pairings, which each signal self-motion around a different axis. In order to further corroborate this finding we decided to use another set of stimuli that also have a high degree of disparity: vestibular yaw and visual pitch rotations.

Experiment 2. Vestibular yaw and visual pitch: Group analysis

A 6 x 3 repeated measures ANOVA with blocks (6) and conditions (3) as factors yielded significant main effects and interaction (all $p<0.0001$). All Bonferroni post-hoc comparisons were significant (all $p<0.0001$; except for block 6 vestibular unimodal threshold not being different form block 2 visual unimodal threshold, and block 4 unimodal visual threshold not being different from block 2 visual unimodal threshold). Next, a general one-tailed bootstrap analysis collapsing across the experimental blocks and participants revealed the following results. There was a significant difference between the visual and vestibular thresholds (vestibular threshold 5.2, visual threshold 4.7; $p=0.01$), and the bimodal threshold differed significantly from the best single cue, i.e. visual (bimodal threshold 3.7; $p=0$) but not from the threshold predicted by the OBE (predicted threshold 3.5; $p=0.06$).

For further analysis we divided the data (pooled across subjects, as described in the Data analysis section and done in Experiment 1) according to the six blocks performed. Figure 3 summarises the experimentally obtained and predicted discrimination thresholds for each of the six experimental blocks. For the yaw-pitch combinations participants' bimodal thresholds were not significantly different from the optimal prediction in all but the second experimental block (one-tailed bootstrap test, $p>0.05$) and in the same blocks the experimentally measured bimodal thresholds were significantly lower than the best single cue estimates ($p<0.05$). In the case of yaw-pitch pairings, subjects therefore optimally integrate the two incongruent cues from the onset and throughout the tested experimental blocks (except block 2).

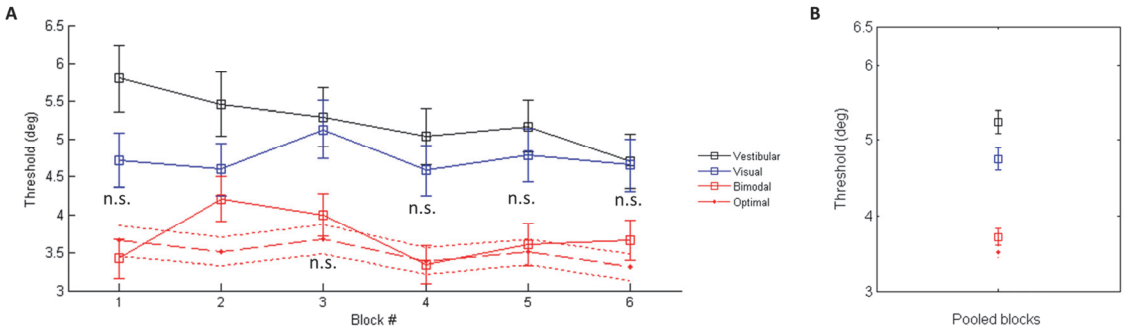

Figure 3. Experiment 2 (vestibular yaw + visual pitch).

A. Integration of vestibular and visual cues in experiment 2 is shown across the six blocks. All blocks except block 2 showed responses compatible with optimal visual-vestibular integration (i.e. no significant difference between the predicted and the experimentally measured threshold). Blocks where the bimodal threshold is not significantly different from the predicted one (i.e. optimal integration) are marked by "n.s." ($p>0.05$, one-tailed bootstrap test). Error bars represent bootstrap standard error.

B. The same analysis performed collapsing across blocks and participants.

As for Experiment 1, we performed a detailed analysis of the discrimination thresholds in each condition over the 6 blocks. The regression and the bootstrap test results are summarised in Table 1. For the unimodal vestibular condition a significant difference was observed between the first and the last experimental blocks ($p=0.022$) due to a linear decrease of the threshold values ($r^2=0.9$, $p=0.004$). For the unimodal visual condition there was no change in the discrimination thresholds over time ($r^2=0.006$, $p=0.88$). There was a significant difference between the two unimodal conditions but only in the first two experimental blocks, once again indicating well-matched single cue discrimination thresholds. In the bimodal condition the threshold values showed no overall linear change ($r^2=0.04$, $p=0.7$) nor a significant difference between the start and end of the experimental session ($p=0.25$).

Experiment 2. Vestibular yaw and visual pitch: Single subject analysis

6 x 3 (block by condition) repeated measures ANOVAs on the values for each subject generated by the bootstrap procedure and subsequent Bonferroni post-hoc comparisons

between the bimodal and the best unimodal cue showed integration for five subjects: for subject 2 in all blocks but for 4 and 6; for subject 3 in all blocks but block 4; for subject 4 in blocks 1, 3 and 4; for subject 5 in all blocks but 1 and 4; and for subject 6 in all blocks but 2 and 3. The results of single subject bootstrap analysis from Experiment 2 are shown in Figures 4 and 5 (see also Table 2). This analysis revealed that seven out of eight subjects in Experiment 2 show optimal integration. The difference between the bootstrap test and the ANOVA is again due to high variance in one block and condition skewing the results of the ANOVA. An example of a participant who integrates throughout Experiment 2 is subject 5 (white bars have a positive value in each experimental block) and this integration is optimal (red lines at the level of or overlapping with the white bars). This is different in subject 4, where the bimodal thresholds are only lower than the best unimodal thresholds in half of the blocks (blocks # 1, 3, 4), and the integration is optimal only in blocks 1 and 4.

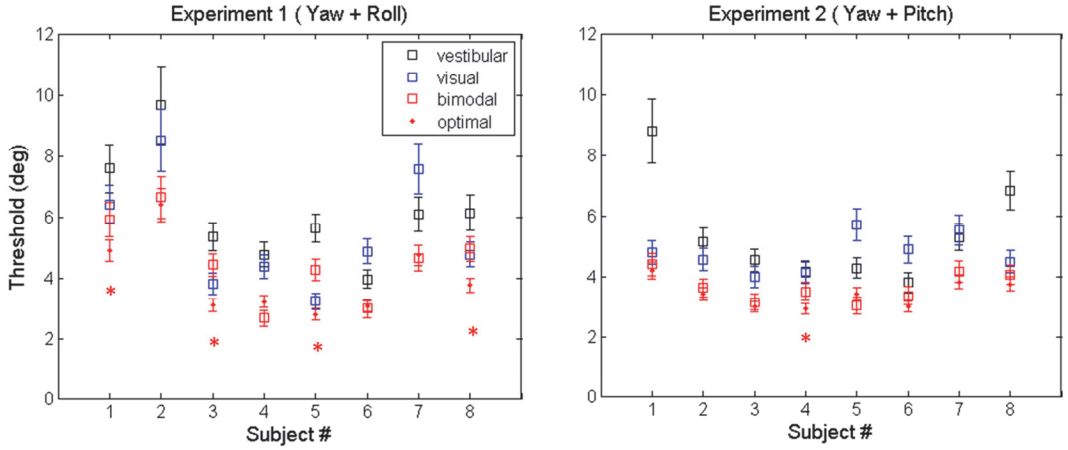

Figure 4. Individual subject data. Vestibular, visual, bimodal and predicted thresholds for each subject for the entire experiment. A red star represents significantly higher bimodal than predicted thresholds (i.e. no optimal integration). *Left panel:* Experiment 1(Yaw + Roll). *Right panel:* Experiment 2 (Yaw + Pitch). Error bars are bootstrap standard errors.

A

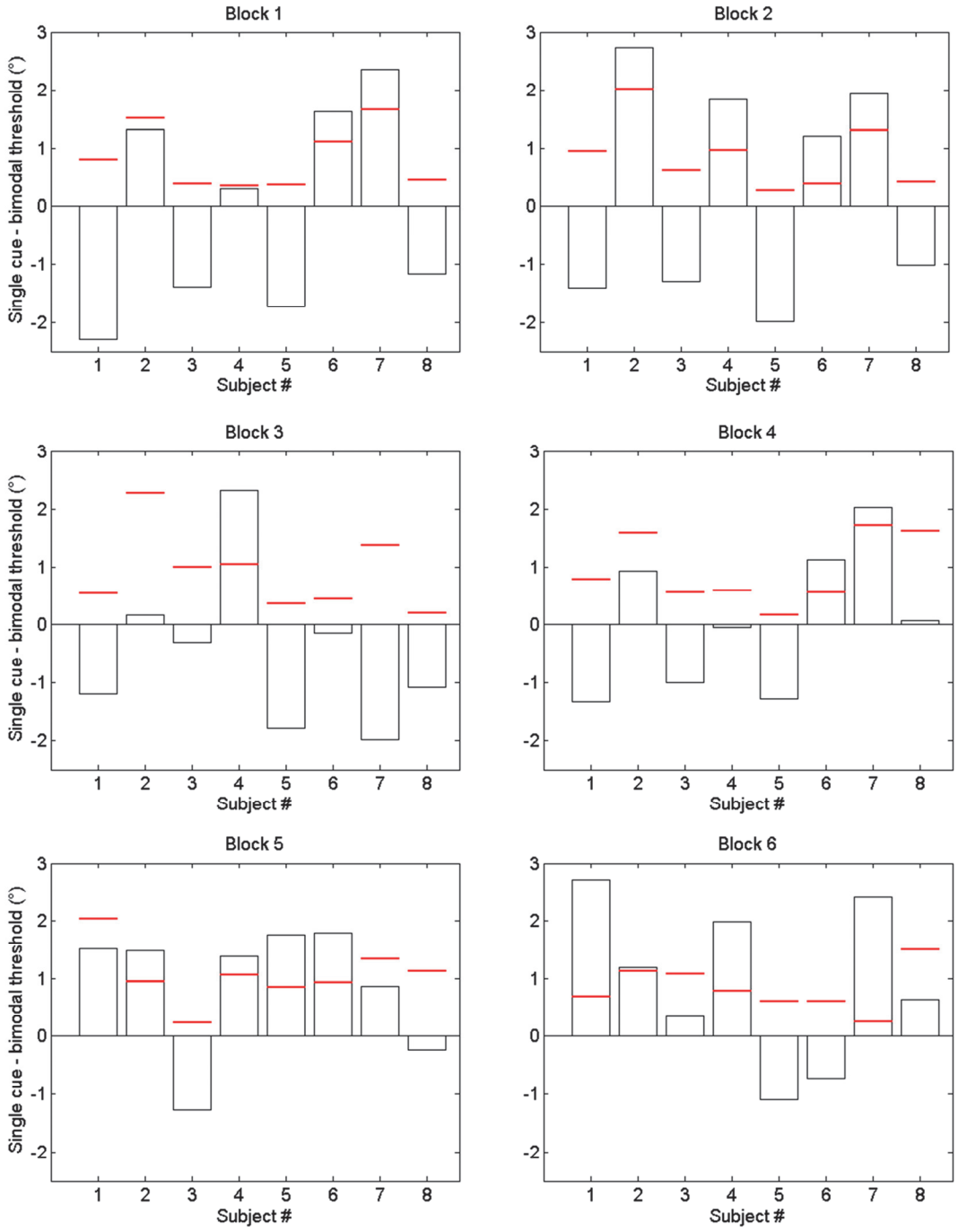
Block 1
Block 2
Block 3
Block 4
Block 5
Block 6
Single cue - bimodal threshold (°)
Subject #
3
2
1
0
-1
-2
1
2
3
4
5
6
7
8

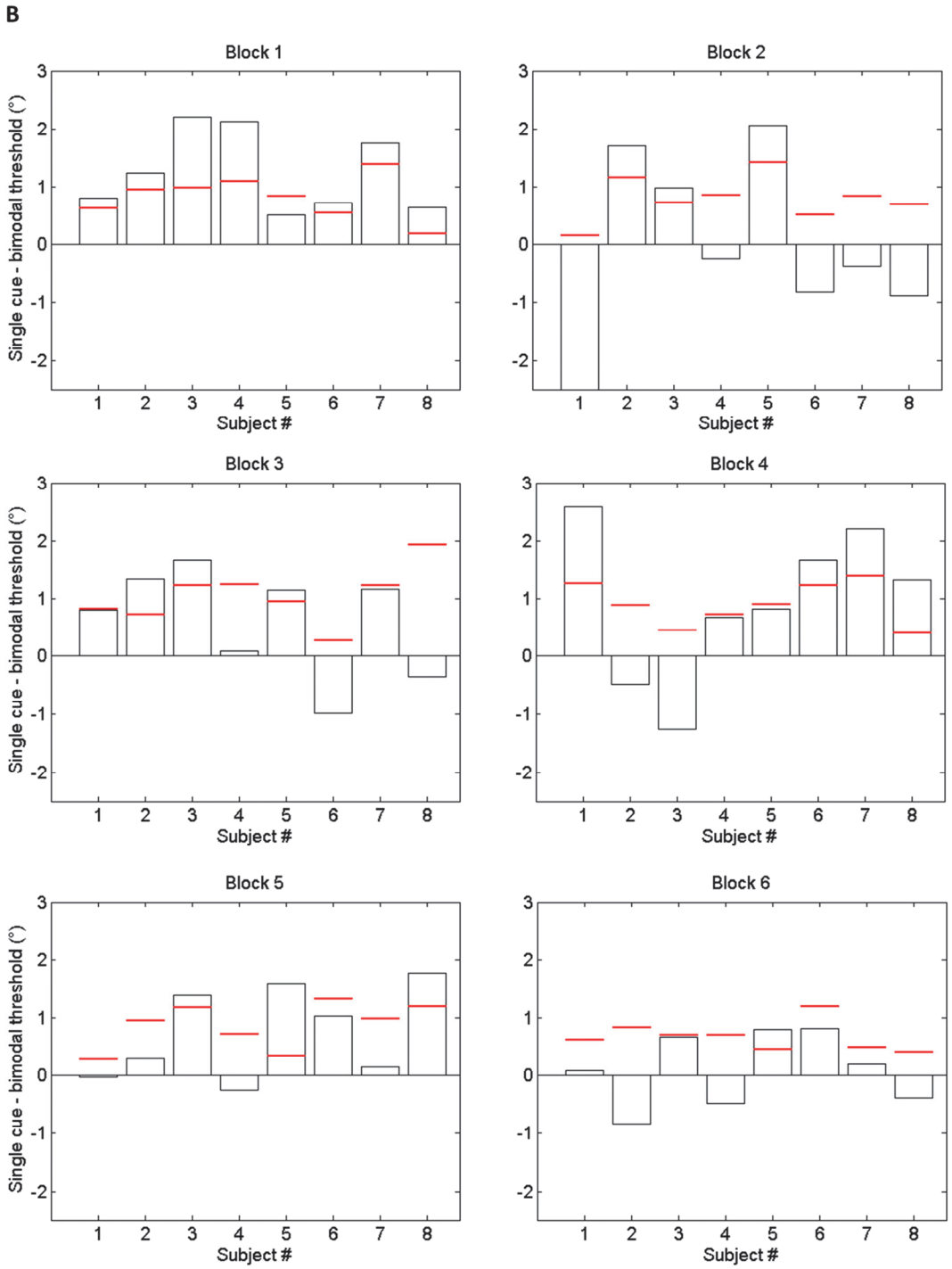

Figure 5. Individual subject data. Difference between the lowest single-cue standard deviation and the measured (white bars) and predicted (red lines) bimodal standard deviations across the six experimental blocks. Positive values indicate integration. *A:* Experiment 1 (Yaw + Roll). *B:* Experiment 2 (Yaw + Pitch)

Discussion

The main finding of the present study is that human observes can optimally integrate or learn to integrate co-occurring multisensory self-motion stimuli when they imply rotations around different axes. In two experiments, we showed that participants' performance was better for directionally conflicting bimodal visuo-vestibular cues than for either vestibular or visual cues alone. In the yaw-roll experiment (Experiment 1) such optimal integration improved over successive blocks, whereas in the yaw-pitch experiment (Experiment 2) it was observed in all but one experimental block. These results extend the previous literature on self-motion perception demonstrating that optimal integration also occurs for stimuli having large, consciously detectable discrepancies. How can we account for these results?

It has been put forward that sensory integration would only occur for stimuli attributed to the same causal event (Körding et al. 2007; Parise, Spence, and Ernst 2012; Shams and Beierholm 2010). The present results would mean that in the bimodal condition instead of experiencing two distinct rotational stimuli as provided by the incongruent visual and vestibular modalities, subjects would perceive one single self-displacement, possibly going in an intermediate direction with respect to the two cues. Compatible with such a proposal are data from previous studies showing that selected visuo-vestibular conflicts are perceived as one single motion (Ishida et al. 2008; Wright, DiZio, and Lackner 2005). Thus, incongruent visual and vestibular cues along the same yaw axis but indicating yaw rotations in the same direction (an ecological conflict: e.g. clockwise vestibular yaw and clockwise visual yaw) are perceived as rotations that depend more strongly on the direction of the visual stimulus, compatible with visual dominance. Findings with the vestibular-ocular reflex (VOR) are also compatible with such visual dominance. The VOR occurs when the head moves or when vection is perceived and keeps the image stable on the retina by moving the eyes in the opposite direction. Ishida et al. (2008) found that the direction of the VOR in cases of non-ecological visual-vestibular stimulus combinations in the yaw axis also reveals such visual dominance and is congruent with the visual stimulus (Ishida et al. 2008). Also of relevance are VOR studies of cross-modal adaptation between visual and vestibular cues (indicating motion in different directions) that have been performed in several species (Schultheis and Robinson 1981; Baker, Wickland, and Peterson 1987; Trillenberg et al.

2003). Subjects were exposed for a certain period of time to simultaneously presented conflicting stimuli (different axis as those employed in the present study) and adaptation was reflected in the change of the direction and gain of the VOR. These studies indicate that a visuo-vestibular conflict, in certain conditions, is formulated by the nervous system into one single percept (i.e. conscious perception of self-motion in one particular direction).

Based on our own finding of optimal integration in Experiments 1 and 2 and these previous findings we argue that in the incongruent visual-vestibular combinations (bimodal conditions) subjects might perceive a single self-displacement. Unfortunately, no subjective reports of the perceived direction of motion have been collected in the present study or in the previous literature. In our study only one subject (in Experiment 2) spontaneously reported after Experiment 2 a single illusory diagonal displacement during the bimodal (yaw + pitch) condition. We propose that future work could extend the present paradigms and additionally record eye movements in order to investigate whether the two conflicting motion directions are combined into a single representation and whether the resulting integrated percept depends more on the vestibular or the visual cue (as reported in related work by Ishida et al. (2008)). Although, the direction of perceived motion might be inferred from the direction of fixating micro-saccades, the use of a stereoscopic visual stimulus necessitating shutter glasses prevented us from recording eye movements by means of video tracking. In previous studies (Ishida et al. 2008; Trillenberg et al. 2003), subjects were exposed to the same continuous stimulation for a prolonged amount of time (one to several hours) before the adaptation could be objectified with the eye-movement recording. The present findings, however, suggest that such motion integration for incompatible directions may occur much faster than previously thought.

The observed visual-vestibular integration may also depend on the demands of the experimental task and the particular stimuli chosen. Thus, multisensory integration in our study could have occurred as a result of the specific task demands, which may have made the directional conflict task-irrelevant. Thus, in previous experiments on multisensory conflicts (including visual-vestibular stimulation, but also other

multisensory stimulus combinations) the response of the subject (e.g. localising a stimulus, judging the number of stimuli, judging perceptual qualities of stimuli) was found to depend on the amount of conflict between the two stimuli. For instance, in a task where subjects are asked to localise a visual stimulus in the presence of an auditory cue from a conflicting location, perceptual unification breaks down and the two modalities bias each other less when the distance between the visual and the auditory cues is too large (e.g. Roach, Heron, and McGraw 2006; Wallace et al. 2004). In the present study, however, the direction of motion was irrelevant to the task we asked our participants to perform because estimating rotation size is independent of rotation direction. As the amount of rotation provided by the visual and the vestibular cues was always the same in the present bimodal conditions one could expect that the extraction of this feature alone could lead to the observed visual-vestibular patterns of integration. This extraction could further have been facilitated by the fact that other stimulus features were matched for the visual and vestibular stimuli despite their directional conflict. Thus, the motion onset, the duration and the spatio-temporal motion profile of both stimuli were matched. In the same vein, previous unpublished research reported, for instance, that simultaneous visuo-vestibular stimuli indicating the same heading direction, but having a different acceleration profile are optimally integrated (Butler et al., 2008). Another unpublished work reported that stimuli designating the same amount of motion and having the same motion profiles (but being temporally offset) can also learned to be integrated (Campos et al., 2009). These data indicate, that despite the fact that some properties of the two stimuli are not matched, integration occurs when the task-relevant features of these stimuli are not in conflict (i.e. most features of the stimuli are correlated). Further work is needed to disentangle the different contributions of stimulus attributes and task demands for the integration process.

Our results show that integration in the bimodal condition occurred from the beginning in Experiment 2 (vestibular yaw + visual pitch), whereas such integration only appeared during the later phases of Experiment 1 (vestibular yaw + visual roll). That is, integration of pitch with yaw was present throughout the experiment, whereas integration of roll with yaw was learned only in later blocks of the experiment. To our knowledge, there exists no anatomical or functional evidence for a facilitated integration

of pitch with yaw versus roll with yaw stimuli. Neither at the level of the vestibular nuclei (Büttner-Ennever 1992; Highstein and Holstein 2006; Naito et al. 1995) nor in the cortex (Arnoldussen, Goossens, and van den Berg 2013) can the pattern of projections from the semicircular canals account for our findings. Although recordings of neural responses to vertical rotations reveal that in the brainstem roll neurons outnumber pitch neurons (Baker et al. 1984; Kasper, Schor, and Wilson 1988; Endo et al. 1995; Bolton et al. 1992; Wilson et al. 1990), optimal activations of cortical vestibular neurons are uniformly distributed over all possible rotation planes (Grüsser, Pause, and Schreiter 1990; Akbarian et al. 1988). Other studies looking at conflicting visuo-vestibular stimuli (e.g. Waespe and Henn 1978; Bockisch, Straumann, and Haslwanter 2003) have failed to provide the comparisons relevant to our study and findings (different stimulation axes and parameters of stimulation). We do not think that our results can be attributed to the fact that participants performed in general better in Experiment 2 (lower thresholds for the unimodal conditions). Nor could this result be attributed to the fact that three subjects participated in both experiments (i.e. learned integration from Experiment 1 influenced thresholds in Experiment 2): their performance was comparable in both experiments and all three subjects showed integration in the majority of experimental blocks in both experiments. Accordingly, we propose that the difference between yaw-roll and yaw-pitch integration may be caused by supra-vestibular directional influences that have been observed previously in cognitive neuroscience. Thus, in Experiment 1 vestibular clockwise (i.e. rightward) yaw was always paired with visual leftward roll, and in Experiment 2 vestibular rightward yaw was always paired with upward pitch. Previous research on spatial compatibility (e.g. Simon effect, spatial Stroop, mental number line) has shown a facilitation effect for stimuli occurring in the same spatial plane (e.g. right + right) and for left-down / right-up pairings (Nicoletti and Umiltà 1984; Nishimura and Yokosawa 2006; Cho and Proctor 2003). For instance participants are faster to respond to visual stimuli presented on the left or at the bottom of the screen with their left hand and to rightward and upward stimuli with their right hand (for a review see Proctor and Cho 2006). Similarly, if vocal responses “right” and “left” are attributed to stimuli presented above or below the midline of the screen, such a random pairing yields faster responses than pairing “right” with below and “left” with above (Weeks and Proctor 1990). Such compatibility effects were also shown for multisensory stimuli. For example, a high frequency tone presented together with a tactile stimulus at

a higher location (and a low frequency tone plus a tactile stimulus at a lower location) are more strongly associated than e.g. a high frequency tone with a tactile stimulus at a lower location (Occelli, Spence, and Zampini 2009). Such cross-modal mechanisms have also been shown for the vestibular system: active head turns (Loetscher et al. 2008) as well as passive displacements (Hartmann, Grabherr, and Mast 2012) to the right and left were found to influence numerical cognition in a magnitude-specific way. Leftward movements facilitate the generation of smaller numbers, whereas right motion that of larger numbers. A related supra-vestibular directional mechanism could have influenced responses in the present two experiments, meaning, that processing the association of the bimodal stimuli we have chosen is *a priori* facilitated due to the correspondence of spatial representations/dimensional overlap of their directions (Kosslyn and Kosslyn 1996; Kornblum, Hasbroucq, and Osman 1990; Li et al. 2014). Given the strong implication of vestibular signals for space perception, the existence of such automatic associations seems highly plausible. Indeed, the pairing of visual (simulated) rightward roll with rightward vestibular yaw and rightward vestibular yaw with upward pitch might represent a "preferred" direction for integration, potentially providing a partial explanation for our results.

Alternatively, other characteristics shared between yaw and pitch stimuli might contribute to the faster integration observed in Experiment 2. For instance the gain of the VOR elicited by both yaw and pitch movement/optic flow is generally close to 1.0, whereas the gain of the torsional VOR elicited by roll movement is generally more limited (Tweed et al., 1994). The optic flow resulting from yaw and pitch movements involves the motion of the whole visual field in one direction, whereas in the roll plane the visual scene rotates around a central point (e.g. Duffy and Wurtz, 1995). Finally, it may be that in daily life combined yaw-pitch head motion (i.e. up and to the right) is more frequent than combined yaw-roll motion, although this speculation has yet to be confirmed by empirical research. These natural constraints may separately or in combination with the mentioned supra-vestibular mechanism result in a multisensory system that is more tolerant to conflicts between stimuli sharing a larger number of common characteristics.

Although of no direct relevance for the integration results we report, it should be noted that the fluctuation of the unimodal thresholds was not the same in the two experiments. During Experiment 1, the unimodal visual threshold became progressively more elevated over consecutive sessions, which was not observed in Experiment 2. We speculate that this change in threshold can be attributed to fatigue or decreased attention over time as the subjects took part in a prolonged experiment requiring a continued high level of visual attention. In Experiment 2, however, the vestibular threshold was reduced over time. We presume that this reduction can be attributed to perceptual learning or improvement as subjects repeatedly experience the same stimulus. It is safe to assume that these idiosyncratic phenomena are also present and affect perception in the same way when the unimodal stimuli are paired with one another in the bimodal condition. The increasing visual thresholds in Experiment 1 and the decreasing vestibular thresholds in Experiment 2 therefore impact the bimodal prediction as well. Despite these changes, the experimental bimodal threshold still closely matched this prediction, thus showing optimal integration.

Finally, our result may be of relevance for visual-vestibular integration in neurological patients. It has been put forward that illusory own body perceptions such as room-tilt-illusions, inversion illusions, and out-of-body experiences are related to abnormal multisensory integration involving the visual and the vestibular senses (Lopez, Halje, and Blanke 2008; Ionta et al. 2011; Blanke, 2012). Our experiments show that conflicting information from these two modalities is optimally integrated by the brain, possibly to produce a single percept and thus merge contradictory visual and vestibular self-motion cues into one coherent representation. We argue that such a single representation may also account for illusory own body perceptions related to self-location and self-motion during such neurological conditions. Abnormal multisensory integration in these illusory own body perceptions could be due to normal integration of an abnormal visual and/or vestibular cue (instead of abnormal integration of a normal visual and/or vestibular cue), which may be providing conflicting information about self-motion and self-location. Neurological patients with out-of-body experiences caused by cortical damage (Ionta et al., 2011) and healthy subjects who are prone to experience an out-of-body experience (e.g. Murray and Fox 2005) may integrate visual and vestibular stimuli across a larger range of stimulus incompatibilities than subjects

without such experiences. This interpretation, however, is to be taken with caution as this is yet to be supported by experimental evidence and as the illusory own body perceptions described above are related to abnormal processing of gravitational information (i.e. depend on the otolith organs), whereas our experimental manipulations involved vestibular yaw rotations and only partly involved visual gravitational stimulation.

References

Akbarian, S., Katharina Berndl, O.-J. Grüsser, W. Guldin, M. Pause, and Ursula Schreiter. 1988. 'Responses of Single Neurons in the Parietoinsular Vestibular Cortex of Primatesa'. *Annals of the New York Academy of Sciences* 545 (1): 187–202. doi:10.1111/j.1749-6632.1988.tb19564.x.

Alais, David, and David Burr. 2004. 'The Ventriloquist Effect Results from near-Optimal Bimodal Integration'. *Current Biology: CB* 14 (3): 257–62. doi:10.1016/j.cub.2004.01.029.

Arnoldussen, D M, J Goossens, and A V van den Berg. 2013. 'Visual Perception of Axes of Head Rotation'. *Frontiers in Behavioral Neuroscience* 7: 11. doi:10.3389/fnbeh.2013.00011.

Baker, J, C Wickland, and B Peterson. 1987. 'Dependence of Cat Vestibulo-Ocular Reflex Direction Adaptation on Animal Orientation during Adaptation and Rotation in Darkness'. *Brain Research* 408 (1-2): 339–43.

Baker, J., J. Goldberg, G. Hermann, and B. Peterson. 1984. 'Spatial and Temporal Response Properties of Secondary Neurons That Receive Convergent Input in Vestibular Nuclei of Alert Cats'. *Brain Research* 294 (1): 138–43. doi:10.1016/0006-8993(84)91318-0.

Bertelson, P, and M Radeau. 1981. 'Cross-Modal Bias and Perceptual Fusion with Auditory-Visual Spatial Discordance'. *Perception & Psychophysics* 29 (6): 578–84.

Bockisch, Christopher J, Dominik Straumann, and Thomas Haslwanter. 2003. 'Eye Movements during Multi-Axis Whole-Body Rotations'. *Journal of Neurophysiology* 89 (1): 355–66. doi:10.1152/jn.00058.2002.

Bolton, P. S., T. Goto, R. H. Schor, V. J. Wilson, Y. Yamagata, and B. J. Yates. 1992. 'Response of Pontomedullary Reticulospinal Neurons to Vestibular Stimuli in Vertical Planes. Role in Vertical Vestibulospinal Reflexes of the Decerebrate Cat'. *Journal of Neurophysiology* 67 (3): 639–47.

Botvinick, Matthew, and Jonathan Cohen. 1998. 'Rubber Hands "feel" Touch That Eyes See'. *Nature* 391 (6669): 756–756. doi:10.1038/35784.

Bresciani, Jean-Pierre, Marc O Ernst, Knut Drewing, Guillaume Bouyer, Vincent Maury, and Abderrahmane Kheddar. 2005. 'Feeling What You Hear: Auditory Signals Can Modulate Tactile Tap Perception'. *Experimental Brain Research. Experimentelle Hirnforschung. Expérimentation Cérébrale* 162 (2): 172–80. doi:10.1007/s00221-004-2128-2.

Butler, J. S., S. T. Smith, J. L. Campos, and H. H. Bulthoff. 2010. 'Bayesian Integration of Visual and Vestibular Signals for Heading'. *Journal of Vision* 10 (11): 23–23. doi:10.1167/10.11.23.

Büttner-Ennever, J A. 1992. 'Patterns of Connectivity in the Vestibular Nuclei'. *Annals of the New York Academy of Sciences* 656 (May): 363–78.

Calvert, Gemma, Charles Spence, and Barry E. Stein. 2004. *The Handbook of Multisensory Processes*. MIT Press.

Cho, Yang Seok, and Robert W. Proctor. 2003. 'Stimulus and Response Representations Underlying Orthogonal Stimulus-Response Compatibility Effects'. *Psychonomic Bulletin & Review* 10 (1): 45–73. doi:10.3758/BF03196468.

Duffy CJ, Wurtz RH (1995) Response of monkey MST neurons to optic flow stimuli with shifted centers of motion. The Journal of neuroscience 15:5192-5208.

Endo, K., D. B. Thomson, V. J. Wilson, T. Yamaguchi, and B. J. Yates. 1995. 'Vertical Vestibular Input to and Projections from the Caudal Parts of the Vestibular Nuclei of the Decerebrate Cat'. *Journal of Neurophysiology* 74 (1): 428–36.

Ernst, M. O. 2007. 'Learning to Integrate Arbitrary Signals from Vision and Touch'. *Journal of Vision* 7 (5): 7–7. doi:10.1167/7.5.7.

Ernst, Marc O, and Martin S Banks. 2002. 'Humans Integrate Visual and Haptic Information in a Statistically Optimal Fashion'. *Nature* 415 (6870): 429–33. doi:10.1038/415429a.

Fetsch, Christopher R., Amanda H. Turner, Gregory C. DeAngelis, and Dora E. Angelaki. 2009. 'Dynamic Reweighting of Visual and Vestibular Cues during Self-Motion Perception'. *The Journal of Neuroscience* 29 (49): 15601–12. doi:10.1523/JNEUROSCI.2574-09.2009.

GEBHARD, J W, and G H MOWBRAY. 1959. 'On Discriminating the Rate of Visual Flicker and Auditory Flutter'. *The American Journal of Psychology* 72 (December): 521–29.

Gepshtein S, Burge J, Ernst MO, Banks MS. The combination of vision and touch depends on spatial proximity. J Vis. 2005 Dec 28;5(11):1013-23.

Gibson, James J. 1950. *The Perception of the Visual World*. Vol. xii. Oxford, England: Houghton Mifflin.

Grüsser, O. J., M. Pause, and U. Schreiter. 1990. 'Vestibular Neurones in the Parieto-Insular Cortex of Monkeys (Macaca Fascicularis): Visual and Neck Receptor Responses.' *The Journal of Physiology* 430 (1): 559–83.

Gu, Yong, Dora E Angelaki, and Gregory C Deangelis. 2008. 'Neural Correlates of Multisensory Cue Integration in Macaque MSTd'. *Nature Neuroscience* 11 (10): 1201–10. doi:10.1038/nn.2191.

Hairston, W. D., M. T. Wallace, J. W. Vaughan, B. E. Stein, J. L. Norris, and J. A. Schirillo. 2003. 'Visual Localization Ability Influences Cross-Modal Bias'. *Journal of Cognitive Neuroscience* 15 (1): 20–29. doi:10.1162/089892903321107792.

Hartmann, Matthias, Luzia Grabherr, and Fred W. Mast. 2012. 'Moving along the Mental Number Line: Interactions between Whole-Body Motion and Numerical Cognition'. *Journal of Experimental Psychology: Human Perception and Performance* 38 (6): 1416–27. doi:10.1037/a0026706.

Highstein, Stephen M, and Gay R Holstein. 2006. 'The Anatomy of the Vestibular Nuclei'. *Progress in Brain Research* 151: 157–203. doi:10.1016/S0079-6123(05)51006-9.

Hillis, J. M., M. O. Ernst, M. S. Banks, and M. S. Landy. 2002. 'Combining Sensory Information: Mandatory Fusion Within, but Not Between, Senses'. *Science* 298 (5598): 1627–30. doi:10.1126/science.1075396.

Ionta, Silvio, Lukas Heydrich, Bigna Lenggenhager, Michael Mouthon, Eleonora Fornari, Dominique Chapuis, Roger Gassert, and Olaf Blanke. 2011. 'Multisensory Mechanisms in Temporo-Parietal Cortex Support Self-Location and First-Person Perspective'. *Neuron* 70 (2): 363–74. doi:10.1016/j.neuron.2011.03.009.

Ishida, Masayuki, Hiroaki Fushiki, Hiroshi Nishida, and Yukio Watanabe. 2008. 'Self-Motion Perception during Conflicting Visual-Vestibular Acceleration'. *Journal of Vestibular Research: Equilibrium & Orientation* 18 (5-6): 267–72.

Jürgens R, Becker W. Perception of angular displacement without landmarks: evidence for Bayesian fusion of vestibular, optokinetic, podokinesthetic, and cognitive information. Exp Brain Res. 2006 Oct;174(3):528-43.

Kapralos, Bill, Daniel Zikovitz, Michael R. Jenkin, and Laurence R. Harris. 2004. 'Auditory Cues in the Perception of Self Motion'. In Audio Engineering Society. http://www.aes.org/e-lib/browse.cfm?elib=12625.

Kasper, J., R. H. Schor, and V. J. Wilson. 1988. 'Response of Vestibular Neurons to Head Rotations in Vertical Planes. I. Response to Vestibular Stimulation'. *Journal of Neurophysiology* 60 (5): 1753–64.

Körding, Konrad P., Ulrik Beierholm, Wei Ji Ma, Steven Quartz, Joshua B. Tenenbaum, and Ladan Shams. 2007. 'Causal Inference in Multisensory Perception'. Edited by Olaf Sporns. *PLoS ONE* 2 (9): e943. doi:10.1371/journal.pone.0000943.

Kornblum, S, T Hasbroucq, and A Osman. 1990. 'Dimensional Overlap: Cognitive Basis for Stimulus-Response Compatibility--a Model and Taxonomy'. *Psychological Review* 97 (2): 253–70.

Kosslyn, Stephen Michael, and Stephen M. Kosslyn. 1996. *Image and Brain: The Resolution of the Imagery Debate*. MIT Press.

Li, Qi, Weizhi Nan, Kai Wang, and Xun Liu. 2014. 'Independent Processing of Stimulus-Stimulus and Stimulus-Response Conflicts'. *PLoS ONE* 9 (2): e89249. doi:10.1371/journal.pone.0089249.

Loetscher, Tobias, Urs Schwarz, Michele Schubiger, and Peter Brugger. 2008. 'Head Turns Bias the Brain's Internal Random Generator'. *Current Biology* 18 (2): R60–R62. doi:10.1016/j.cub.2007.11.015.

Lopez, C, P Halje, and O Blanke. 2008. 'Body Ownership and Embodiment: Vestibular and Multisensory Mechanisms'. *Neurophysiologie Clinique = Clinical Neurophysiology* 38 (3): 149–61. doi:10.1016/j.neucli.2007.12.006.

Lunghi, Claudia, Maria Concetta Morrone, and David Alais. 2014. 'Auditory and Tactile Signals Combine to Influence Vision during Binocular Rivalry'. *The Journal of Neuroscience: The Official Journal of the Society for Neuroscience* 34 (3): 784–92. doi:10.1523/JNEUROSCI.2732-13.2014.

Mendonça, Catarina, Jorge A Santos, and Joan López-Moliner. 2011. 'The Benefit of Multisensory Integration with Biological Motion Signals'. *Experimental Brain Research. Experimentelle Hirnforschung. Expérimentation Cérébrale* 213 (2-3): 185–92. doi:10.1007/s00221-011-2620-4.

Murray, Craig D, and Jezz Fox. 2005. 'Dissociational Body Experiences: Differences between Respondents with and without Prior out-of-Body-Experiences'. *British Journal of Psychology (London, England: 1953)* 96 (Pt 4): 441–56. doi:10.1348/000712605X49169.

Naito, Y, A Newman, W S Lee, K Beykirch, and V Honrubia. 1995. 'Projections of the Individual Vestibular End-Organs in the Brain Stem of the Squirrel Monkey'. *Hearing Research* 87 (1-2): 141–55.

Nicoletti, R, and C Umiltà. 1984. 'Right-Left Prevalence in Spatial Compatibility'. *Perception & Psychophysics* 35 (4): 333–43.

Nishimura, Akio, and Kazuhiko Yokosawa. 2006. 'Orthogonal Stimulus–response Compatibility Effects Emerge Even When the Stimulus Position Is Task Irrelevant'. *The Quarterly Journal of Experimental Psychology* 59 (6): 1021–32. doi:10.1080/17470210500416243.

Occelli, Valeria, Charles Spence, and Massimiliano Zampini. 2009. 'Compatibility Effects between Sound Frequency and Tactile Elevation:' *NeuroReport* 20 (8): 793–97. doi:10.1097/WNR.0b013e32832b8069.

Ohmi, Masao. 1996. 'Egocentric Perception through Interaction among Many Sensory Systems'. *Cognitive Brain Research* 5 (1-2): 87–96.

Parise, Cesare V., Charles Spence, and Marc O. Ernst. 2012. 'When Correlation Implies Causation in Multisensory Integration'. *Current Biology* 22 (1): 46–49. doi:10.1016/j.cub.2011.11.039.

Pick, Herbert L., David H. Warren, and John C. Hay. 1969. 'Sensory Conflict in Judgments of Spatial Direction'. *Perception & Psychophysics* 6 (4): 203–5. doi:10.3758/BF03207017.

Proctor, Robert W., and Yang Seok Cho. 2006. 'Polarity Correspondence: A General Principle for Performance of Speeded Binary Classification Tasks'. *Psychological Bulletin* 132 (3): 416–42. doi:10.1037/0033-2909.132.3.416.

Prsa, M., S. Gale, and O. Blanke. 2012. 'Self-Motion Leads to Mandatory Cue Fusion across Sensory Modalities'. *Journal of Neurophysiology* 108 (8): 2282–91. doi:10.1152/jn.00439.2012.

Prsa, Mario, Steven Gale, and Olaf Blanke. 2012. 'Self-Motion Leads to Mandatory Cue Fusion across Sensory Modalities'. *Journal of Neurophysiology* 108 (8): 2282–91. doi:10.1152/jn.00439.2012.

Recanzone, Gregg H. 2003. 'Auditory Influences on Visual Temporal Rate Perception'. *Journal of Neurophysiology* 89 (2): 1078–93. doi:10.1152/jn.00706.2002.

Roach, N. W, J. Heron, and P. V McGraw. 2006. 'Resolving Multisensory Conflict: A Strategy for Balancing the Costs and Benefits of Audio-Visual Integration'. *Proceedings of the Royal Society B: Biological Sciences* 273 (1598): 2159–68. doi:10.1098/rspb.2006.3578.

Schultheis, L W, and D A Robinson. 1981. 'Directional Plasticity of the Vestibuloocular Reflex in the Cat'. *Annals of the New York Academy of Sciences* 374: 504–12.

Shams, Ladan, and Ulrik R Beierholm. 2010. 'Causal Inference in Perception'. *Trends in Cognitive Sciences* 14 (9): 425–32. doi:10.1016/j.tics.2010.07.001.

Stein, Barry E. 2012. *The New Handbook of Multisensory Processing*. Mit Press.

Trillenberg, P, M Shelhamer, D C Roberts, and D S Zee. 2003. 'Cross-Axis Adaptation of Torsional Components in the Yaw-Axis Vestibulo-Ocular Reflex'. *Experimental Brain Research. Experimentelle Hirnforschung. Expérimentation Cérébrale* 148 (2): 158–65. doi:10.1007/s00221-002-1285-4.

Tweed D, Sievering D, Misslisch H, Fetter M, Zee D, Koenig E (1994) Rotational kinematics of the human vestibuloocular reflex. I. Gain matrices. Journal of neurophysiology 72:2467-2479.

Van Beers, R J, A C Sittig, and J J Denier van der Gon. 1996. 'How Humans Combine Simultaneous Proprioceptive and Visual Position Information'. *Experimental Brain Research. Experimentelle Hirnforschung. Expérimentation Cérébrale* 111 (2): 253–61.

———. 1999. 'Localization of a Seen Finger Is Based Exclusively on Proprioception and on Vision of the Finger'. *Experimental Brain Research. Experimentelle Hirnforschung. Expérimentation Cérébrale* 125 (1): 43–49.

Waespe, W, and V Henn. 1978. 'Conflicting Visual-Vestibular Stimulation and Vestibular Nucleus Activity in Alert Monkeys'. *Experimental Brain Research. Experimentelle Hirnforschung. Expérimentation Cérébrale* 33 (2): 203–11.

Wallace, M.T., G.E. Roberson, W.D. Hairston, B.E. Stein, J.W. Vaughan, and J.A. Schirillo. 2004. 'Unifying Multisensory Signals across Time and Space'. *Experimental Brain Research* 158 (2). doi:10.1007/s00221-004-1899-9. http://springerlink.metapress.com/openurl.asp?genre=article&id=doi:10.1007/s00221-004-1899-9.

Warren, Rik, and Alexander H. Wertheim. 2014. *Perception and Control of Self-Motion*. Psychology Press.

Weeks, Daniel J., and Robert W. Proctor. 1990. 'Salient-Features Coding in the Translation between Orthogonal Stimulus and Response Dimensions'. *Journal of Experimental Psychology: General* 119 (4): 355–66. doi:10.1037/0096-3445.119.4.355.

Welch, R B, and D H Warren. 1980. 'Immediate Perceptual Response to Intersensory Discrepancy'. *Psychological Bulletin* 88 (3): 638–67.

Wilson, V. J., Y. Yamagata, B. J. Yates, R. H. Schor, and S. Nonaka. 1990. 'Response of Vestibular Neurons to Head Rotations in Vertical Planes. III. Response of Vestibulocollic Neurons to Vestibular and Neck Stimulation'. *Journal of Neurophysiology* 64 (6): 1695–1703.

Wozny, D. R., and L. Shams. 2011. 'Recalibration of Auditory Space Following Milliseconds of Cross-Modal Discrepancy'. *Journal of Neuroscience* 31 (12): 4607–12. doi:10.1523/JNEUROSCI.6079-10.2011.

Wright, W G, P DiZio, and J R Lackner. 2005. 'Vertical Linear Self-Motion Perception during Visual and Inertial Motion: More than Weighted Summation of Sensory Inputs'. *Journal of Vestibular Research: Equilibrium & Orientation* 15 (4): 185–95.

6.2

Paper V – Learning to integrate contradictory multisensory self-motion cue pairings.

Visuo-neural discrepancies modulate the sense of agency for brain-machine actions

Nathan Evans[1,2], Steven Gale[1,2], Aaron Schurger[1,2], Olaf Blanke[1,2,3]

[1] Center for Neuroprosthetics, École Polytechnique Fédérale de Lausanne, Switzerland
[2] Laboratory of Cognitive Neuroscience, Brain-Mind Institute, École Polytechnique Fédérale de Lausanne, Switzerland
[3] Department of Neurology, University Hospital Geneva, Switzerland

Corresponding Author:
Olaf Blanke
Center for Neuroprosthetics & Brain-Mind Institute
Bertarelli Foundation Chair in Cognitive Neuroprosthetics
School of Life Sciences
École Polytechnique Fédérale de Lausanne
Station 19
CH – 1015 Lausanne
Tel: +41 21 693 69 21
E-mail: olaf.blanke@epfl.ch

Abstract

Recent advances in neuroscience and engineering have led to the development of technologies that permit the control of external devices through real-time decoding of brain activity (brain-machine interfaces; BMI). Though the feeling of controlling bodily movements (sense of agency; SOA) has been well studied and a number of well-defined sensorimotor and cognitive mechanisms have been put forth, very little is known about the SOA for BMI-actions. Exploiting a novel experimental framework, we describe the SOA for BMI-actions and demonstrate that discrepancies between decoded neural activity and its resultant real-time sensory feedback are associated with a decrease in the SOA, compatible with SOA mechanisms proposed for bodily actions. For certain poorly controlled BMI-actions, if the feedback discrepancy is corrective, then the SOA can be high and increase with increasing discrepancy, demonstrating the dominance of visual feedback on the SOA. Nevertheless, a small but significant amount of residual variance could be accounted for on the basis of brain signals alone, suggesting that mechanisms of monitoring may also be involved, even if largely overruled by visual feedback. Although these results demonstrate that bodily and BMI-actions rely on common mechanisms of sensorimotor integration for agency judgments, they also demonstrate that in the absence of any overt bodily movements and proprioceptive feedback, visual feedback dominates the SOA, however erroneous that feedback may be.

Introduction

Human action is associated with a sense of agency (SOA) characterized by the feeling that one's movements and their consequences are self-generated and not externally produced (Gallagher, 2000; David et al., 2008; Pacherie, 2008). Many behavioral (Fourneret and Jeannerod, 1998; Tsakiris et al., 2005), modeling (de Vignemont and Fourneret, 2004; Jeannerod and Pacherie, 2004), and neuroimaging studies (Farrer and Frith, 2002; Farrer et al., 2003; David et al., 2007) have investigated the brain mechanisms of the SOA. These studies have demonstrated that the SOA for bodily actions is attenuated when spatial and temporal conflicts are inserted between the action and its sensory consequences (Knoblich and Sebanz, 2005; Sato and Yasuda, 2005; Jeannerod, 2006; Farrer et al., 2008; Kannape et al., 2010). Predictive theoretical accounts link the SOA to internal forward models of motor control, where efferent copy signals related to motor commands (Sperry, 1950; von Holst and Mittelstaedt, 1950) are used to make predictions about the sensory consequences of the movement (Wolpert et al., 1995; Miall and Wolpert, 1996). Discrepancies between the predicted and the actual sensory feedback weaken the evidence for a causal connection between action and feedback and reduce the SOA (Frith et al., 2000; Blakemore et al., 2002). By contrast, cognitive or postdictive theories (Wegner, 2002, 2003) hold that the SOA is based on the comparison between high-order movement intentions, anticipation, cognitive priors, and sensory outcomes.

Recent advances in brain-machine interfaces (BMI) have made it possible to decode cortical activity and generate machine-controlled actions without concomitant bodily action (Taylor et al., 2002; Velliste et al., 2008; Hochberg et al., 2012). It is likely that BMIs will be increasingly exploited for purposes of neural rehabilitation (*e.g.* Borton et al., 2013; Thakor, 2013), as well as by patients and healthy individuals who wish to restore and augment movement or communication capacity (Nicolelis, 2003; Millán et al., 2010). Yet, we currently lack empirical evidence and scientific understanding of the SOA for BMI-actions

and knowledge of whether it relies on the same brain mechanisms as those described for body-driven actions.

To examine if BMI-actions are associated with a SOA, and to explore whether and how experimental manipulations used to study the SOA for bodily actions also impact BMI-actions, we used a real-time, motor imagery-based, non-invasive BMI (Guger et al., 2000) and introduced systematic conflicts between decoded motor signals and their resultant sensory consequences (visual feedback). Thus, whereas experimenters previously introduced delays between the movement and its visual consequence (visuo-motor delay; *e.g.* Farrer et al., 2013), we injected systematic delays between the decoded cortical activity and its visual consequence ("visuo-neural delay"). Furthermore, we introduced spatial conflicts by manipulating the direction of the cursor to be either congruent or opposite (incongruent) to the trained directional association. As participants in our experiments controlled the sensory consequences directly via brain activity, this paradigm allowed for investigation of the SOA in a novel setting where motor and movement-associated proprioceptive and tactile signals are absent (Fig. 1).

Materials and Methods

Two experiments were conducted with independent subject samples. For study 1, we tested the SOA for BMI-actions by introducing a wide range of visuo-neural delays. In study 2 we aimed to reconfirm findings in a different study sample and extend our investigation into the effects observed in study 1. As such, we utilized shorter visuo-neural delays, and further performed a control experiment to verify that BMI control was performed without overt muscle contractions.

Subjects

Eight healthy, right-handed participants were recruited for study 1 (2 females; aged 26.5 ± 3.5 years, *mean* ± *SD*) and seven healthy participants for study 2 (7 males; 1 left-handed; aged 26 ± 2.3 years). All participants provided informed consent prior to participation and the present studies were undertaken in accordance with the Declaration of Helsinki and approved by the local ethics research committee at the University of Lausanne.

Electroencephalography (EEG)

27-channel electroencephalography (EEG) was sampled at 128 Hz (*g.tec*, Schiedelberg, Austria) and were saved and processed in real-time using a custom Simulink model (*Mathworks*, Natick, Massachusetts, USA). The electrode grid was centered over sensorimotor cortex, grounded with an additional electrode placed on the forehead, and re-referenced to an electrode attached to the right earlobe. Electrode placement and real-time data processing methods are described in detail in (Guger et al., 2000).

Electromyography (EMG)

For study 1, we ensured that cursor control was not based on overt muscle movements via visual inspection of the participants while performing the task and by reminders to participants to remain motionless. However, in order to more

objectively verify that cursor control was not based on limb muscle artifacts, we measured EMG activity in study 2. EMG data were collected in a supplementary experimental block of 40 trials (20 left hand; 20 right), where participants were asked to physically clasp their left or right hand according to the directional cue. EMG activity was sampled at 128Hz from electrode pairs placed on the left and right forearm flexor muscles midway between the wrist and elbow. The EMG signals were rectified and an average amplitude ratio (motor imagery divided by the maximum voluntary contraction; MVC) was constructed separately for left- and right-cued trials. Further details on data processing and analysis can be found in Wolpaw and McFarland, 2004.

Brain-machine interface training procedure

Participants first trained to perform a lateralized motor imagery task without visual feedback (Pfurtscheller et al., 1997). Participants sat at a table with their hands on their laps (palms up) and their vision of their hands was occluded. They were instructed to relax and to avoid blinking and other body movements. An experimenter visually assured compliance with these instructions throughout the experiment and provided reminders throughout the experiment in the case of negligence. A black fixation cross was first presented for 2000ms. Next, as a preparation cue, the fixation cross turned red for 500ms and was then overlaid with a left or right arrow for 1250ms indicating whether participants should imagine clasping their left or right hand, respectively. Following the directional cue, a fixation cross was presented for 4.25s while participants performed motor imagery.

Training with visual feedback

Coefficients were computed for a binary linear classifier discriminating between left and right imagined hand movements (see *EEG data processing*, below) and used in a second training phase with visual feedback. This training phase was used for the participants to learn the temporal and spatial dynamics of the

relationship between their imagined movements and the movement of the visual cursor. The presentation of the stimulus was the same as for the task without visual feedback, except that following the directional cue, the fixation cross and cue disappeared and were replaced by a horizontally-oriented, rectangular cursor that participants were instructed to move to the cued edge of the screen using the trained motor imagery association. The cursor was controlled by real-time classifier output until the cursor touched one of the edges of the screen, or until 6s had passed without reaching either edge.

Using the set of possible cursor velocities, we computed the minimum and maximum theoretical time to reach an edge (1.48s and 66.41s, respectively). We performed a simulation of 10,000 iterations where the cursor moved according to a random-walk and found it to never reach a target (mean absolute cursor distance traveled as a percentage of the target: 0.071 ± 0.054%; maximum distance traveled in an iteration as a percentage of the target: 32.29%). By contrast, our empirical data showed that participants were able to control the cursor to reach a target in 3.31s ± 0.48 for study 1 and 3.25s ± 0.40 for study 2 (average across trials, experimental conditions and subjects).

After each training block of 40 trials (20 left cues, 20 right), proficiency in controlling the cursor was estimated by computing the real-time classification performance (percentage of time steps classified in the direction of the cue) on a trial-by-trial basis. If participants were unable to achieve >75% mean performance across trials in the training block, or did not verbally report that they felt able to move the cursor in the desired direction, the full training procedure was repeated until these criteria were met (generally 1 to 4 training blocks of 40 trials; study 1: 80 ± 37 trials *mean* ± *SD*; study 2: 80 ± 56 trials). This procedure was repeated up to five training blocks, after which participants still unable to sufficiently control the cursor were dismissed and did not take place in the experiments (study 1: two participants; study 2: six participants). We elected to

dismiss participants if they were unable to control the BMI during the training phase in order to closely follow studies investigating the SOA for body movements, where participants are generally able to perform the required motor task (*e.g.* Blakemore et al., 1999; Sato and Yasuda, 2005; Farrer et al., 2008).

Experimental protocol and measurements

The presentation of the stimulus in the main experiments followed that of the training blocks with visual feedback (see *Training with visual feedback*). In both studies the visual consequences were experimentally manipulated by inserting a buffered delay into the real-time classifier output (Fig. 2, *bottom*). Six delay conditions were tested in study 1 (0 to 3750ms at 750ms intervals). As the SOA is generally tested for shorter visuo-motor delays, we tested a range of sub-second delays in study 2 (0 to 1000ms at 250ms intervals and 3750ms). Thus, in both studies, the cursor position was updated at every time step and was displaced according to classifier output associated with the brain activity from the current time step, or up to 3750ms prior to the current time step. In study 1, an additional manipulation of cursor direction was made: for incongruent trials, classifier output was multiplied by -1, resulting in an inverted velocity mapping between classifier output and cursor position with respect to the learned directional association (Fig. 2, *top*). Thus, in incongruent trials where the participants imagined left hand clasping, the cursor moved to the right, whereas for congruent trials the cursor moved in the direction of the imagined movement.

An additional control condition (henceforth referred to as the ‘random-feedback’ condition) was included in both studies in which the cursor moved on a random trajectory decoupled from the neural activity. We used the following algorithm to generate the random trajectory: at a random interval (uniformly sampled between 250 and 1500 ms), the cursor velocity was randomly sampled (with replacement) from the vector of velocities used to linearly map classification output to cursor feedback. As this experimental condition was the same for both studies, data

analyses were performed on data collapsed across all participants in both studies (resulting in 288 analyzed trials).

Trials were presented in experimental blocks (study 1: 5 blocks of 13 conditions x 3 trial repetitions; study 2: 4 blocks of 6 conditions x 7 repetitions + 1 block of 40 trials for electromyography). Within each block of trials, experimental conditions were randomized and interleaved. Participants were instructed to imagine clasping the cued hand, even if the cursor was not moving as desired.

Sense of agency measurement

SOA was gauged on a trial-by-trial basis with a yes-no response to the statement: "*I felt as if I was controlling the cursor I saw on the screen.*" Responses were transformed into a percentage of yes answers, resulting in a single percentage per subject, per experimental condition.

BMI classification performance measurement

Classification performance was taken as the percentage of time samples that the classifier output corresponded to the cued direction, regardless of where the (potentially) manipulated visual cursor was displaced. Thus, classification performance is also an indicator of the amount of time that participants spent in the brain state associated with the learned coupling between BMI-action and consequence.

Statistical and psychometric analyses

Differences in SOA responses and classification performance across experimental conditions in study 1 were assessed using a 2 x 6 repeated-measures ANOVA with factors Congruency x Delay. After observing a significant interaction, we tested for the main effect of delay separately for congruent and incongruent trials with 1 x 6 repeated-measures ANOVAs. For any significant

main effects we used post-hoc two-tailed, paired t-tests to assess differences across individual experimental conditions. Full statistical results from these tests can be found in Table 1.

Trial-by-trial psychometric analyses

Our inclusion criteria for the experiment led to a high overall classification performance for all subjects (see *Results*). In order to test for an explicit relationship between SOA and classification performance on a trial-by-trial basis over a fuller range of classification performances and a larger data set, trials were pooled across participants and binned (2% classification performance width) such that each SOA response was paired with its corresponding classification performance in four conditions: 1) congruent, no delay; 2) congruent, high delay (3.75s); 3) incongruent, no delay and 4) incongruent, high delay. For study 2, only the first two conditions were used. Psychometric curves were then fit to the binned group data in these four conditions using binomial, logistic regression (glmfit logit function, Matlab, Mathworks, Natick, Massachusetts, USA; *e.g.* Farrer et al., 2013). The same procedure was used to build psychometric curves between SOA and the percentage of time that the cursor was displaced toward the cued direction (for the analysis leading to Figs. 6 and 7C).

For each of the four conditions, two measurements were collected from the best psychometric fit. First, the point of subjective equality (PSE) was taken as the classification percentage closest to 50% SOA (resolution 0.001%). Second, we measured the sensitivity (slope) of the psychometric fit (Stetson et al., 2006). Standard errors on these values were obtained using the bootstrap method with 10,000 iterations and statistical differences across conditions were assessed using a one-tailed bootstrap test (Prsa et al., 2012).

EEG data processing

Offline classifier computation

EEG data from the motor imagery period of the classifier training session were visually inspected for eye blink and muscle artifacts and trials with artifacts were removed. To further increase the robustness of the classifier in study 2, artifact-free trials were combined from two classifier-training sessions (in contrast to one training session for study 1). Thus, the number of artifact-free trials used to train the per-subject classifiers was 38 ± 2 (*mean* ± *SD*) for study 1 and 51 ± 14 for study 2. Of the remaining artifact-free trials used to train each participant's classifier, approximately half (53.4% ± 1 SD) were left and half were right.

Data from the training session was used to compute common spatial patterns (CSPs) for each subject (Blankertz et al., 2008). In study 1, CSPs were computed for motor imagery data from a fixed window (0.25 – 1.25s following the directional cue). In study 2, we further optimized the CSPs by selecting a per-subject window position that maximized the classification performance on the training set (from a 1.5s window at 0.5s intervals, between 0.25 – 4.25s following the cue).

Next, feature vectors were constructed by bandpass filtering the raw EEG in the mu (sensorimotor alpha oscillations; Pfurtscheller et al., 1997) and beta frequency bands (8–30 Hz), reducing the dimensionality of the data by re-projecting it through the first two and last two CSPs, and then computing the log variance across a sliding window of timeframes (*see below*) in each of these four dimensions of the filtered signals. The per-subject classifiers (linear discriminant analysis; McLachlan, 2004) and per-subject CSPs were only computed during the classifier training phase without visual feedback and were held fixed throughout the remainder of the experiment.

Real-time preprocessing, classification, and visual feedback

Real-time EEG data were bandpass filtered, projected through the offline-

computed CSPs, and log variance was taken using the Simulink model. Visual feedback was provided in the form of a rectangular cursor that could move to the left or right of its current position with a velocity proportional to the magnitude of the distance of the feature vector from the linear decision boundary (Fabiani et al., 2004; Wolpaw and McFarland, 2004). The cursor trajectory was additionally smoothed by taking a sliding average (1s window) of the log variance. Thus, features (average log variance across this time window for each of the four CSP dimensions) were computed for each EEG sample and fed to the classifier, resulting in classifier output that translated to a new cursor position every ~8ms.

Additional verification of BMI control signals

To ensure that participants used sensorimotor rhythm modulation rather than non-EEG artifacts to control the cursor, we plotted topographies of the statistically derived common spatial pattern filter weights for single subjects (for methods on the computation of the weights see *Offline classifier computation*, above). The weights were normalized between -1 and 1 and projected for each channel onto a topographical EEG map (*e.g.* Guger et al., 2000; Blankertz et al., 2008).

We verified the presence of classical electrophysiological neuromarkers of motor imagery during real-time cursor control, namely the suppression of sensorimotor mu/beta band-power (8–30 Hz) in contralateral versus ipsilateral imagery (Pfurtscheller et al., 1997). To do so, we first computed the mu- and beta-band power spectral density for all participants (Fast Fourier Transform; Matlab, Mathworks, Natick, Massachusetts, USA) during the cursor control period separately for left and right imagery trials and in electrodes lying in close proximity to sensorimotor hand regions (C3 and C4) as well as in a central control electrode (FCz). Next, we computed the log power ratio (LPR) of contralateral versus ipsilateral imagery trials and took the mean across participants. Thus, the LPR indicates the relative power modulation between right

imagery trials as compared to left imagery trials (at electrode C3) and left imagery trials as compared to right imagery trials (at electrode C4). The LPR at the control electrode was taken as the ratio of left imagery versus right imagery. Log power ratios (LPR) are approximately log-normal, and since a LPR of 0 indicates no difference in the power spectral density (PSD) between contralateral and ipsilateral motor imagery trials, we performed two-tailed t-tests (Bonferonni corrected for multiple comparisons) of the LPR distributions against a distribution with mean 0.

Results

Sense of agency (study 1)

The SOA was higher for congruent than for incongruent feedback (main effect of congruency: $F_{(1,7)} = 43.3$; $P < 0.001$; Fig. 3A). Furthermore, the SOA depended differently on delay for congruent and incongruent trials as reflected by a delay × congruency interaction ($F_{(5,7)} = 5.76$; $P = 0.001$). For congruent trials, the SOA decreased with increasing delay (from 84% to 58%; $F_{(5,7)} = 5.33$; $P = 0.001$). By contrast, for incongruent trials, the SOA was low and did not depend on visuo-neural delay (20% to 34%; $F_{(5,7)} = 1.87$; $P = 0.13$; see Table 1 for full statistical results). To further analyze the effect of delay on the SOA, we also performed linear regression separately on congruent and incongruent trials and found that SOA decreases with increasing delay for congruent ($r^2 = 0.25$, $P < 0.001$), but not for incongruent trials ($r^2 = 0.08$, $P > 0.05$). In summary, these results indicate that subjects felt a higher SOA for congruent BMI-actions and that this SOA decreased as a function of visuo-neural delay. On the other hand, directional incongruence led to a large decrease in the SOA and for these trials, the SOA was insensitive to visuo-neural delay.

Classification performance and EEG analysis (study 1)

We analyzed BMI classification performance across participants and found that it remained higher than chance levels (76.7 ± 8.77 vs. 53.4% ± 1; *mean* ± *SD*; $P < 0.001$; *one-tailed T-test*) in all conditions and exhibited no significant difference across the experimental conditions ($F_{(5,7)} = 1.36$; $P > 0.25$; *two-way ANOVA*; Fig. 3B). In order to test for learning effects, we additionally analyzed classification performance across participants as a function of trial order and found no significant effect of trial order ($F_{(7,194)} = 0.96$; $P = 0.64$; *one-way ANOVA*).

To investigate whether participants modulated the expected mu-/beta-band oscillations over bilateral sensorimotor cortex to control the cursor movements, we first projected the statistically derived classification features (common spatial patterns) to topographical EEG maps for each participant. The resulting spatial filters revealed the importance of electrodes C3 and C4 (located over left and right sensorimotor hand regions) in discriminating between left and right motor imagery, for all individuals (Fig. 4A). Next, we performed spectral analysis which showed mu- and beta-band power to be suppressed at both electrode C3 (-1.08 ± 0.24; *mean*±*SEM*; *two-tailed T-test; P = 0.003*) and electrode C4 (-1.02 ± 0.33; *P = 0.018*) in contralateral imagery trials as compared to ipsilateral trials, but not at control electrode FCz (0.098 ± 0.14; *P = 0.5*; Fig. 4B). Taken together, these classification performance and EEG results show that the differences observed in the SOA between our experimental conditions cannot be accounted for by differences in decoder performance, and that the BMI-action was generated by sensorimotor networks classically recruited during motor imagery.

Trial-by-trial psychometric analyses: SOA as a function of classification performance (study 1)

Next, we performed a trial-by-trial psychometric analysis between classification performance and the SOA. We generated psychometric SOA curves for the pooled, group data and fit them to the EEG classification performance for the two extreme delay conditions (see *Materials and Methods*). For congruent trials, this analysis revealed that low classification performance was associated with a low SOA and that high classification performance was associated with a high SOA (Fig. 5, *left*). For any given classification performance, delay insertion led to a decrease in SOA and a shift in the point of subjective equality (PSE) from 43.4% to 62.1% (*one-tailed bootstrap test; P* = 0.015). Delay insertion was further associated with higher SOA variance characterized by a decrease in the absolute slope of the psychometric curve (*one-tailed bootstrap test; P* = 0.03). Thus, although average classification performance was not influenced by visuo-neural

delay (Fig. 3B), visuo-neural delay altered the relationship between classification performance and the SOA. In particular, delay introduced uncertainty into the SOA judgments and in order to report an equivalent SOA in delayed trials, participants remained longer in the brain state associated with the learned BMI-action consequence (*i.e.* higher classification performance).

For incongruent trials, this analysis also showed visuo-neural delay to yield higher SOA variance (absolute slope decrease; $P = 0.04$). However, in contrast to congruent trials, low classification performance for incongruent trials was associated with a higher SOA and high classification performance was associated with a lower SOA (Fig. 5, *right*). Though low classification performance generally indicates poor BMI control (*e.g.* Guger et al., 2000), these data show that one does not necessarily have to successfully control the BMI to feel a high SOA for incongruent BMI-actions. In addition, and in contrast to congruent BMI-actions, the SOA increased with visuo-neural delay for any given classification performance (PSE shift: 50.7% to 62.9%; $P = 0.02$). In other words, to report an equivalent SOA in delayed trials as for non-delayed trials, participants remained longer in the brain state associated with the subject-and-machine learned, but now reversed BMI-action mapping. For example, our subjects spent more time imagining right movement for a right-cued trial for an equivalent SOA, despite the cursor moving to the left (and vice versa for left-cued trials). These data demonstrate that the mechanisms for the SOA for incongruent BMI-actions differ from those observed for bodily actions, where task performance is generally linked to the SOA in the opposite manner (*e.g.* as observed for congruent BMI-actions). Furthermore, since our experimental manipulations of incongruent and delayed trials may effectively correct for poor BMI-control, such as in cases where participant's poor BMI control inadvertently causes the manipulated cursor to move toward the cued direction, these results suggest that the SOA for incongruent or delayed BMI-actions may be based on the congruency of the visual feedback with the cued direction.

Cognitive or postdictive mechanisms and the SOA for BMI-actions

To test for cognitive mechanisms influencing the SOA for BMI-actions, we next fit psychometric SOA curves to the percentage of time that the cursor was displaced in the cued direction for each trial, irrespective of BMI performance. This analysis revealed that participants have a high SOA when the visual cursor frequently moves in the cued direction and a low SOA when the cursor rarely moves in the cued direction (Fig. 6). This relationship held for all tested BMI-actions, that is, for congruent non-delayed (PSE: 62.2; slope: 0.019), congruent delayed (PSE: 62; slope: 0.014), incongruent non-delayed (PSE: 68.2; slope: 0.015), and incongruent delayed (PSE: 66.7; slope: 0.018) trials. No difference in slope or PSE was found across the experimental conditions (all one-tailed bootstrap tests; $P > 0.05$).

SOA for "BMI-actions" where the sensory consequences are decoupled from brain activity

Analysis of the 'random-feedback' condition, where the cursor was displaced independently with respect to the decoded motor signals, revealed that the SOA on these trials was highly variable across individuals (38.89 ± 27.15; *mean* ± *SD*; Fig. 7A). Classification performance for this condition, however, remained high and did not differ from the main experimental conditions in studies 1 and 2 (79.92 ± 9.87; *two-tail T-test*; all $P > 0.05$), indicating that the observed changes in the SOA could not have been due to differences in decoder performance.

For these random-feedback trials, psychometric analyses between the SOA and classification performance resulted in a poor psychometric fit that led to an undefined PSE and slope (Fig. 7B). On the other hand, a psychometric fit for the percentage of time in the cued (intended) direction versus the SOA again

revealed a clear relationship: when the cursor rarely moved in the intended direction, the SOA was low, and when it moved often in the cued direction, the SOA was high (PSE: 65%; Fig. 7C).

Taken together, these psychometric analyses demonstrate that the SOA is highly variable for BMI-actions where sensory feedback is decoupled from the decoded motor signals and that this SOA is best predicted by the coherence of the visual feedback with the intended direction, rather than by a participant's trial-by-trial classification performance. This again highlights the predominance of the visual feedback in accounting for the SOA for the BMI-actions used in this context.

SOA for BMI-actions: Classification performance or visual feedback?

Finally, we assessed whether BMI classification performance was a contributing factor to the SOA, or if the SOA was based solely on the congruence of the visual feedback with the cued direction. To this end, we performed a stepwise regression to see if any residual variance in the SOA curves could be accounted for by classification performance. This analysis revealed that classification performance accounts for 0.07% of the residual variance in SOA judgments ($P < 0.01$; stepwise regression; fixed-effects model). Though this analysis confirms that the visual feedback clearly dominates the SOA for BMI-actions, it also suggests that participants are at least partially basing their SOA on the classifier-driving sensorimotor brain activity.

Sense of agency (study 2)

Analysis on the shorter visuo-neural delays tested in study 2 confirmed the effect of delay on the SOA (main effect of delay: $F_{(5,6)} = 7.82$; $P = 0.0001$; Fig. 8A). However, visuo-neural delays below 1s did not modulate the SOA for the BMI-actions we tested (all pairwise tests $P > 0.05$).

Classification performance, EEG, and EMG analysis (study 2)

Classification performance did not vary across the tested visuo-neural delays (81.70 ± 10.78; *mean* ± *SD*; $F_{(1,6)} = 0.19; P = 0.97;$ *one-way ANOVA*; Fig 8B). Furthermore, no difference was found in classification performance as a function of trial order ($F_{(6,167)} = 0.88; P > 0.84;$ *one-way ANOVA*).

As for study 1, we confirmed that BMI control was driven by mu-/beta-band modulation over bilateral sensorimotor cortex by projecting the spatial filter weights as scalp topographies. For all individuals, electrodes C3 and C4, located over left and right hand motor areas, respectively, showed the greatest influence of discrimination between left and right hand motor imagery (Fig. 8C).

Finally, analysis of the EMG data revealed low muscle contraction ratios for all participants (Fig. 8D) that were not significantly different from periods of rest ($P < 0.01$; *two-tailed T-test*), suggesting that the SOA judgments for BMI-actions were not associated with small limb movements or covert muscle contractions. For illustrative purposes, Figure 8E displays single EMG traces during cursor control (motor imagery) and voluntary overt movements (MVC) for participant 2 in characteristic left- and right-cued imagery trials.

Discussion

Based on work from the cognitive neuroscience of action awareness and motor control, we introduced spatio-temporal conflicts between decoded cortical motor signals and their resultant sensory consequences during the real-time brain-control of a visual cursor (here defined as BMI-actions). In two experiments, we found that congruent BMI-actions were associated with a robust SOA that was

perturbed by the insertion of visuo-neural delay. Classification performance was high across the experimental conditions and the cursor was controlled by mu- and beta-band oscillations (8 – 30 Hz) over bilateral sensorimotor cortex in the absence of overt muscle activity.

Although it is well described that bodily actions are associated with a SOA that is reduced by visuo-motor (Farrer et al., 2008), audio-motor (Sato and Yasuda, 2005), and somato-motor (Blakemore et al., 1999) delays between the bodily action and its sensory outcomes, this is the first study (to our knowledge) to target the SOA for BMI-actions. Investigating the SOA in this novel, 'disembodied' context avoids some of the confounds of earlier work. In particular, bodily actions are normally accompanied by re-afferent proprioceptive and tactile signals that were absent in the present experiments, as BMI-actions are generated without full involvement of the central nervous and musculoskeletal systems (Wolpaw, 2007).

Despite this unique context, our analyses showed that congruent BMI-actions are associated with a robust SOA that decreases with increasing discrepancy between the predicted and actual sensory feedback, as for bodily actions. This suggests that the SOA for these two types of actions is at least partially based on common brain mechanisms and may recruit some of the same regions that have been described for the SOA for bodily actions, including the supplementary motor area, ventral premotor cortex, posterior parietal cortex, temporo-parietal junction, and/or cerebellum (review in David et al., 2008).

We also observed differences between the SOA for congruent BMI- and bodily actions, suggesting distinct brain mechanisms for these types of actions. For instance, the present data show the SOA for congruent BMI-actions without

visuo-neural delay to be ~85%. Most studies report higher SOA values for bodily actions in comparable experimental conditions (Fourneret and Jeannerod, 1998; Sato and Yasuda, 2005; Farrer et al., 2008). Moreover, the temporal sensitivity of the SOA for congruent BMI-actions was lower than for bodily actions: study 2 revealed that participants were insensitive to visuo-neural delays of less than 1s, whereas previous SOA studies for bodily actions have reported visuo-motor or audio-motor delays of 150-300 ms to significantly perturb the SOA (Sato and Yasuda, 2005; Farrer et al., 2008, 2013). The most likely explanation for these differences is an increased latency in BMIs between the brain's "movement"-related signals and the end effector. Moreover, the signal-to-noise ratio (*i.e.* overall end-effector control reliability) is much lower for the BMI-actions utilized in the present context than for the overlearned bodily actions of previous SOA studies. A low signal-to-noise ratio for BMI-actions might arise from the lack of tactile-proprioceptive feedback, imperfections implicit to the selected neural decoding process, subject selection (our investigations only included participants able to control our BMI with a certain competency), and the novelty of a motor imagery task. Indeed, recent work demonstrated that the SOA for bodily actions increases with learning of novel overt motor tasks (Wel et al., 2012).

The results for incongruent BMI-actions are in contrast to our observations for congruent BMI-actions and to previous findings concerning the SOA for bodily actions. Notably, our psychometric analyses for incongruent BMI-actions revealed a high SOA during periods of poor performance that was further increased by additional temporal feedback discrepancy. This indicates that participants have a SOA for a BMI-action even if their classified EEG signals do not match the trained patterns they had learned to couple their neural activity to the associated visual consequences, making it unlikely that the SOA for incongruent BMI-actions can be accounted for by predictive SOA accounts (Wolpert et al., 1995; Miall and Wolpert, 1996; Frith et al., 2000). According to these accounts, the large mismatch between the decoded motor commands and

the visual feedback ought to yield a low SOA, and additional mismatch should further reduce the SOA. Furthermore, by assessing classification performance (Fig. 3B) alongside the SOA (Fig. 3A), we observed that participants generated similar mu-/beta-band oscillations in sensorimotor cortex in all experimental conditions, even though the SOA changed as a function of congruence and visuo-neural delay. This dissociation between the SOA and classification performance for incongruent BMI-actions indicates that the SOA was not based on a comparison between the mu-/beta-band oscillations in sensorimotor cortex and brain signals associated with the visual feedback.

Considering this, how could our participants form a SOA? Postdictive SOA theories hold that the SOA is based on comparing cognitive cues (*e.g.* intentions and goals) with the sensory outcomes (Wegner, 2002). In the present context, a high SOA for poorly controlled BMI-actions could occur if the cursor displacements were to match the subject's cued (and likely intended) direction. Our paradigm, and in particular incongruent BMI-actions, allowed us to test the special situation where a mismatch between the decoded brain signals and the sensory consequences yields congruence between the cued cursor direction and the actual cursor displacement. Indeed, our trial-by-trial analyses revealed, for all experimental conditions, a distinct relationship between the SOA and the match of the visual feedback with the cued direction. Incongruent trials when analyzed with respect to classification performance (Fig. 5, *right*) and the directional feedback (Fig. 6, *right*) leads to a divergence which is compatible with the proposal that the SOA for incongruent BMI-actions (and perhaps congruent BMI-actions) depends on cognitive agency signals and may be independent of the motor imagery-based signals in sensorimotor cortex. This interpretation is further supported by our SOA analysis in the 'random-feedback' condition (Fig. 8). Collectively, these findings suggest that the SOA for BMI-actions is largely reliant on comparison of the re-afferent visual cues with visual feedback rather than with the motor signals used to control the BMI.

Nevertheless, we also found classification performance to account for a small but significant portion of the variance in the SOA responses. This analysis suggests that some form of self-monitoring is at play (*e.g.* comparison of the decoded sensorimotor signals to the sensory outcomes). The small effect may be due to the strong dominance of visual feedback in the SOA for BMI-actions, or for novel or unreliable actions in general. The present experiments do not elucidate whether such monitoring on the part of the brain is predictive (as per the "predictive-coding" framework) or related to other mechanisms (*e.g.* the brain may infer a SOA for BMI-actions by monitoring the relative amplitude of mu-band oscillations in the two hemispheres versus an encoding for the cued direction). Further research is required to assess the relative roles of sensory feedback versus predictive models of sensorimotor brain activity in BMI-actions. These results confirm that the SOA for BMI-actions can be based almost purely on visual feedback (if proprioceptive feedback and overt movement is absent), while a small amount of SOA variance could be accounted for by brain signals alone, suggesting that internal models may be at work but were overridden by the visual feedback.

Thus, we argue that cognitive, postdictive agency theories rather than predictive best account for congruent, incongruent, and ‘random-feedback’ EEG-based BMI-actions. Alternatively, recent multifactorial theories (Pacherie, 2008; Synofzik et al., 2008, 2013; Knoblich and Repp, 2009; Moore et al., 2009; Farrer et al., 2013; Kawabe, 2013), allow for relative contextual weighting of predictive and postdictive information in the formation of the SOA. This unified framework has been used to explain how the SOA can emerge for joint actions in human dyads (Wel et al., 2012), a situation that may be analogous to the “joint” action between human and machine needed to generate BMI-actions. Our findings, which show that some combination of visual feedback and internal monitoring of sensorimotor activity best explains the SOA for BMI-actions, fit favorably within

such a framework. Further research is needed to better understand the relative weighting of predictive and postdictive cues in forming a SOA for BMI-actions and differences in weighting with respect to the SOA for bodily actions. For instance, it could be the case that for bodily actions, predictive mechanisms play a much larger role in determining the SOA, whereas for BMI-actions, postdictive mechanisms dominate in the presence of sensory feedback.

In our quest for repair, substitution, and augmentation, we will likely witness an increase in the use of brain-controlled technologies (Nicolelis, 2003; Millán et al., 2010). Experimental setups such as the present one allow for the investigation of the SOA for these new types of “actions” and provide empirical, neuroscience-based data for the unique ethical and moral challenges raised with respect to responsibility for machine-controlled actions (Blanke and Aspell, 2009; Haggard and Tsakiris, 2009; Moretto et al., 2011).

References

Blakemore S, Wolpert DM, Frith CD (2002) Abnormalities in the awareness of action. 6:237–242.

Blakemore SJ, Frith CD, Wolpert DM (1999) Spatio-temporal prediction modulates the perception of self-produced stimuli. J Cogn Neurosci 11:551–559.

Blanke O, Aspell J (2009) Brain technologies raise unprecedented ethical challenges. Nature 458:2009 Available at: http://www.nature.com/nature/journal/v458/n7239/full/458703b.html [Accessed February 16, 2014].

Blankertz B, Tomioka R, Lemm S, Kawanabe M, Muller K-R (2008) Optimizing Spatial filters for Robust EEG Single-Trial Analysis. IEEE Signal Process Mag 25:1–12.

Borton D, Micera S, Millán JDR, Courtine G (2013) Personalized neuroprosthetics. Sci Transl Med 5:210rv2 Available at: http://www.ncbi.nlm.nih.gov/pubmed/24197737 [Accessed January 21, 2014].

David N, Cohen MX, Newen A, Bewernick BH, Shah NJ, Fink GR, Vogeley K (2007) The extrastriate cortex distinguishes between the consequences of one's own and others' behavior. Neuroimage 36:1004–1014 Available at: http://www.ncbi.nlm.nih.gov/pubmed/17478105 [Accessed January 25, 2014].

David N, Newen A, Vogeley K (2008) The "sense of agency" and its underlying cognitive and neural mechanisms. Conscious Cogn 17:523–534 Available at: http://www.ncbi.nlm.nih.gov/pubmed/18424080 [Accessed January 23, 2014].

De Vignemont F, Fourneret P (2004) The sense of agency: a philosophical and empirical review of the "Who" system. Conscious Cogn 13:1–19 Available at: http://www.ncbi.nlm.nih.gov/pubmed/14990237 [Accessed January 26, 2014].

Fabiani G, McFarland D, Wolpaw J, Pfurtscheller G (2004) Conversion of EEG activity into cursor movement by a brain-computer interface (BCI). Neural Syst Rehabil Eng IEEE Trans 12:331–338 Available at: papers://248a3614-0a46-4871-940a-2d2e9866e6d0/Paper/p671.

Farrer C, Bouchereau M, Jeannerod M, Franck N (2008) Effect of distorted visual feedback on the sense of agency. Behav Neurol 19:53–57.

Farrer C, Franck N, Georgieff N, Frith CD, Decety J, Jeannerod M (2003) Modulating the experience of agency: a positron emission tomography study. Neuroimage 18:324–333 Available at: http://linkinghub.elsevier.com/retrieve/pii/S1053811902000411 [Accessed January 23, 2014].

Farrer C, Frith CD (2002) Experiencing oneself vs another person as being the cause of an action: the neural correlates of the experience of agency. Neuroimage 15:596–

603 Available at: http://www.ncbi.nlm.nih.gov/pubmed/11848702 [Accessed January 23, 2014].

Farrer C, Valentin G, Hupé JM (2013) The time windows of the sense of agency. Conscious Cogn 22:1431–1441 Available at: http://dx.doi.org/10.1016/j.concog.2013.09.010.

Fourneret P, Jeannerod M (1998) Limited conscious monitoring of motor performance in normal subjects. Neuropsychologia 36:1133–1140.

Frith CD, Blakemore SJ, Wolpert DM (2000) Abnormalities in the awareness and control of action. Philos Trans R Soc Lond B Biol Sci 355:1771–1788 Available at: http://www.pubmedcentral.nih.gov/articlerender.fcgi?artid=1692910&tool=pmcentrez&rendertype=abstract [Accessed January 26, 2014].

Gallagher S (2000) Philosophical conceptions of the self: implications for cognitive science. Trends Cogn Sci 4:14–21.

Guger C, Ramoser H, Pfurtscheller G (2000) Real-time EEG analysis with subject-specific spatial patterns for a brain-computer interface (BCI). IEEE Trans Rehabil Eng 8:447–456.

Haggard P, Tsakiris M (2009) The Experience of Agency: Feelings, Judgments, and Responsibility. Curr Dir Psychol Sci 18:242–246 Available at: http://cdp.sagepub.com/lookup/doi/10.1111/j.1467-8721.2009.01644.x [Accessed February 16, 2014].

Hochberg LR, Bacher D, Jarosiewicz B, Masse NY, Simeral JD, Vogel J (2012) Reach and grasp by people with tetraplegia using a neurally controlled robotic arm. Nature 485:372–375 Available at: http://dx.doi.org/10.1038/nature11076.

Jeannerod M (2006) Motor cognition: What actions tell the self. Oxford University Press.

Jeannerod M, Pacherie E (2004) Agency, Simulation and Self-identification. Mind Lang 19:113–146 Available at: http://doi.wiley.com/10.1111/j.1468-0017.2004.00251.x.

Kannape O a, Schwabe L, Tadi T, Blanke O (2010) The limits of agency in walking humans. Neuropsychologia 48:1628–1636 Available at: http://www.ncbi.nlm.nih.gov/pubmed/20144893 [Accessed February 16, 2014].

Kawabe T (2013) Inferring sense of agency from the quantitative aspect of action outcome. Conscious Cogn 22:407–412 Available at: http://dx.doi.org/10.1016/j.concog.2013.01.006.

Knoblich G, Repp BH (2009) Inferring agency from sound. Cognition 111:248–262 Available at: http://www.ncbi.nlm.nih.gov/pubmed/19306996 [Accessed January 25, 2014].

Knoblich G, Sebanz N (2005) Agency in the face of error. Trends Cogn Sci 9:259–261.

McLachlan G (2004) Discriminant analysis and statistical pattern recognition. Available at: http://books.google.com/books?hl=en&lr=&id=O_qHDLaWpDUC&oi=fnd&pg=PR7&dq=Discriminant+analysis+and+statistical+pattern+recognition&ots=6EShNOFVSS&sig=FqclSsEsrJJTWDeNHLUMMgm7vuY [Accessed February 16, 2014].

Miall R, Wolpert D (1996) Forward models for physiological motor control. Neural networks Available at: http://www.sciencedirect.com/science/article/pii/S0893608096000354 [Accessed February 16, 2014].

Millán JDR, Rupp R, Müller-Putz GR, Murray-Smith R, Giugliemma C, Tangermann M, Vidaurre C, Cincotti F, Kübler a, Leeb R, Neuper C, Müller K-R, Mattia D (2010) Combining Brain-Computer Interfaces and Assistive Technologies: State-of-the-Art and Challenges. Front Neurosci 4:1–15 Available at: http://www.pubmedcentral.nih.gov/articlerender.fcgi?artid=2944670&tool=pmcentrez&rendertype=abstract [Accessed January 21, 2014].

Moore JW, Wegner DM, Haggard P (2009) Modulating the sense of agency with external cues. Conscious Cogn 18:1056–1064 Available at: http://www.ncbi.nlm.nih.gov/pubmed/19515577 [Accessed January 30, 2014].

Moretto G, Walsh E, Haggard P (2011) Experience of agency and sense of responsibility. Conscious Cogn 20:1847–1854 Available at: http://dx.doi.org/10.1016/j.concog.2011.08.014.

Nicolelis M (2003) Opinion: Brain–machine interfaces to restore motor function and probe neural circuits. Nat Rev Neurosci 4:417–422 Available at: file:///Users/nathan/Documents/Papers/2003/Nicolelis/Opinion Brain–machine interfaces to restore 2003 Nicolelis.pdf.

Pacherie E (2008) The phenomenology of action: a conceptual framework. Cognition 107:179–217 Available at: http://www.ncbi.nlm.nih.gov/pubmed/17950720 [Accessed January 24, 2014].

Pfurtscheller G, Neuper C, Flotzinger D, Pregenzer M (1997) EEG-based discrimination between imagination of right and left hand movement. Electroencephalogr Clin Neurophysiol 103:642–651.

Prsa M, Gale S, Blanke O (2012) Self-motion leads to mandatory cue fusion across sensory modalities. J Neurophysiol 108:2282–2291 Available at: papers://248a3614-0a46-4871-940a-2d2e9866e6d0/Paper/p914.

Sato A, Yasuda A (2005) Illusion of sense of self-agency: discrepancy between the predicted and actual sensory consequences of actions modulates the sense of self-agency, but not the sense of self-ownership. Cognition 94:241–255 Available at: http://www.ncbi.nlm.nih.gov/pubmed/15617673 [Accessed January 24, 2014].

Sperry R (1950) Neural basis of the spontaneous optokinetic response produced by visual inversion. J Comp Physiol Psychol 43.

Stetson C, Cui X, Montague PR, Eagleman DM (2006) Motor-sensory recalibration leads to an illusory reversal of action and sensation. Neuron 51:651–659 Available at: http://www.ncbi.nlm.nih.gov/pubmed/16950162 [Accessed January 22, 2014].

Synofzik M, Vosgerau G, Newen A (2008) Beyond the comparator model: a multifactorial two-step account of agency. Conscious Cogn 17:219–239 Available at: http://www.ncbi.nlm.nih.gov/pubmed/17482480 [Accessed January 22, 2014].

Synofzik M, Vosgerau G, Voss M (2013) The experience of agency : an interplay between prediction and postdiction. 4:1–8.

Taylor DM, Tillery SIH, Schwartz AB (2002) Direct cortical control of 3D neuroprosthetic devices. Science 296:1829–1832 Available at: http://www.ncbi.nlm.nih.gov/pubmed/12052948 [Accessed January 24, 2014].

Thakor N V (2013) Translating the brain-machine interface. Sci Transl Med 5:210ps17 Available at: http://www.ncbi.nlm.nih.gov/pubmed/24197734.

Tsakiris M, Haggard P, Franck N, Mainy N, Sirigu A (2005) A specific role for efferent information in self-recognition. Cognition 96:215–231 Available at: http://www.ncbi.nlm.nih.gov/pubmed/15996559 [Accessed January 23, 2014].

Velliste M, Perel S, Spalding MC, Whitford AS, Schwartz AB (2008) Cortical control of a prosthetic arm for self-feeding. Nature 453:1098–1101 Available at: http://www.ncbi.nlm.nih.gov/pubmed/18509337 [Accessed January 21, 2014].

Von Holst E, Mittelstaedt H (1950) No Title. Naturwissenschaften 37.

Wegner D (2002) The illusion of conscious will. MIT Press. Available at: http://books.google.com/books?hl=en&lr=&id=eQnlRg56piQC&oi=fnd&pg=PR7&dq=The+illusion+of+conscious+will&ots=ZXxqHuT3HZ&sig=0G0xPLYNksTCohSmlyOPKZEc_jk [Accessed February 16, 2014].

Wegner DM (2003) The mind’s best trick: how we experience conscious will. Trends Cogn Sci 7:65–69 Available at: http://linkinghub.elsevier.com/retrieve/pii/S1364661303000020 [Accessed January 23, 2014].

Wel RPRD Van Der, Sebanz N, Knoblich G (2012) The sense of agency during skill learning in individuals and dyads. Conscious Cogn 21:1267–1279 Available at: http://dx.doi.org/10.1016/j.concog.2012.04.001.

Wolpaw JR (2007) Brain-computer interfaces as new brain output pathways. J Physiol 579:613–619 Available at: http://www.pubmedcentral.nih.gov/articlerender.fcgi?artid=2151370&tool=pmcentrez&rendertype=abstract [Accessed February 5, 2014].

Wolpaw JR, McFarland DJ (2004) Control of a two-dimensional movement signal by a noninvasive brain-computer interface in humans. Proc Natl Acad Sci U S A 101:17849–17854.

Wolpert DM, Ghahramani Z, Jordan MI (1995) An internal model for sensorimotor integration. Science (80-) 269:1880–1882 Available at: papers://248a3614-0a46-4871-940a-2d2e9866e6d0/Paper/p835.

Figures

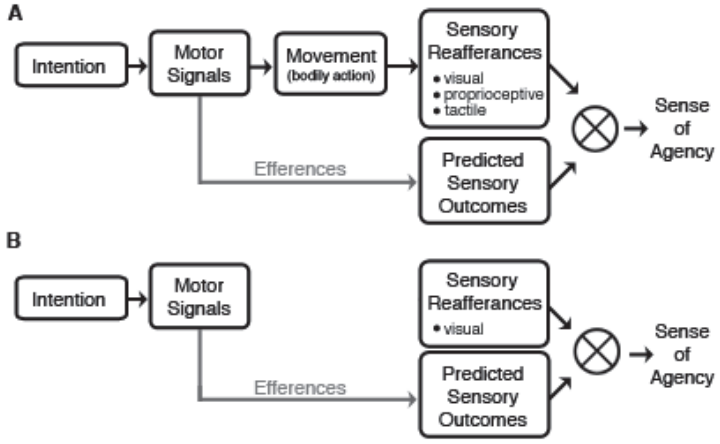

Figure 1. Schematic diagrams contrasting bodily and brain-machine actions in the context of predictive frameworks for the sense of agency (SOA). (A) Inspired by models of motor control, previous work on the SOA for bodily actions has theorized that a perturbed SOA stems from discrepancies between one's predicted (efferent) and actual (re-afferent) sensory outcomes. These re-afferent signals may come from internal (*e.g.* proprioceptive and tactile signals stemming from muscle activity) or external sources (*e.g.* a visual flash on a screen). **(B)** In contrast to these previous paradigms, the current setup was designed to investigate the SOA for BMI-actions that lack bodily movement and the concomitant re-afferent tactile and proprioceptive signals. In this context, the SOA may depend on the comparison of one's efferent motor commands (from motor imagery) or intended goal states with the re-afferent sensory outcomes. Schematic diagrams are based on (David et al., 2008).

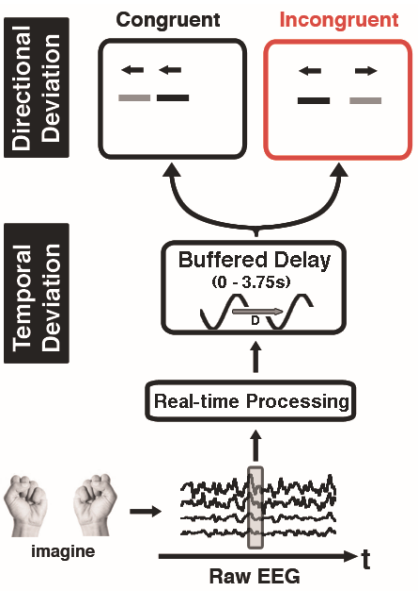

Figure 2. Task and experimental manipulations. Participants were asked to imagine clasping their left or right hand. EEG signals were measured, processed, and decoded in real-time in order to displace a cursor on a monitor to the left or right. For each trial of cursor control, one of six temporal deviations was applied using a buffered delay on the decoded motor signal. Additionally, a directional deviation was applied to the cursor position such that in half of the trials, the coupling between the classifier output and the cursor displacement was reversed (incongruent; red) from the learned association (congruent; black). For instance, for incongruent trials, left imagery resulted in right cursor displacement.

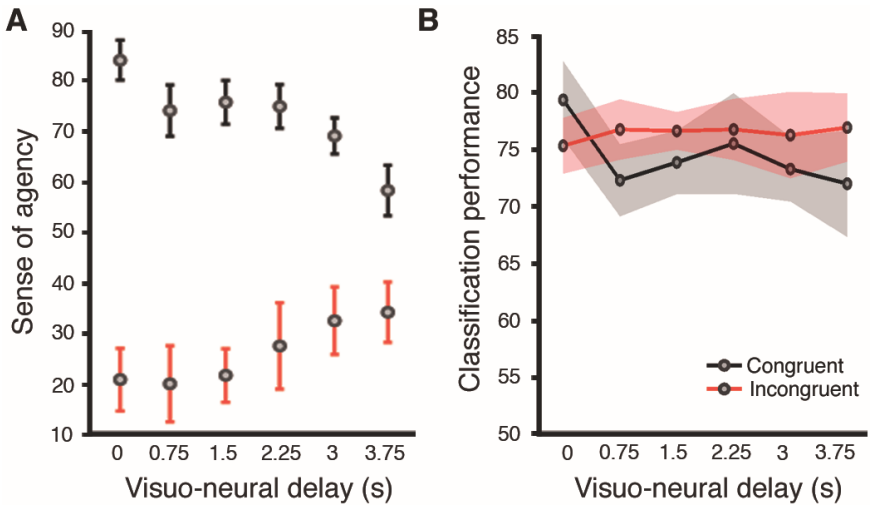

Figure 3. Brain-machine actions are associated with a sense of agency (SOA) that is modulated by visuo-neural delay. ***(A)*** SOA (% yes answers) for congruent (black) and incongruent (red) BMI-actions plotted as a function of visuo-neural delay. ***(B)*** Classification performance (% real-time decoder performance) remained constant across experimental conditions. Error bars and shaded regions indicate SE of the mean.

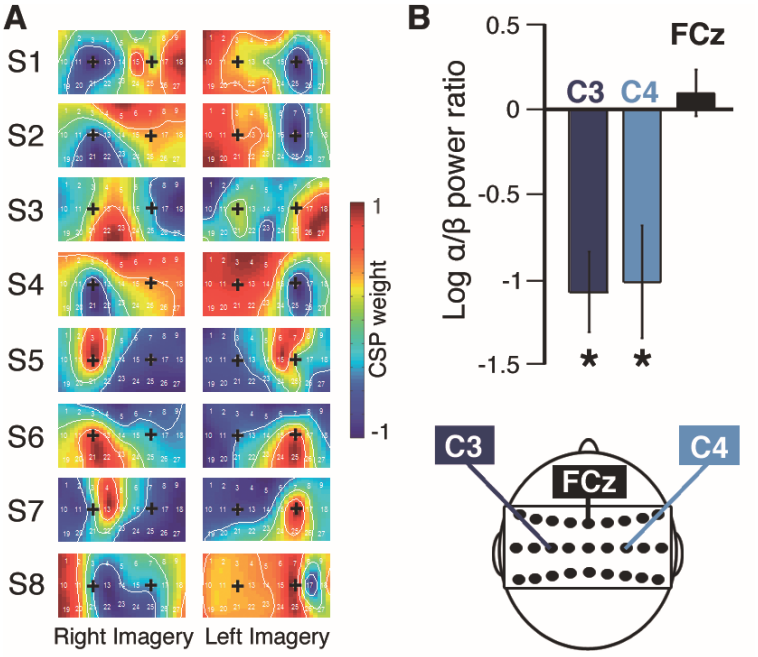

Figure 4. Cursor control driven by bilateral sensorimotor mu- and beta-band modulations. ***(A)*** Normalized, per-channel common spatial pattern weights for each electrode during left and right motor imagery for each participant (S1-S8) collected during the BMI training period (without visual feedback). On each topographic map, '+' labels are placed over electrodes C3 and C4 for orientation. ***(B)*** Contralateral divided by ipsilateral log power ratios for 8–30 Hz oscillations at electrodes C3, C4, and control electrode FCz. * indicates significant suppression ($P < 0.05$; *two-tailed T-test*) with respect to a log power ratio of 0 (*i.e.* no difference between ipsilateral and contralateral power). Error bars represent SE of the mean.

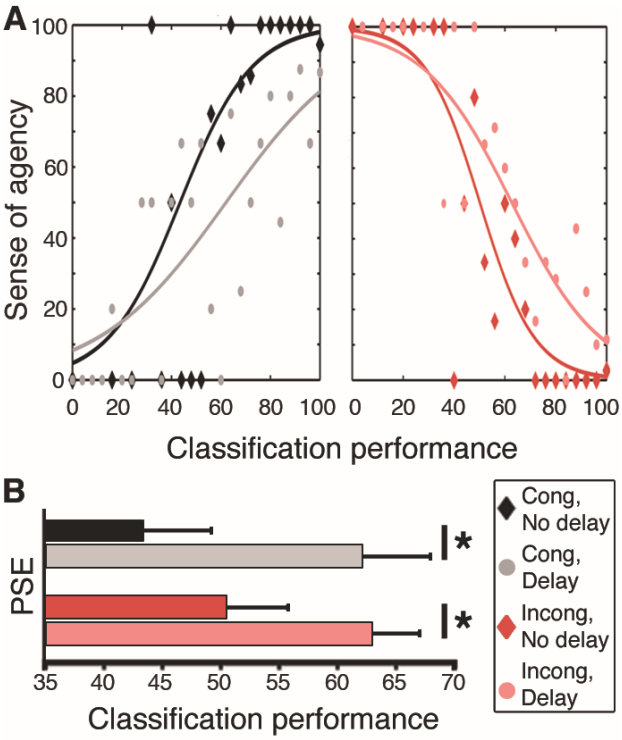

Figure 5. Trial-by-trial psychometric relationship between the sense of agency (SOA) and classification performance. ***(A)*** SOA as a function of classification performance at zero and high delay (3.75s) for congruent and incongruent trials. Data points represent mean SOA across all trials for all participants in 4% classification performance bins. Curves indicate best-fit logistic regression. ***(B)*** Point of subjective equality for each psychometric curve in *(A)*. Error bars represent SE of the mean and * indicates a significant difference between conditions (*P < 0.05; one-tailed bootstrap test*).

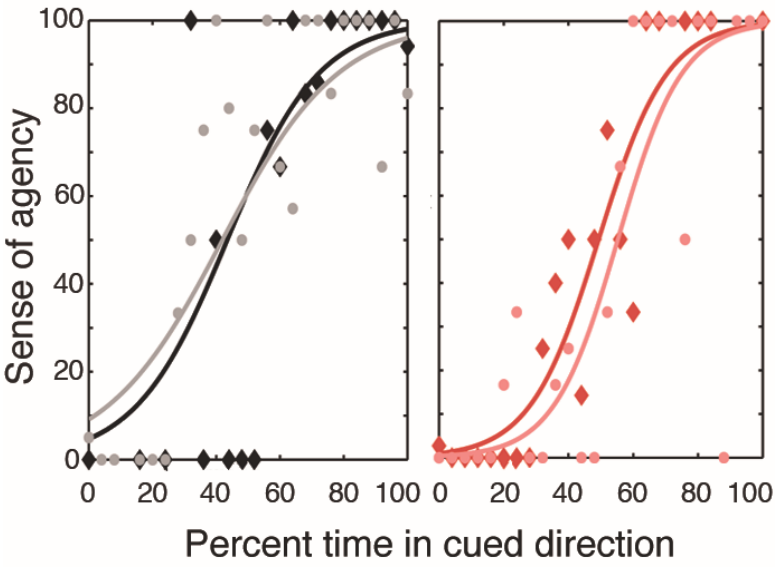

Figure 6. Sense of agency (SOA) for BMI-actions depends on the match between one's intended direction and the resultant sensory consequences. Psychometric SOA curves (best-fit logistic regression) are plotted as a function of the percentage of time the cursor spent moving in the cued direction for zero-delay congruent (black), high-delay congruent (grey), zero-delay incongruent (red), high-delay incongruent (pink) trials. Data points represent mean SOA across all trials for all participants in 4% bins (of percent time in cued direction).

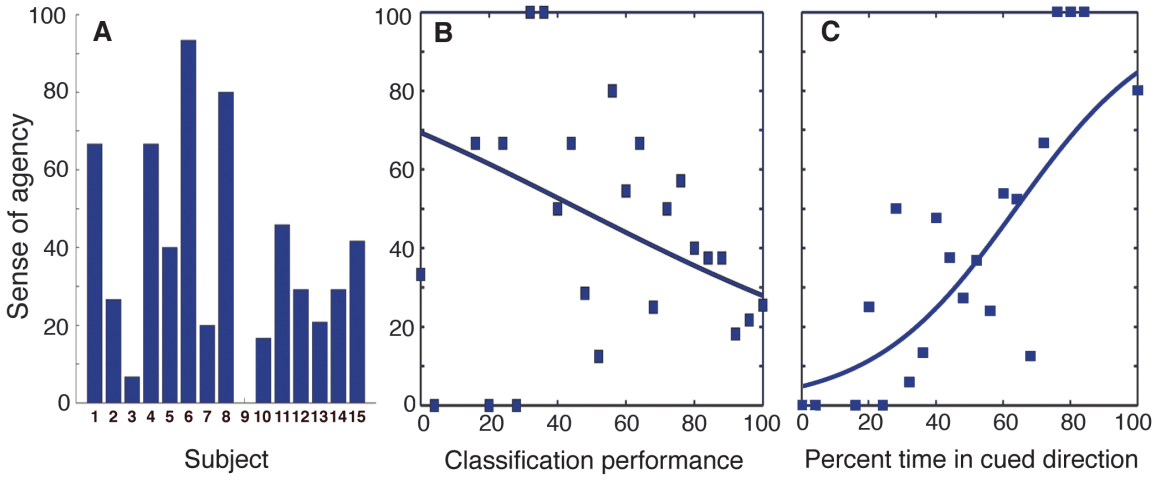

Figure 7. Sense of agency (SOA) for brain-machine actions where sensory consequences are generated independently to brain activity (random-feedback condition). (A) SOA in the random-feedback condition for all subjects across studies 1 and 2 (study 1: subjects 1-8; study 2: subjects 9-15). Individuals reported a wide range of feeling in control over the cursor that moved independently to their brain activity. **(B)** Fitting procedure for SOA as a function of classification performance showed no psychometric relationship between SOA and classification performance on a trial-by-trial basis. **(C)** Psychometric fit (point of subjective equality: 65%) for SOA as a function of the percentage of time the cursor moved in the cued direction. In panels (B) and (C), data points represent mean SOA across all random-feedback condition trials for all participants (in studies 1 and 2) in 4% classification performance or percentage in cued direction bins. Taken alongside Figures 5 and 6, these results suggest that SOA for BMI-actions relies on the match between the sensory outcomes (visual cursor position) to one's intended (cued) direction, rather than to one's ability to reliably generate the learned motor activity patterns (classification performance).

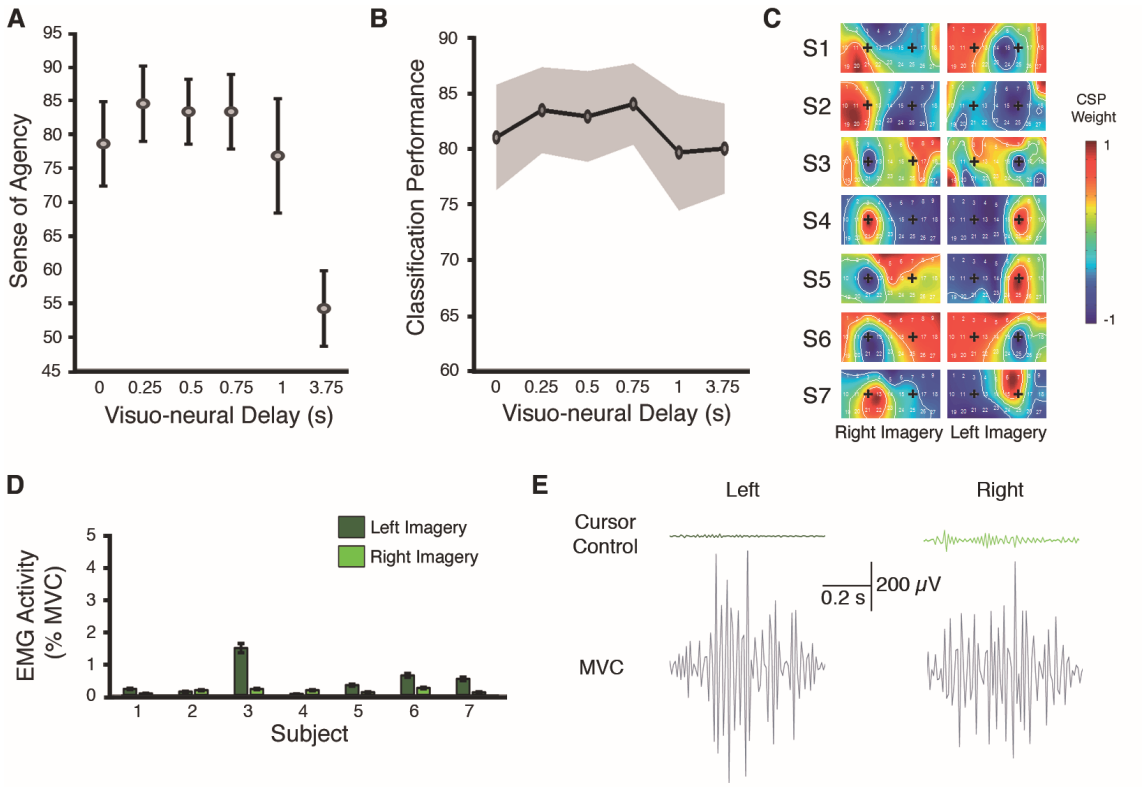

Figure 8. Study 2 results. ***(A)*** Sense of agency and ***(B)*** classification performance as a function of visuo-neural delay. ***(C)*** Per-subject, per-channel, normalized spatial filter weights for each electrode during left and right motor imagery for study 2. On each topographic map, '+' labels are placed over electrodes C3 and C4 for orientation. ***(D)*** Mean electromyographic (EMG) activity of left and right forearm flexor muscles during motor imagery. Activity was averaged across trials and conditions for each subject and a ratio was computed to their maximum voluntary contraction (MVC), resulting in very low ratios (all < 2%). ***(E)*** Sample EMG traces from participant 2 during left and right cursor control and during MVC trials. In all panels, error bars and shaded regions indicate SE of the mean.

Table 1. Statistical results for sense of agency measures in study 1 and study 2. All statistical contrasts used to assess differences across experimental conditions in SOA judgments (see *Methods* for details). For all pairwise T-test contrasts, only significant differences ($P < 0.05$) are reported.

Study 1	F / t	P	Study 2	F / t	P
2 x 6 ANOVA Interaction Congruency Delay	5.76 43.3 --	0.001 < 0.001 > 0.6	1 x 6 ANOVA effect of delay (congruent trials)	7.817	0.0001
1 x 6 ANOVA effect of delay (congruent trials)	5.33	0.001	T-Tests: 0 > 3.75s 0.25 > 3.75s 0.5 > 3.75s 0.75 > 3.75s 1 > 3.75s	all > 2.86	all < 0.03
1 x 6 ANOVA effect of delay (incongruent trials)	1.87	0.125			
T-Tests: congruent > incongruent (at all delays)	all > 3.77	all < 0.007			
T-Tests: (within congruent) 0 > 3s 0 > 3.75s 1.5 > 3.75s 2.25 > 3.75s 3 > 3.75s	all > 2.86	all < 0.03			

7. ACKNOWLEDGEMENTS

One of the most interesting parts of completing a PhD is looking way, way back to how it all began. How did I become an expert in watching people spin in circles? The simple answer is not on my own. Reminiscing about this academic odyssey, the faces of the people that helped get me to this point come flooding back to me. I think of a relaxed summertime chat with **Prof. Phillipe Renaud** that convinced me to choose EPFL over big city life in Paris. I think of my mentor **Prof. Carl Petersen** giving me my first lectures in neuroscience, inspiring me to expand on my curiosity of how the brain worked and get down to the business of research. And of course I think of my supervisor, **Prof. Olaf Blanke**, who most of all showed me how to think big and take chances.

But the story doesn't end there! I could write pages about the epic adventures of **The Beard Brothers**, my good friends **Nathan** and **Pär**. I spent more hours with Nathan during my PhD than anybody else, but our hairy bond goes much deeper than cumulative hours. Battling science demons during the day, composing music late into the night at the studio, or boogying down for marathon dance sessions, for all these things and more I send a hearty thanks and beardy salute. Pär, your zen presence and sage guidance during the early days of my PhD helped me more than you know. I've learned so much from you, both in terms of science and life. A strangely salient memory of my first days in the lab is looking down the row of desks at these two fine fellows, bopping their heads to some funky beat while I wistfully wished I was able to connect to their Airfoil Speakers and listen in.

Of course the bassist for **Love Bunker,** the LNCO mega-band for whom I served as roadie/VJ, needs to be mentioned here; from **Lukas** I learned just how superior Basel is to every other place on earth. So many others! **Aaron,** who helped carry me through the final leg of my PhD and for tolerating me on all those boat trips to Thonon. **Polona** for our countless hours of people watching and chatting by the window, and of course drawing class in Renens. **Silvia** for the beboppo, hallway breakdancing, and explorations of Pully. **Olli** for mapping my body movements to a T.rex avatar after a long day in the rotator room (still one of my favourite memories). **Mario** for our spirited political debates and Seinfeld quotes. **Silvio** for the random adventures. **Roy "The Boy" Solomon** for our many afternoon chats about science and life. **Elin** for our pioneering work as student representatives and being a great neighbour. And of course: **Dr. Joachim Forget, Bruno**, **Mariia, Christian, Christophe, Estelle, Jane, Roberto, Nathan 2.0, Fosco, Michiel, Sebastien, Michel, Petr, Javier, Lucie, Roberta, Elisa,** and all the rest of the LNCO/BMI/CNP/SV crew.

Finally, a huge thank you to my **parents,** easily my biggest fans, whose open ears and helpful guidance kept me on track when the road took an unexpected turn. I should also thank my older **brothers**, who lifted me up like only brothers can. Surprisingly, I also had a life outside of school, so to all of my great **friends**, **Soul Warriors, tai chi-ers**, and **travel buddies**, thanks for keeping me sane!

<insert beautiful quote that satisfies everybody and brings joy to the world>

8. CURRICULUM VITAE

STEVEN GALE

EPFL, Lausanne | +41 21 693 1681 | steven.gale@epfl.ch

EMPLOYMENT

Laboratory of Cognitive Neuroscience [LNCO]
Ecole Polytechnique Fédérale de Lausanne [EPFL]
Research Assistant – Doctoral Candidate **2010-2014**

Danfoss Solar Inverters A/S [Denmark]
Electronics Engineer **2007-2008**

PowerLynx A/S [Denmark]
Power Electronics IAESTE Intern **2006-2007**

TEACHING + LEADERSHIP

EPFL, Life Science Faculty
Teaching Assistant – "Neuroscience for Engineers" **2010-2013**

EPFL, Neuroscience Department
PhD Student Representative **2010-2013**

EPFL, Life Science Faculty
Teaching Assistant – "Practical Laboratory – EEG" **2010-2011**

EDUCATION

Laboratory of Cognitive Neuroscience [LNCO]
Ecole Polytechnique Fédérale de Lausanne [EPFL]
PhD Candidate in Neuroscience **2010-2015**

Ecole Polytechnique Fédérale de Lausanne [EPFL]
MSc in Microengineering **2008-2010**

Western University
B.Esc in Electrical Engineering **2001-2006**

PUBLICATIONS

Gale S, Prsa M, Schurger A, Gay A, Paillard A, Herbelin B, Guyot JP, Lopez C, Blanke O
Oscillatory neural responses evoked by natural vestibular stimui in humans (submitted)

Gale S, Schurger A, Blanke O
Temporal dynamics of cortical oscillations under natural vestibular stimulation (in prep)

Evans N, Gale S, Schurger A, Blanke O
Visuo-neural discrepancies modulate the sense of agency for brain-machine actions (submitted)

Prsa M, Gale S, Blanke O
Self-motion leads to mandatory cue fusion across sensory modalities
Journal of Neurophysiology 108:2282-2291 (2012)

Kaliuzhna M, Prsa M, Gale S, Lee S, Blanke O
Learning to integrate contradictory multisensory self-motion cue pairings
Journal of Vision (in press)

CONFERENCES PROCEEDINGS

Society for Neuroscience (2011-13) | **Alpine Brain Imaging Conference** (2012) | **Lemanic Neuroscience Annual Meeting** (2011-12)

LANGUAGES

English – mother tongue | French – intermediate | Danish – intermediate

LIFE

Travel. Music + Film +Art. Tinkerer + Maker.